A Holistic Framework of Synthesis and Characterization of Waste-based Geopolymers for Civil Engineering Applications

by

Mengxuan Zhao

A Dissertation
Submitted to the Faculty
of the
WORCESTER POLYTECHNIC INSTITUTE
in partial fulfillment of the requirements for the
Degree of Doctor of Philosophy
in
Civil, Environmental, and Architectural Engineering
April 2023

APPROVED:

_____

Professor Mingjiang Tao, Major Advisor, CEAE department, WPI

_____

Professor Tahar EI-Korchi, Co-Advisor, CEAE department, WPI

_____

Professor Aaron Sakulich, Committee member, CEAE department, WPI

_____

Professor Sergio Granados-Focil, Committee member, School of Chemistry and Biochemistry, Clark University

ABSTRACT

The cement industry is responsible for about 8% of all human-made CO_2 emission and 2-3% of energy use in the world, and thus achieving sustainable concrete becomes imperative with the ever-growing worldwide demand for concrete. Geopolymers, as a promising greener alternative to ordinary portland cement (OPC), are investigated in this Ph.D. study, with a focus on the development of a holistic framework for synthesizing and characterizing their mechanical properties, durability, and volume change behavior. Red mud slurry-Class F fly ash-based geopolymers and metakaolin-based geopolymers were synthesized and investigated through an integrated multiscale experimental approach.

In the first part of this study, red mud slurry and class F fly ash (RMSFFA) - based geopolymers were successfully synthesized, and the relationship among synthesis factor-mechanical property-microstructure of RMSFFA geopolymer has first been examined.

Then two different aspects of geopolymers were evaluated in the second part of this study: (i) to examine whether the current chemical shrinkage testing procedure of OPC is suitable for geopolymers by using metakaolin as the raw material, and (ii) to characterize the chemical volume change of the more complicated geopolymer system – RMSFFA geopolymers. A comprehensive experimental study was first performed to investigate the influence of different filling solutions (i.e., deionized water-DIW and activator solution-AS) on geopolymerization and the chemical volume change behavior of metakaolin-based geopolymer (MKG). Four stages in chemical volume change of MKGs were confirmed: Shrinkage, Expansion, Shrinkage, and Stable stages. Based on the testing results by Scanning Electron Microscopy-energy Dispersive X-ray (SEM-

EDX), Isothermal Conduction Calorimetry (ICC), Fourier Transform Infrared Spectroscopy (FTIR), Brunauer-Emmett-Teller (BET), and Inductively Coupled Plasma Mass Spectrometry (ICP-MS) techniques, AS filling solution generally caused the formation of more geopolymer gels, while the DIW filling solution intervened or dampened the geopolymerization process to some extent, especially on the surface portion. The filling solutions affect the geopolymerization of MKGs and thus their micro-characteristics and chemical volume change, largely through chemical exchanges between the filling solutions and geopolymer slurry, particularly diffusion-based leaching or ingress of Na^+ and OH^-. Then the chemical volume change behavior of RMSFFA geopolymers was investigated to shed light on the more practical geopolymer system.

In the third part of this study, freeze-thaw (F-T) durability of RMSFFA geopolymers was also investigated, with an emphasis on the influence of chemical compositions and curing conditions (i.e., curing time and curing temperature). F-T durability was evaluated on the basis of the sustained mechanical strength of RMSFFA geopolymer specimens after subjected to 50 F-T conditioning cycles. The change in their chemical bonding, mineralogy, and pore characteristics at various F-T conditioning cycles was examined with FTIR, X-ray diffraction (XRD), and BET testing, respectively, to reveal the underlying processes during F-T conditioning. The results of both mechanical strength and microstructural characterization indicate that curing conditions influence F-T resistance of RMSFFA geopolymer samples through affecting their strength development. For 14-day cured RMSFFA samples at 50 °C, they experienced further geopolymerization at the early stage of F-T conditioning but the partial dissolution of geopolymer gels at the later stage of F-T conditioning. For 28-day cured samples at 50 °C, only the partial dissolution of geopolymer gels was likely to occur during the F-T conditioning because the strength development was likely to complete prior to the conditioning.

Lastly, the results of RMSFFA geopolymer samples were used to illustrate how a holistic framework can be applied to synthesize and characterize geopolymers and other cementitious materials.

ABSTRACT

I dedicated this thesis to

My Mother Ai'jun, my Father Liang, my Husband Ning and my Daughter Yuxi

For being in my life

ACKNOWLEDGMENT

The best way to begin this thesis I feel would be by acknowledging my gratitude towards all the brilliant individuals responsible for its successful completion.

It is a great pleasure to acknowledge my deepest thanks and gratitude to my advisor Professor Mingjiang Tao for his guidance, expertise, continued support and friendship throughout my Ph.D. journey in WPI. I would also like to thank my committee members Professor Tahar El-Korchi, Professor Aaron Sakulich, and Professor Sergio Granados-Focil for being part of my Ph.D. committee, and for their time and continued support. I would like to appreciate Professor Chunyuan Liu for providing me the opportunity to pursue my doctorate here.

I would like to sincerely thank the lab managers Russ Lang, Wenwen Yao, and Donald Pellegrino for not only their expertise, but also their friendship. I really enjoyed the time we spent together in the lab.

I would like to give special thanks to Agata Lajoie, Marylou Horanzy, Cynthia Bergeron, Maryann Watts, and Joan Langlois. They were always there when I needed. I would like to thank my fellow graduate students for their friendship: Mo Zhang, Xiaokong Yu, Wenwen Yao, Jessica Rosewitz, Chao Wang and Shuai Wang.

I would like to thank the Department of Civil, Environmental and Architectural Engineering at WPI for the financial support being the teaching assistant for so many years.

I also would like to thank the U.S. National Science Foundation for the partial financial support to this research (Grant No. CMMI-1301048).

More than all, I would like to thank my family, especially my husband, this could not have been done without his support. Thanks to my parents, who have provided me through all those tough years in my life. Thanks to my best friend Ye Tong, I could not have gone so far without your continued support and friendship. Thanks to my daughter Yuxi, I am grateful to have you along the way.

TABLE OF CONTENTS

LIST OF FIGURES

LIST OF TABLES

CHAPTER I – INTRODUCTION

1.1 LITERATURE REVIEW

1.1.1 Background of Geopolymers

The world-wide demand for concrete is ever-growing and approaching 30 billion tons per year [1]. However, ordinary Portland cement (OPC) manufacturing is an energy-intensive process that requires high-temperature firing of raw materials such as limestone at 1400-1500°C, and energy-consuming grinding. Moreover, this manufacturing process emits a large quantity of CO_2. In fact, it is estimated that producing 1.0 ton cement yields approximately 1.0 ton CO_2 emission according to the reaction $CaCO_3 \rightarrow CaO + CO_2$, and concrete industry is responsible for about 8% of all human-made CO_2 in the world. Furthermore, the raw materials readily available for cement production have been over-consumed, and the cement production process is highly non-sustainable. Therefore, the global construction materials industry has been searching for a new viable, greener, and economical alternative to replace OPC, in order to reduce CO_2 emission, conserve energy, and slow down the current global warming process.

More recently, a new class of materials, inorganic geopolymers, has attracted great attention in the research community. Geopolymers are synthetic mineral products that combine properties of polymers, ceramics, and cements [15], and thus possess a series of distinct properties and advantages: (1) they are exceptionally heat/fire resistant (e.g., stable up to 1200°C) [2, 3]; (2) it is easy to make and handle geopolymers, since they can transform and polycondense rapidly at low or room temperatures; (3) they are highly resistant to organic solvent, acid, and sulfate attack and other corrosive processes (e.g., anti-biofouling) [4, 5]; (4) they are nontoxic, “green” materials

since their production saves energy and does not emit CO_2 [6-8]; (5) they are made from low-cost materials, such as metakaolin, fly ash, and furnace slag; and (6) they do not incorporate hydration water within the polymeric structure, unlike Ca-based cements, and hence have higher mechanical properties (e.g., surface hardness, compressive strength) than Portland cement [9, 10]. Therefore, geopolymers are very promising to be used as a durable, high-strength cementitious material for diverse applications. For instance, they can be used as a much cheaper (if produced from wastes) cementitious structural material to replace OPC, as adhesives, or as a waste (even radioactive wastes) encapsulation material. Geopolymers have been studied as a viable alternative to organic polymers and inorganic cements in diverse applications, including military [11], aircraft [12, 13], high-tech ceramics [14], thermal insulating foams [15], protective coatings [16], refractory adhesives [17], and hybrid inorganic-organic composites [18, 19], due to their exceptionally high thermal and chemical stability and adhesive/cementitious strength. Different from their organic counterparts, geopolymers are inorganic materials synthesized from silicate- and aluminate-bearing materials and even wastes at ambient or low (<150°C) temperatures (hence low or no energy consumption). It involves polycondensing tetrahedral silica (SiO_4) and alumina (AlO_4) into final amorphous or semi-crystalline polymeric structures:

$$M_n^+\{\text{-}(SiO_2)_z\text{-}AlO_2\text{-}\}n[e.g., (\text{-}Si\text{-}O\text{-}Al\text{-}O\text{-})_n, (\text{-}Si\text{-}O\text{-}Al\text{-}O\text{-}Si\text{-}O\text{-})_n, (\text{-}Si\text{-}O\text{-}Al\text{-}O\text{-}Si\text{-}O\text{-}Si\text{-}O\text{-})_n],$$

Where M^+ = an alkali cation (K^+, Na^+) for balancing negative charges; n = degree of polymerization; and z=Si/Al molar ratio. By varying Si/Al ratio (i.e., typically z=1-15, up to >300) [20], geopolymers exhibit different properties: low ratios result in three-dimensional cross-linked rigid networks with stiff and brittle properties (e.g., those of ceramics and cements); ratios >3 and >15 result in 2-D network and linearly linked polymeric structures with adhesive and rubbery properties, respectively. Geopolymer formation consists of two basic steps [15, 21-23]: (1) the

generation of reactive species by alkali activation, which is the dissolution of amorphous phases of feedstock (e.g., fly ash, furnace slag, metakaolin) by alkali solution to produce reactive silica and alumina; and (2) the actual setting reaction, which is the polycondensation process leading to the formation of aluminosilicate polymers. In particular, the presence of reactive alumina ($Al(IV)$ or Al^{4+}) and alkali-activation are two key requisites for geopolymerization, as illustrated by the following two reactions [24]:

$$n(Si_2O_5, Al_2O_2) + 2nSiO_2 + 4nH_2O + \frac{NaOH}{KOH} \rightarrow Na^+, K^+ n(OH)_3\text{-}Si\text{-}O\text{-}Al^-\text{-}O\text{-}Si\text{-}(OH)_3 \quad (1\text{-}1)$$

$$(OH)_2$$

(Si-Al material) (Geopolymer precursor)

$$n(OH)_3\text{-}Si\text{-}O\text{-}Al^-\text{-}O\text{-}Si\text{-}(OH)_3 + NaOH/KOH \rightarrow (Na^+, K^+)\text{-}(\text{-}Si\text{-}O\text{-}Al^-\text{-}O\text{-}Si\text{-}O\text{-}) + 4nH_2O \quad (1\text{-}2)$$

$$(OH)_2 \qquad\qquad O \quad O \quad O$$

(Geopolymer backbone)

Therefore, geopolymerization also presents a viable, economical, and environmentally friendly approach to recycling and reusing various industrial wastes. In this Ph.D. study, red mud slurry, Class F fly ash, and metakaolin were used to synthesize geopolymers. The detailed introductions of the raw materials are described in the following sections.

1.1.2 Raw Materials

In principle, a wide range of materials, including the natural minerals and industrial wastes and residues that are rich in amorphous silica and/or alumina, are potential feedstocks to synthesize geopolymers. For instance, metakaolin [25, 26], red mud [27, 28], fly ash [29, 30], or the mixture

of the above [31], have been used to successfully synthesize geopolymers. The raw materials used in this Ph.D. study are summarized below:

1.1.2.1 Red Mud Slurry

Red mud slurry (denoted as RMS) is the major waste in the production of alumina from the Bayer process [32-36]. The annual production of red mud slurry is estimated about 200 million tons worldwide [34, 35, 37], with an increment of 120 million tons annually [36, 38]. Due to different bauxite ore sources and refining processes, RMS has variable physical, chemical, and mineralogical properties, with a pH value of ~10-13 [32, 35, 39, 40]. The main compositions of RMS are iron oxide and alumina-silicate oxides. The management and reuse of RMS have been challenging because of its enormous quantity, high alkalinity, high water content, presence of various heavy metals [41], which pose serious disposal problems in the mining industry [33]. In recent years, many researchers have attempted to develop new ways to recycling or reusing RMS, one of which is geopolymerization [36] by taking advantage of its high alkalinity and the presence of aluminosilicates. The high alkalinity can partially replace the alkaline solution in geopolymer synthesis, and aluminosilicates present in RMS can participate in geopolymerization reactions and act as non-reactive fillers in the resulting geopolymer. In addition, the application of geopolymerization technology in civil engineering can consume RMS in large quantities. However, based on previous studies [36, 42], the reactivity of RMS in geopolymerization at ambient conditions is poor or limited. To achieve better mechanical properties of geopolymer products, other raw materials with high reactivity in geopolymerization must be added, such as metakaolin or fly ash. In addition, RMS still needs to be dried and ground to powders prior to

geopolymer synthesis, which consumes extra energy and adds more costs than directly using RMS in geopolymer synthesis.

1.1.2.2 Fly Ash

Fly ash, one of the four main by-products of coal-burning power plants, is obtained from the combustion of coal, consisting of the inorganic matter that did not burn during the process. Fly ash is composed of fine, spherical aluminosilicate particles generally recovered from the smokestack of a power plant. The exact chemical composition of fly ash depends on the type of coal burned. If a sub-bituminous coal used, the resulting ash will be classified as type C due to its higher amount of calcium [43]. This type of ash does not always require an activator and will display cementitious properties when exposed to water, which means that in theory water is the only additive needed to hydrate this material and form cementitious products similar to those obtained from OPC. If a bituminous coal used, the resulting by-product is classified as class F fly ash, which has a relatively low calcium with no self-cementing properties and is a pozzolan [44]. More than 750 million ton fly ash is generated worldwide each year.

Fly ash is rich in silicate and aluminates, both of which are main reactants in geopolymerization processes. The reuse of fly ash is environmentally friendly in three ways. It reduces the amount of virgin material that needs to be extracted to make OPC, as well as displaces the greenhouse gases, and reduces energy consumption, during the processing of that virgin material. Moreover, fly ash can also be used as the raw material to produce alkali-activated fly ash in a highly alkaline medium (i.e., geopolymer) [45].

Most of the aluminum plants that generate red mud also generate fly ash from their captive power plants, which make these two industrial wastes a good combination for geopolymer

synthesis due to low transportation costs [46]. Red mud and fly ash-based geopolymer has been synthesized by a number of researchers in recent years [41, 47].

1.1.2.3 Metakaolin

Metakaolin is a dehydroxylated form of kaolin clay, one of the most widely mined minerals in the world, produced by the calcination of kaolin at a temperature of 600 to 850 degree Celsius [48]. Metakaolin contains nearly exclusively amorphous silica and alumina, and therefore it is highly reactive during the alkali activation. Although metakaolin is not necessarily more cost-effective or greener than fly ash/slag [49], it is an ideal raw material that produces relatively pure geopolymer binders. Thus, it was often chosen in previous research studies as a starting point for exploratory investigations to avoid complexity and uncertainties associated with impurity present in other feedstocks with complex compositions (e.g., fly ash, red mud, blast furnace slag). Despite the improved purity of metakaolin-based geopolymers (MKGs), MKGs have not been seriously considered as alternative binders for mainstream construction products because it is inherently more expensive than industrial by-products and there lacks information about MKGs' long-term performance and durability [49]. However, in nuclear and hazardous waste encapsulation applications, the higher cost of metakaolin is not an issue and chemical consistency of the resulting product is more important [50].

1.1.3 Mechanical Properties of Geopolymers

Mechanical properties are a key indicator in geopolymer system, which is the most important factor to be considered in geopolymer synthesis. Mechanical and physical properties, in general including the unconfined compressive strength (UCS), the failure strain, bulk density, and Young's

modulus, were evaluated by numerous researchers on various geopolymer systems. Chemical composition, curing time, and curing temperatures are the most common synthesis factors investigated on their effects on various geopolymer systems. In the literature studies, Si/Al molar ratio and Na/Al molar ratios are used to control the geopolymer synthesis. The UCS values of geopolymer with different chemical compositions can vary from a few MPa to more than 100 MPa [20, 51]. In addition, UCS of geopolymers is affected by curing humidity, the composition of alkali activators, and especially the curing temperatures and curing time. Fast evaporation of water from the geopolymer structure with the presence of high curing temperature and longer duration of exposure may reduce the structural integrity of the matrix and thus lower its mechanical strength.

1.1.4 Microstructure of Geopolymers and Geopolymer Gels

1.1.4.1 Geopolymer Gels

It is imperative to understand basic structures and properties, and compatibility of geopolymer gel because it is the major constituent for strength development and bonding agent in geopolymer. So far, there are two major alkali activated materials: (i) low calcium alkali activated materials (e.g., Class F fly ash and metakaolin); and (ii) higher calcium alkali activated materials (e.g., ground granulated blast slag (GGBS) and Class C fly ash). For low calcium alkali activated materials, the reaction product is an amorphous counterpart of an aluminosilicate zeolitic structure. Such geopolymers are commonly activated with sodium hydroxide or sodium silicates with relatively high pH values (e.g., >12). Geopolymeric gel and calcium silicate hydrate (C-S-H, the main product of OPC hydration) were found to co-exist in alkali activated materials in the literature. The formation of C-S-H was mainly attributed to dissolved calcium ions from the surface of the source materials that react with available silicate species in an alkali environment. It was also

proposed that the simultaneous formation of the geopolymeric gel and the C-S-H may help to bridge gaps in the matrix and hence increase the compressive strength of geopolymers, especially at early ages. For high calcium alkali activated materials, the reaction product is “aluminum substituted calcium silicate hydrate (C-A-S-H). This gel is similar to tobermorite in its structure and generally can be compared to the C-S-H gel resulted from the hydration of OPC. Substitution of Al in the C-S-H structure leads to a higher degree of polymerization and crosslinking between tobermorite chains. When the content of alumina is relatively low in the precursors, the formed gel is dominantly C-S-H.

1.1.4.2 FTIR

García-Lodeiro et al. [52] successfully synthesized C-S-H and N-A-S-H gels from laboratory reagents at different pH values through sol-gel process. C-S-H gels and N-A-S-H gels were synthesized with same theoretical Ca/Si ratio (=1) and Si/Al ratio (=1), respectively, but at different pH values. The FTIR results of C-S-H gels are shown in **Figure 1**. The main band of C-S-H gel, band e, became narrower and shifted towards lower wavenumbers as the pH value increased. Two conclusions were drawn: (1) when pH <11, main Si-O band was wide and centered at higher frequency (~1041 cm^{-1} in this paper), which indicates a higher content of SiO_2 and higher degree of polymerization; and (2) when pH >11, main Si-O bond was narrow and centered at a lower frequency (~975 cm^{-1} in this paper), which indicates higher Ca content in the micro-structure of the gel (conventional C-S-H gel) and lower polymerization. In addition, because of the existence of Ca, some C-O vibration bands (c, d and f) were found in these spectra. The FTIR results of N-A-S-H gels are shown in **Figure 1-1**. When pH< 12.5, the main band slightly shifted towards lower wavenumbers as pH value increased. And when pH>12.5, the main band became identical, which

was around 1006 cm^{-1}. So the authors believe at high pH>12.5, it is N-A-S-H gel, but at relatively low pH value, it is a mixture of N-A-S-H and silica gels. All the bands in FTIR spectra associated with C-S-H, silica and N-A-S-H gels are summarized in **Table 1-1**.

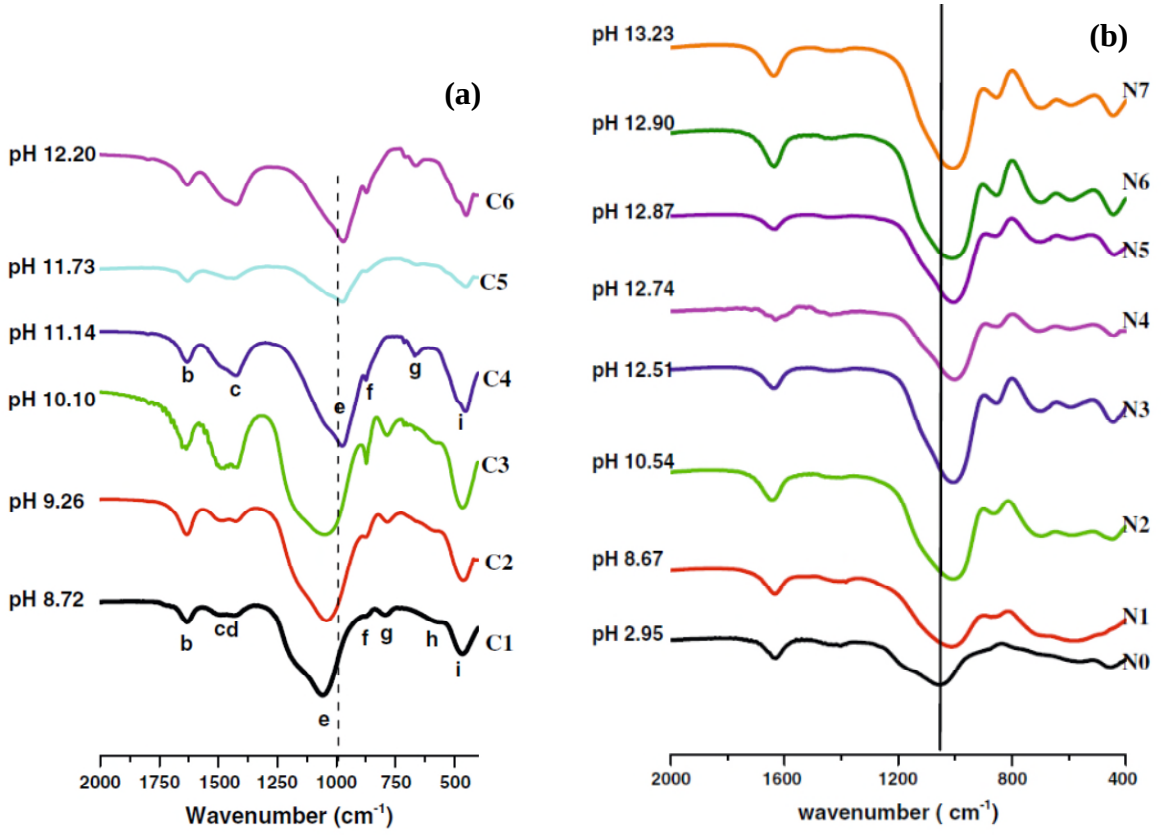

Figure 1-1 (a) FTIR spectra for C-S-H gels. (b) FTIR spectra for N-A-S-H gels

Table 1-1 Summary of FTIR results of C-S-H, N-A-S-H and Silica gels.

Gel type	Wavenumber (cm^{-1})	Bond
C-S-H gel	~450, 658	typical of C-S-H gel
	660	Si-O-Si bending band (typical C-S-H gel)
	835,815	Si-O bond symmetric stretching vibrations (Q^1)
	870 – 875, 1470-1400	carbonate C-O stretching vibrations in carbonates
	970	Si-O bond asymmetric stretching vibrations (typical C-S-H gel)(generated by Q^2 units)
Silica gel	1040-1080, 1140-1180, and 1486	Q^3 and Q^4 silicon tetrahedral in silica gels
N-A-S-H gel	1006	T-O bond asymmetric stretching vibrations
	650-500	the presence of double rings
	594	TO4 external vibrations
	690-700	TO_4 internal symmetric bending vibrations
	860	Si-O terminal bonds (double ring structure)
	1085-990	Si-O (Si) bridge bonds (in double ring structure)

The authors also tried to blend the N-A-S-H gel and C-S-H gel together, and FTIR was conducted on the blended material. Only some ambiguous conclusions were drawn, based on different ratios of N-A-S-H gel and C-S-H gel added in, there is no clear trend to follow. And the characterization method failed to distinguish the N-A-S-H gel and C-S-H gel. In addition, Takashima attack was performed on C-S-H gel and blended gel. Takashima attack is a chemical separation method with methanol and salicylic acid, in which C-S-H gel can dissolve, but silica gel and $CaCO_3$ cannot. Based on this method, the C-S-H gels are not pure gels, which is a mixture of C-S-H gel, silica gel and $CaCO_3$.

Although the main component of these two gels is silicate, the basic molecular structures of C-S-H gel and N-A-S-H gel are totally different. The C-S-H gel is a layered structure with linear chains of linked silicate tetrahedral and CaO membrane, while N-A-S-H gel is a three-dimensional

structure with silicon and aluminum tetrahedral randomly distributed. The cations in N-A-S-H gel are bounded to gel surfaces to balance the negative charge generated by the substitution of Al^{3+} to Si^{4+}. The structures are schematically shown in **Figure 1-2.**

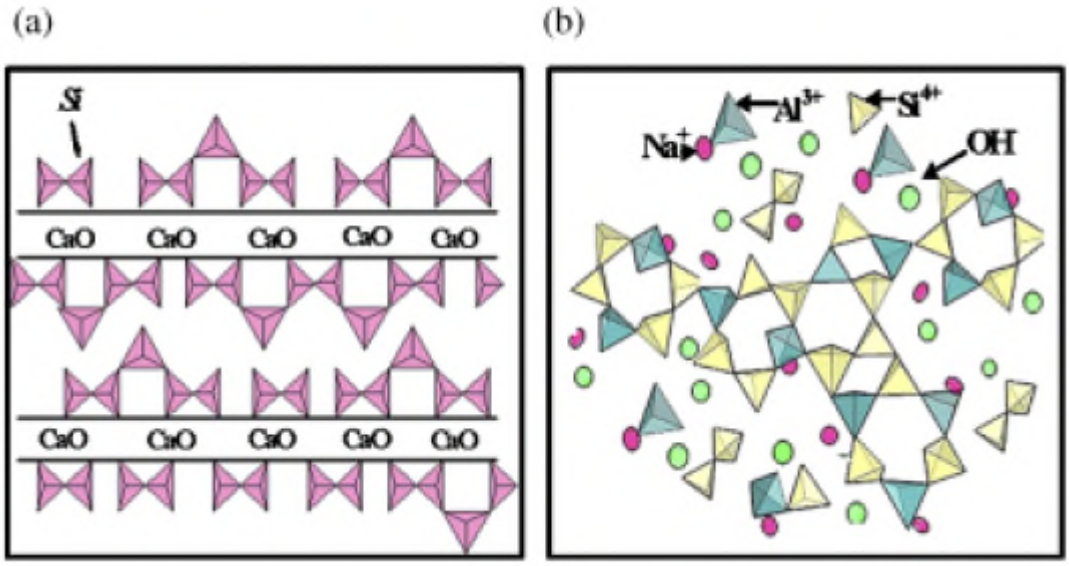

Figure 1-2 (a) C-S-H gel structure. (b) N-A-S-H gel structure.

The main band in the control group shifted to higher wavenumbers and became broader after aluminum and sodium being added. This is interpreted as arising from the formation of Si-O-Al cross-linkages from what was previously Si-O-H or Si-O-Ca groups. The more acidic Al^{3+} ion (relative to H^+ or Ca^{2+}) draws electron density away from the neighboring Si-O bond, weakening it and resulting in a peak shift to lower wavenumbers. However, the remaining Si-O bonds in what were previously the pairing silicate tetrahedral may experience an increase in strength due to the resulting change in polarization at the O on the Si-O-Al linkage, leading to higher wavenumber contributions to the main Si-O band and consequent broadening of the band around 970 cm^{-1}. The 3635 cm^{-1} band corresponding to portlandite shown in the control sample disappeared in the samples containing Al and Na. The reasons are: 1) a reduction in $Ca(OH)_2$

crystallinity; 2) the pH reduction permitting $Ca(OH)_2$ solubility; and 3) a redistribution of Ca adsorbed onto surfaces of a modification product (e.g., a sodium aluminosilicate hydrate (N-A-S-H) gel).

There is no significant change in FTIR spectra and morphological differences in TEM results between the control group (N-A-S-H gels) and experimental group (N-A-S-H gels with calcium additions). However, a big difference can be found in EDX results, which is shown in **Figure 1-3**.

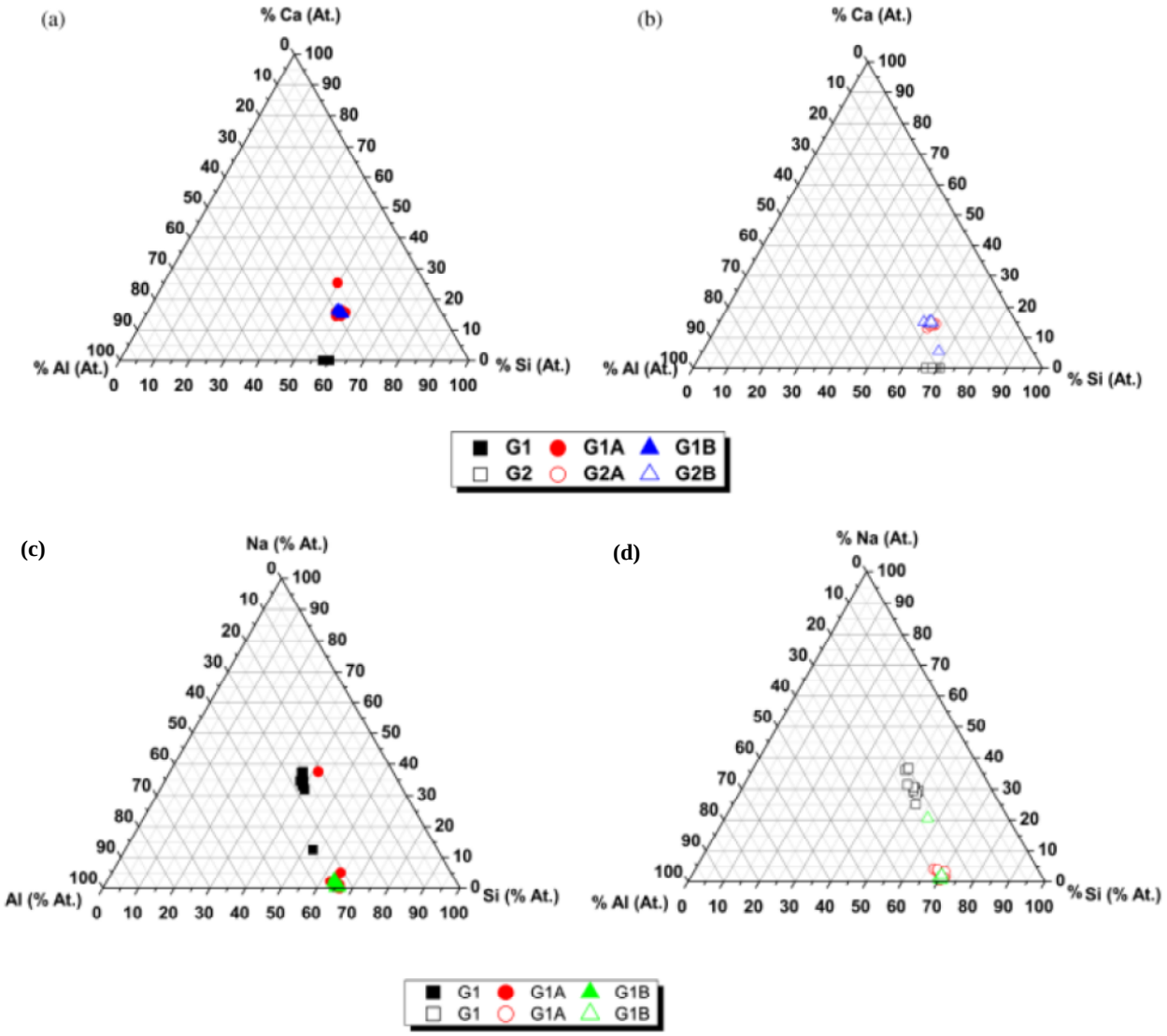

Figure 1-3 EDX analysis (1) Ca-Al-Si system (a) G1, G1A, and G1B; (b) G2, G2A, and G2B. (2) Na-Al-Si system (c) G1, G1A, and G1B; (d) G2, G2A, and G2B.

The actual Si/Al ratios estimated from EDX for G1 and G2 are 1.45±0.03, 2.19±0.11, respectively. It can be found that nearly no sodium left in the gels with calcium additions, which means calcium is adsorbed preferentially and sodium is only adsorbed when there is no sufficient calcium.

1.1.4.3 NMR

^{29}Si NMR, ^{27}Al NMR, and ^{23}Na NMR were conducted on the geopolymer gels by Noftz et al. [53]. For ^{27}Al NMR, a single peak located at around +56 to +58 ppm attributed to tetrahedral aluminum, and a small peak located at around +5 ppm associated to the octahedral aluminum that may be attributable to the appearance of AF_m. But the participation of calcium doesn't change the modification in this structure. For ^{23}Na NMR, the intensity of sodium decreased as the amount of calcium added increased, which was also observed in EDX. And for ^{29}Si NMR, it was believed that the signals appeared in the -72 to -81 ppm interval were associated to Q^2 units, and the signals appeared at values higher than -100 ppm were associated to Q^4 units. Noftz et al. [53] studied the effect of different cations on the ^{29}Si spectra for different types of aluminosilicate glass and showed that the width of the NMR resonances increased towards high field (more negative chemical shifts) in the following order Na<Li<Ca<Mg. The ^{29}Si NMR spectra were deconvoluted and the areas of deconvoluted components for control and resulting gels are shown in **Figure 1-4**. In the control gels, the amounts of Q^4(4Al) and Q^4(3Al) are main components in gel G1, and Q^4(3Al) and Q^4(2Al) are main components in gel G2. The Q^4(2Al) and Q^4(1Al) increased significantly in gels with calcium. Moreover, the amount of Q^4(1Al) for gels with initial Si/Al ratio of 1 is smaller than that for gels with initial Si/Al ratios of 2. The authors believed there are two possibilities: (1) Si-O-Al linkages are disrupted by the polarizing influence of Ca^{2+} to form Si-O-Ca (thus reducing the Q^4(4Al) and Q^4(3Al) units, or (2) Al is lost from the 3D structure to produce secondary phases with Ca. The appearance of octahedral Al by NMR would tend to support this, indicating a rather poorly crystalline AFm-type phase type monocarboaluminates (not observed by XRD).

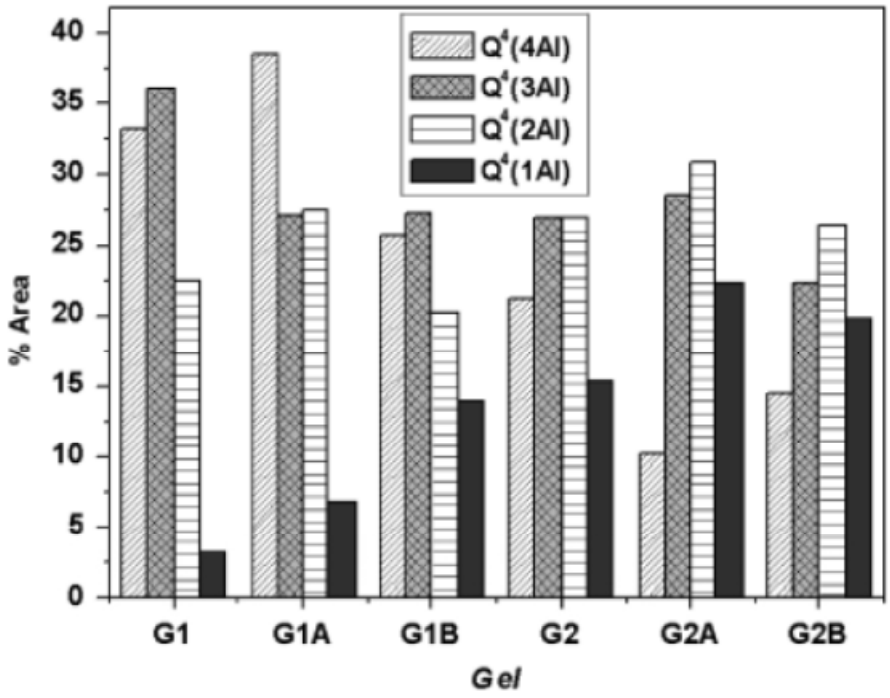

Figure 1-4 Areas of deconvoluted components on spectra for gels G1(control), G1A, and G1B; G2(control), G2A and G2B.

All ^{29}Si measurements were acquired using a resonance frequency of 79.5 MHz and spinning rate was 10 KHz, and referenced against TMS (tetramethylsilane), with a MAS single pulse of 5 μs and a 10 s. The ^{27}Al MAS-NMR and ^{23}Na MAS-NMR spectra were acquired at 104.3 MHz, 105.8 MHz, and the spinning rate was 10 KHz, using $Al(H_2O)_6^{3+}$ and NaCl as external standards (both with a MAS single pulse of 2 μs and a relaxation delay of 5s).

In conclusion, the 3D structures of N-A-S-H gels appear to be preserved, the orientation or distribution of aluminate and silicate tetrahedral changed by the introduction of Ca. In the authors' previous study [54], high concentrations of alkaline oxides to C-S-H gel structures increased the degree of silicate polymerization (increasing Q^2) in the gel, even in the very early stages of reaction. In this paper, the effects on C-S-H gels with aluminum and sodium additions. The

synthesis pH decreased after the aluminum and sodium added, and the synthesis pH of NA4 is higher than NA2, which has higher amount of aluminum. This can be interpreted as the initial high pH is likely to promote hydrolysis of available silicates and support condensation (polymerization) of (alumina)silicates available from solution or surface sites. The pH reduces when aluminum nitrite is added, which means the high polymerization degree of more available Al which is known to form bridges between silicates tetrahedral. The NMR results are shown in **Table 1-2**. NMR results show that the existence of stratlingite, and there is no silicate connectivity higher than Q^2 (possibly Q^3).

Table 1-2 NMR results of control gel NC and sample gels with aluminum and sodium additions NA2 and NA4.

	peak (ppm)	Assigned to	Notes
^{29}Si spectrum	-78.31	tetrahedral end-of-chain Q^1 silicates	
	-83.62	tetrahedral mid-chain Q^2 silicates	
	-89.6	Q^3 silicate	
	-81	Q^2(1Al)	
	-81	Q^2(2Al)	shown in stratlingite
	-84	Q^1(2Al)	
	-87	Q^2	
	-91	Q^3(2Al)	
^{27}Al spectrum	62	Al[4]	
	9.9	Al[6]	

The presence of aluminum at high pH will enhance the geopolymerization in aluminosilicates. This is due to aluminate species' tendency to form bridging tetrahedral between silicate units, and bridging of tetrahedral extend to three-dimensional structures rather than just two. Faucon et al. [55] proposed that 4-coordinated aluminum replaces the silicon in both the bridging and paired tetrahedral in the drierkette chains of C-S-H gel but Taylor [56] had previously

reported that aluminum only replaces silicon in bridging tetrahedral. But the enhanced degree of cross-linking is limited, which can be seen from the above NMR results. There is no silicate connectivity higher than Q^2 (possibly Q^3). The high alkali concentrations will increase the linkages between tetrahedral and also levels of hydrolysis of the aluminosilicate.

1.1.5 Volume Change Behavior of Geopolymers

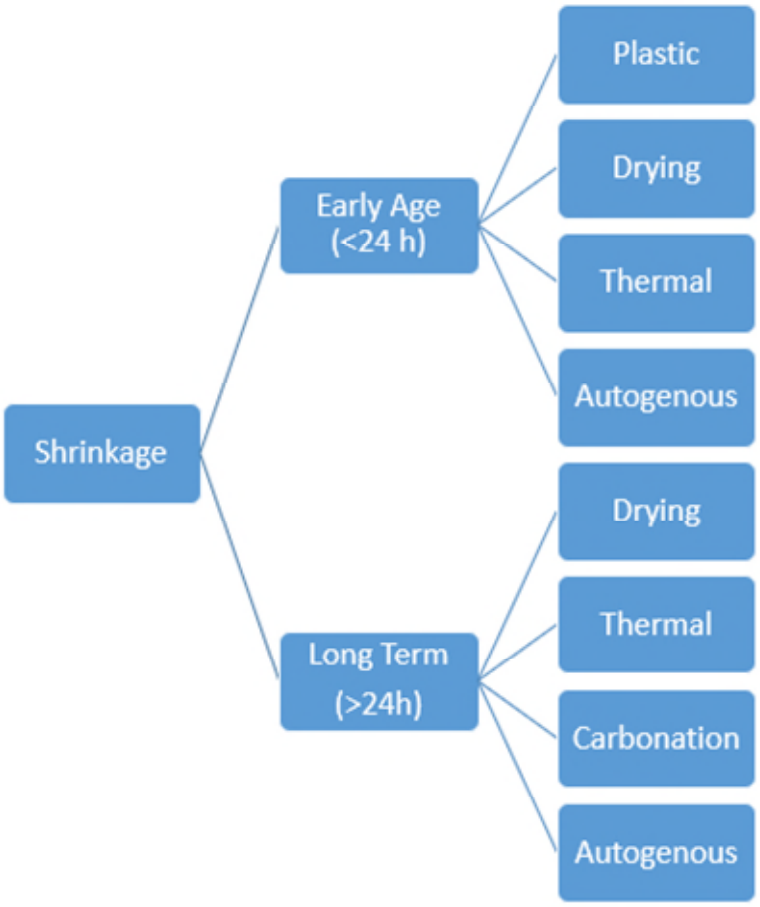

Figure 1-5 Types of Shrinkage

Despite being confirmed as a promising alternative to OPC by numerous laboratory experimental studies [47, 57, 58], geopolymer has not been widely applied in civil engineering mainly because

of several main barriers, one of which is the lack of information and knowledge about their volume change (refer to shrinkage to OPC) behavior during synthesis process.

Shrinkage of cementitious materials has been the interest of numerous research studies owing to its important effect on micro and macro cracking that in turn often results in deterioration, non-structural damage, or even catastrophic failure to concrete structures [59-63]. Shrinkage can lead to early-age cracking, which reduces mechanical properties such as compressive strength and provides aggressive media (primary chlorine ions) easy access to reinforcing steel. The reaction between aggressive media and reinforcing steel creates expansive corrosion products, which create stresses that cause (and later accelerate) cracking. This cycle leads to a relatively quick deterioration in the properties of the concrete structure. Although the shrinkage of geopolymers would have significant influence on whether geopolymer will crack or not under the restrained condition and thus its durability, it has received comparatively little attention [64-68] and the mechanism of shrinkage of geopolymers is far from being well understood.

The types of shrinkage are illustrated in **Figure 1-5**. Shrinkage and shrinkage related stresses have been studied over several decades, along with the progress of cement and concrete technologies [69]. Shrinkage can be classified as early age shrinkage and long-term shrinkage, or restrained shrinkage and unrestrained shrinkage. The exact definition of ‘early age’ depends on the context and time frame of the measurements [70].

The main forms of shrinkage are chemical, autogenous, and dying shrinkage. Chemical and autogenous shrinkages are two main forms that occur for reasons unrelated to water leaving the cementitious system; they would occur even if the system were completely sealed from the external environment [70]. Proper curing practices (or, more accurately, proper external curing

practices, since water is provided only to the exterior of the system) such as curing in a lime-saturated bath in the laboratory or applying wet burlap to the surface of the structure in the field, can help to counteract two forms of early-age shrinkage: autogenous shrinkage and drying shrinkage [71].

1.1.5.1 Chemical Volume Change

Chemical shrinkage, also called “hardening shrinkage” [49, 72-82], is “internal”, which does not affect the overall volume of the system and begins at the moment that activating solution and raw materials come into contact. Chemical shrinkage is the absolute volume change between the reactants and the products during the chemical reaction process. The volume change is mainly caused by the density difference between the products and the reactants, which is called Le Chatelier’s contraction [76]. As the hydration is completed, this shrinkage can represent approximately 10% of the initial volume of OPC [76]. Initially, this reduction in volume is accommodated by deformation of the fresh paste, but after being set, the system resists deformation and pores are created [83]. The porosity of the system will continue to increase for as long as hydration reactions (or their equivalents) are occurring. Therefore, chemical shrinkage is an indicator of the extent of a chemical reaction, and is proportional to the degree of hydration [72].

As chemical shrinkage has no external effect, it can only be measured indirectly. M. Bouasker et al. summarized the three principal measurement methods of chemical shrinkage based on Le Chatelier’s contraction [76], which was first listed by Justnes et al.[84]. The three principal measurement methods are Gravimetry, Thermostated bath, and Pycnometry, and are depicted in **Figure 1-6 [76]**. Gravimetry is the most common method, which is used in the ASTM C1608

standard for the chemical shrinkage measuring of cement. M. Bouasker et al. reported the equivalence of the results got from dilatometry and gravimetry was proved by Garcia-Boivin theoretically and experimentally in 1999 [76].

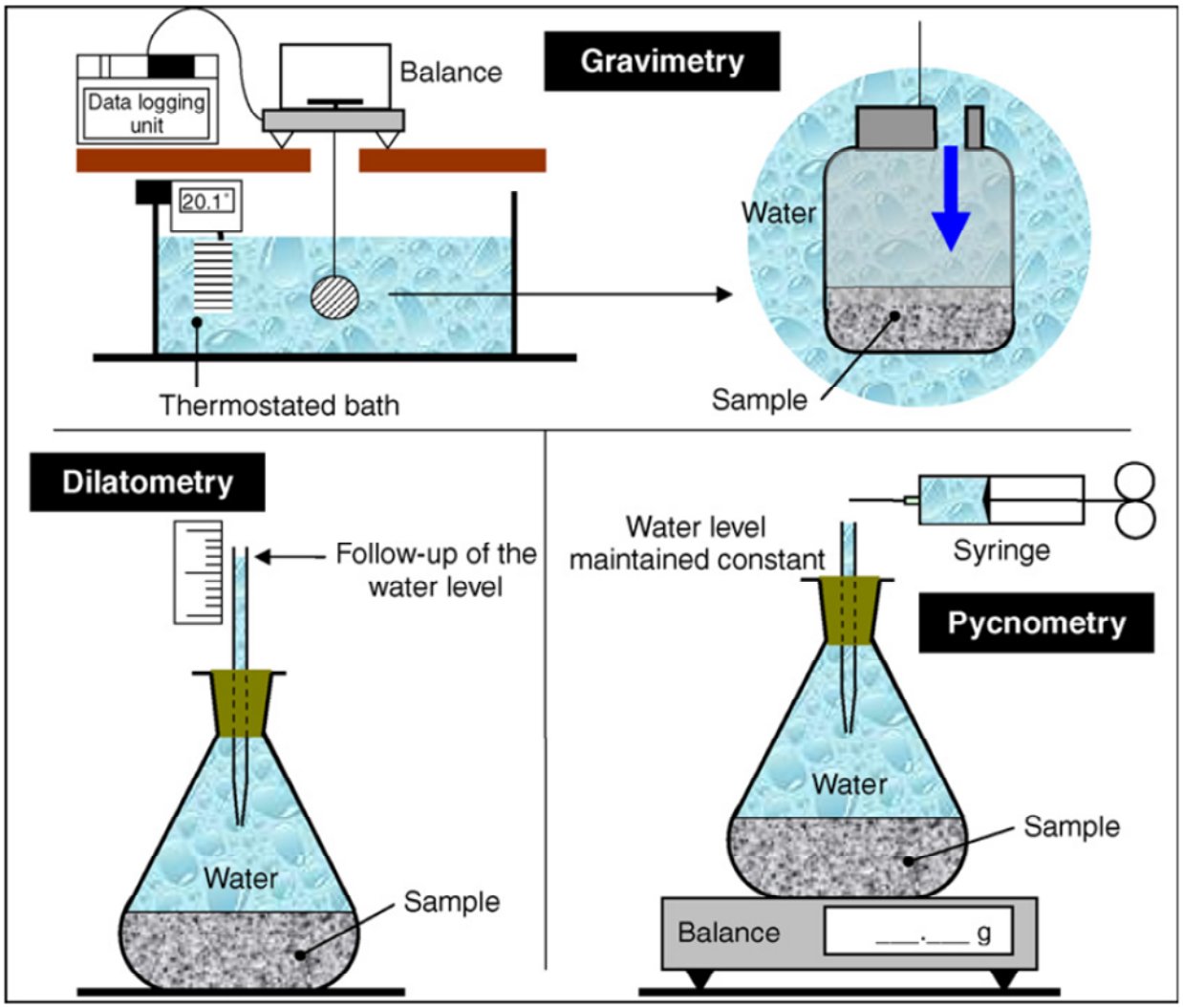

Figure 1-6 Three principal measurement methods of chemical shrinkage based on Le Chatelier's contraction: Gravimetry, Dilatometry, and Pycnometry [66].

In recent years, the chemical shrinkage of slag-based geopolymer system has been studied by many researchers. Due to the instability of the slag-based geopolymer system, chemical

shrinkage was affected by a series of factors, such as chemical composition of the raw material, solution type, pH value, and so on. The most studied system is alkali-activated fly ash-slag.

N.K. Lee et al. [82] used the ASTM method which is dilatometry method shown in **Figure 1-6**. This method is conducted by placing a capillary tube filled with water above a thin specimen [85]. Depercolation of the capillary porosity, which may occur as cement hydrates, is a concern during this test as it will make transport of water to the pores more difficult [86]. Over time, as porosity is created, external water will enter the pores and the level in the capillary tube will decrease, showing the internal volumetric change. The calculation equations (which are the same with the ones described in ASTM C1608[85] are shown below:

$$M_{cement} = \frac{M_{vial+paste} - M_{vialempty}}{(1.0+\frac{w}{c})} \quad (1\text{-}3)$$

$$cs(t) = \frac{[h(t) - h(60\ min)]}{M_{cement}} \quad (1\text{-}4)$$

Where M_{cement}= the mass of cement in the vial (g);

$M_{vial+paste}$=the mass of the glass vial with the added cement paste (g);

$M_{vialempty}$= the mass of empty vial (g);

w/c = water to cement ratio;

$cs(t)$= the chemical shrinkage at time t (mL/g);

$h(t)$=the water level in the capillary tube at time t [87]

Hojati et al. [72] studied the effects of fly ash/slag ratio and activating solution on the chemical shrinkage and mechanical properties of alkali activated fly ash-slag samples. Hojati et al. modified the ASTM measuring procedure by using gravimetry method and by replacing the solution on top of the paste from water to reaction solution. The device was drawn in **Figure 1-7** based on the description in this dissertation. In this paper, samples activated by solution with lower

pH value have shorter initial and final setting time. For a given activating solution, the more amount of slag, the shorter setting time the sample has. The chemical shrinkage was obtained at 10 days. Hojati et al. indicated that the difference in chemical shrinkage is due to the variations of the products formed. For a given activating solution, raw material with smaller amount of slag results in more less C-A-S-H gels, but more N-A-S-H gels, which has lower molar volume. Therefore, a system with more N-A-S-H gel will have larger chemical shrinkage. For a given amount of slag, the use of activating solution with large pH value results in a larger reaction extent, then definitely larger chemical shrinkage.

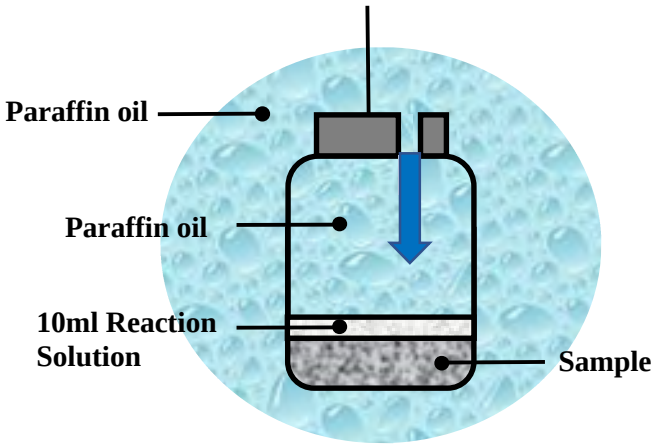

Figure 1-7 Modified device based on ASTM measuring method used in Hojati's paper. (This device is drawn only based on the description by the author)

The equation used for this method is shown below:

$$V_{cs} = \frac{\Delta V_{paste}}{g_{fly\ ash+slag}} = \frac{W_{sub}(t) - W_{sub}(30)}{\rho_{oil} \times g_{fly\ ash+slag}} \qquad (1\text{-}5)$$

Where V_{cs}= the chemical shrinkage (ml/g);

ΔV_{paste}=the volume change of the paste [87];

$g_{fly\ ash+slag}$= the mass of cementitious material content in the AAFS paste sample (g);

$W_{sub}(30)$ = the mass of the sample 30 minutes after the first contact between the cementitious material and the activating solution (a reference point) (g);

$W_{sub}(t)$= the recorded submerged mass of the sample at time t (g); and

ρ_{oil}= the density of the paraffin oil (0.863 g/ml at 23°C).

N.K. Lee et al. stated that compressive strength is increasing with the increasing amount of slag, which is consistent with the findings of M. Hojati's study. However, N.K. Lee et al. stated that more slag results in larger chemical shrinkage, which is opposite with M. Hojati's observations. But this paper only observed the chemical shrinkage for 2 days, while M. Hojati's observation period was10 days. The trend might change in the following days.

As an emerging cementitious material, pure geopolymers (mainly N-A-S-H gel)' volume change behavior during geopolymerization process is much less clear or well understood, for the following reasons: i. There lacks a well-accepted laboratory testing procedure for measuring chemical volume change of geopolymers, particularly the selection of appropriate filling solution and the required monitoring time period; ii. Very limited research studies have been performed on the chemical volume change of geopolymers; and iii. Underlying chemical processes and its concomitant volume change during geopolymerization is far from well understood. Due to different chemical reactions of geopolymer synthesis (geopolymerization instead of hydration for OPC) and thus potential intervention of using deionized water as the filling solutions on geopolymerization, the standard dilatometry method for measuring chemical shrinkage of OPC might not be directly applicable to geopolymers.

Most of the previous studies focused on autogenous shrinkage or dying shrinkage of the blended geopolymer-related systems. Therefore, very limited data are available regarding the

chemical volume change of geopolymer-related systems, even fewer for N-A-S-H geopolymer systems (i.e., the geopolymers without appreciable amount of Ca). Hojati et al. [88] investigated the shrinkage behavior of alkali-activated fly ash-slag binder system, indicating that the binders activated at high pH values experienced larger chemical shrinkage, but lower autogenous and drying shrinkage. Chemical, autogenous, and drying shrinkage of the similar system were determined by Lee et al. [89]. It was reported that higher sodium silicate and slag contents in the mixture caused more shrinkage but resulted in a higher compressive strength. There is no consensus about which filling solution is suitable for quantifying chemical volume change of geopolymer, nor systematic study on the influence of filling solution on geopolymerization and thus the accuracy of measured volume change. In addition, inconsistent chemical volume change has been reported in the literature. Hojati et al. [88] and Lee et al. [89] used activator solution to test the chemical volume change of alkali-activated fly ash-slag system; Sakulich et al. [90] utilized distilled water to investigate the chemical volume change of alkali-activated slag system; and Cartwright [91] used a NaOH solution with an equivalent pH of the activator solution as the filling solution to characterize the chemical volume change of alkali-activated slag system. The chemical volume change of metakaolin-based geopolymer (MKG) was first investigated by Li et al. [92], largely following the chemical shrinkage testing procedure developed for OPC but using the activator solution (i.e., a mixture of sodium hydroxide solution and sodium silicate solution) as the filling solution. Unlike OPC, the chemical deformation of MKGs does not show monotonic chemical shrinkage but exhibits three stages of different chemical deformation: chemical shrinkage, chemical expansion, and chemical shrinkage, during 14-day monitoring time. They further linked different volume change stages with geopolymerization processes as follows: the first chemical shrinkage stage was attributed to the dissolution of metakaolin, the chemical

expansion stage was due to the formation of Al-rich geopolymer gel, and the formation of Si-rich geopolymer network gel attributed to the second chemical shrinkage. Lolli et al. [93] also studied on the volume change behavior of MKGs based on the testing procedure for chemical shrinkage of OPC but using paraffin oil as the filling solution. Lolli et al. [93] reported that the geopolymers undergo early-stage chemical expansion instead of shrinkage.

Despite recent progress made in testing procedure and understanding of chemical volume change of geopolymer, the volume change behavior (shrinkage or expansion) of geopolymer systems and its dependence on the synthesis factors remain poorly understood. In addition, potential intervention of filling solutions (e.g., deionized water or activator solution) on the geopolymerization and the resulting geopolymer gel has not been systematically investigated, which is the main barrier for establishing a well-accepted laboratory testing procedure.

1.1.5.2 Autogenous Shrinkage

Autogenous shrinkage is a macroscopic reduction in length under constant temperature and without any moisture migration to or from the concrete [49, 66, 72-75, 79-82, 94-104]. Like chemical shrinkage, autogenous shrinkage occurs without water leaving the system; however, autogenous shrinkage is “external” and decreases the overall volume of the system. Porosity and voids present in the binder initially contain a large amount of solution. As hydration reactions continue, the internal humidity of the systems drops and pore solution begins to migrate into the binder, where it is consumed in further hydration reactions. This cycle leads to a continuous decrease in the amount of solution present in pores generally referred to as “self desiccation.” At some point, menisci form in pore solution due to surface tension, which creates stresses that attempt to pull the walls of the pore towards each other. This causes a macroscale decrease in the

volume of the system that can be measured with length comparators, strain gauges, etc. and may take the form of distributed microcracking or visible through-cracks that severely degrade the mechanical properties of a structure [105]. When proper curing techniques are used, externally supplied water replaces water consumed during hydration reactions, pores remain filled with fluid longer, and the stresses that cause autogenous shrinkage are reduced. On the other hand, more water may mean a higher degree of reaction in the system, thus more chemical shrinkage and a greater degree of porosity.

The relationship between chemical and autogenous shrinkage is not simple [106]. Tazawa et al. [73] note the case of expansive cements, where an overall increase in volume (i.e. negative autogenous shrinkage, more simply called autogenous expansion) is observed due to the production of ettringite or portlandite. However, chemical shrinkage still occurs in expansive cements when phases such as C-S-H undergo hydration, therefore chemical shrinkage and autogenous shrinkage cannot necessarily be easily related. Chemical shrinkage is, however, relatable to the degree of hydration, which can be inferred from non-evaporable water content and a variety of other physio-chemical methods.

1.1.5.3 Drying Shrinkage

When a cementitious body is placed, it will try to reach equilibrium with its environment not just in temperature, but also in internal humidity. When placed in a low-humidity environment, water will leave the body, enter the environment, and the body will shrink. This is referred to as drying shrinkage [49, 50, 66, 67, 72, 80-82, 94, 96-99, 102, 103, 107-125].

The mechanism behind this is similar to that involved with autogenous shrinkage: pores will empty, starting with the largest first, menisci will be created, and these menisci will create

forces that pull the pore walls together, resulting in a measurable shrinkage [71]. One considerable difference is location: whereas autogenous shrinkage will take place anywhere in the sample where hydration reactions are consuming pore solution, drying shrinkage is mainly confined to surfaces exposed to the environment. The shape of a body has little effect (generally speaking) on autogenous shrinkage, however, a body with a greater surface (e.g., a T-shaped beam) will have a higher degree of drying shrinkage than a body with a lower surface area (e.g., a box-shaped beam). Many building codes account for the effect of geometry on drying shrinkage with provisions calling for ‘theoretical’ or ‘hypothetical’ thickness calculations.

There is no one experiment in which drying and autogenous shrinkages can easily be separated. Whereas drying shrinkage can easily be prevented simply by sealing the specimen off from the surrounding environment, allowing autogenous shrinkage to be measured independently, there is no such a way to mitigate autogenous shrinkage without affecting drying shrinkage. Therefore, total shrinkage and autogenous shrinkage are usually measured, with the former subtracted from the latter. Alternatively, mass loss during drying can be measured to determine the amount of water that has evaporated, which can indicate the degree of drying shrinkage.

1.1.6 Freeze-thaw Durability of Geopolymers

Although mechanical properties of geopolymers synthesized from the mixture of red mud and FFA have been confirmed in the laboratory by a number of researchers [47, 126-130], their durability under different conditions needs to be investigated before it can be used in civil engineering applications. Generally speaking, geopolymers are usually more durable compared to conventional Portland cement concrete. However, the durability of specific geopolymer is not always ensured for the following reasons: 1. For geopolymers synthesized from industrial wastes, their variable

chemical compositions might have negative effect on their durability; and 2. different synthesis conditions (e.g., chemical composition of raw materials and curing conditions) can result in different mechanical properties and durability of the resulting geopolymers. The durability of red mud-fly ash based geopolymer in sulfuric acid and deionized water was studied by the authors' group [131], which confirmed that red mud-FFA based geopolymer has a good resistance to sulfuric acid and deionized water and is comparable to OPC. However, its F-T resistance has not been systematically investigated. F-T often causes damages to concrete structures in cold areas and undermines their long-term performance [132]. When the critically saturated concrete is subjected to temperature fluctuating above and below freezing, the freezing front continuously sucks water from the adjacent region and makes the ice lens getting bigger and bigger, which results in repeated loss of concrete surface and deterioration of its mechanical properties [133]. Good F-T resistance of various geopolymers was confirmed by few laboratory studies [132, 134-139]. Sun and Wu [134] and Li et al. [138] investigated the F-T durability of fly ash-based geopolymer mortar and geopolymer paste. Compared to OPC, both of the geopolymer paste and geopolymer mortar have good F-T resistance, in light of the small deterioration in their mechanical strength in the range of 5% to 20% relative to their respective initial strength after subjected to 15 and 300 F-T conditioning cycles, respectively. F-T resistance of fluidized bed combustion bottom ash-based geopolymers and coal bottom ash-based geopolymers were investigated by Slavik et al. [135] and Topcu et al. [136], respectively. Almost all of the samples were reported to have good F-T resistance after subjected to 50 and 100 F-T conditioning cycles, respectively, with less than 20% reduction in compressive strength compared to the unconditioned specimens. A similar study conducted by Topcu et al. in 2014 [137] indicates that coal bottom ash-based geopolymer lost only 6.77% of its initial strength after 30 F-T cycles. Zhang et al. [140] reported that the PVA short

fiber reinforced metakaolin and fly ash-based geopolymer mortar composites have excellent F-T resistance, based on their high remaining impact resistance after subjected to 20 F-T cycles. In most of the above studies, F-T durability is inferred from the changes in mechanical properties of geopolymer specimens before and after F-T conditioning cycles. However, the changes in microstructure, chemical bonding, and pore characteristics of geopolymers during F-T conditioning processes have not been systematically examined, neither are the fundamental processes underlying the deterioration of mechanical properties of geopolymer samples during the conditioning. In addition, the effects of synthesis factors (e.g., curing conditions, Si/Al and Na/Al molar ratios, water content, and pH values) on F-T durability of geopolymers have not been studied.

1.2 RESEARCH MOTIVATIONS AND OBJECTIVES

The main goal of this study is to develop a holistic framework of synthesis and characterization of waste-based geopolymers for civil engineering applications. The technological impact of this project is the development of next generation, “green” cementitious binder for sustainable civil engineering. For the scientific impact, three main motivations are developed for: (i) helping fill the knowledge gap in the understanding of the chemical composition - mechanical properties - durability behavior relationship of waste-based geopolymer through an integrated multiscale experimental approach; (ii) using red mud slurry instead of processed red mud powder, mixed with fly ash to synthesize geopolymers and examine their durability; and (iii) exploring the volume change behavior and freeze-thaw resistance of RMSFFA geopolymers.

To achieve the above goal, three hierarchically structured objectives are proposed as follows:

(i) To synthesize RMSFFA geopolymers, and to obtain the mechanical properties of RMSFFA geopolymers.

(ii) To explore the testing procedure for the chemical volume change behavior of geopolymers and investigate the chemical volume change behavior of different geopolymer systems.

(iii) To investigate the freeze-thaw resistance property of RMSFFA geopolymers.

1.3 OUTLINE OF DISSERTATION

This dissertation consists of five chapters. A comprehensive literature review on geopolymers was presented in Chapter 1, with the focus on geopolymer synthesis, microstructural characterization, volume change behavior, and durability properties. The influence of curing condition (e.g., temperature and curing time) and chemical composition (e.g., Si/Al molar ratio and Na/Al molar ratio) on the mechanical strength and microstructures (e.g., micromorphology, mineralogy and porosity) of the resulting geopolymers, as well as the reaction kinetics that have been largely investigated with mechanical tests, XRD, SEM-EDX, FTIR, BET and ICC was reviewed. The raw materials used for the geopolymer synthesis in this dissertation, including metakaolin, red mud slurry and class F fly ash, were also introduced.

Chapters 2, 3, and 4 are devoted to synthesis and characterization of the geopolymers from two abundant industrial materials: red mud slurry and Class F fly ash. RMSFFA geopolymers were successfully synthesized and the mechanical properties are investigated and represented in Chapter 2.

In Chapter 3, two different aspects are evaluated: (i) to examine whether the existing volume change testing procedure of OPC is suitable for quantifying the volume change of geopolymers by using metakaolin as the raw material, and (ii) to characterize the volume change of the more complicated geopolymer system - RMSFFA geopolymers. A comprehensive experimental study was performed to investigate the influence of different filling solutions (i.e., deionized water-DIW and activator solution-AS) on the chemical volume change of metakaolin-based geopolymer (MKG). SEM-EDX, ICC, FTIR, BET, ICP-MS techniques were used to shed light on the influence of filling solutions on the geopolymerization process and thus the chemical volume behavior of MKG. The chemical volume change behavior of RMSFFA geopolymers was also investigated, which had the overall expansion chemical volume behavior.

In Chapter 4, freeze-thaw (F-T) durability of geopolymers synthesized from the mixture of red mud slurry-Class F fly ash (RMSFFA) was investigated, with an emphasis on the influence of chemical compositions and curing conditions (i.e., curing time and curing temperature). F-T durability was evaluated on the basis of the sustained mechanical strength of RMSFFA geopolymer specimens after subjected to 50F-T conditioning cycles. The change in their chemical bonding, mineralogy, and pore characteristics at various F-T conditioning cycles was examined with Fourier transform infrared spectroscopy, X-ray diffractometer, and Brunauer-Emmett-Teller testing, respectively, to reveal the underlying processes during F-T conditioning.

Chapter 5 summarizes the major findings from this research study and establishes the processing-composition-microstructure-property relationships by evaluating the relationships between the composition (e.g., Si/Al ratios, Na/Si ratios, curing time), microstructure (e.g., porosity), and engineering properties (e.g., strength, Young’s modulus, failure strain, durability) of the geopolymers. These correlations not only provide a comprehensive understanding of the

processing and engineering properties of the geopolymers but can also be used to develop a readily applicable design chart for tailoring desired geopolymer composites for specific applications where different strength or failure strains are required. This chapter also provides some recommendations for future studies.

CHAPTER II – RELATIONSHIP AMONG SYNTHESIS FACTORS-MICROSTRUCTURE-MECHANICAL PROPERTIES OF RED MUD SLURRY - CLASS F FLY ASH-BASED GEOPOLYMERS (RMSFFA)

2.1. INTRODUCTION

Geopolymer, a family of aluminosilicate materials, has been successfully synthesized from various raw materials rich in silicates and/or aluminates. Synthesized geopolymers are of the composite nature and constituted of geopolymer gel, crystals, unreacted impurities, and unreactive fillers, where geopolymer gel has amorphous to semi-crystalline structures[6, 141]. As a sustainable alternative to OPC, geopolymers need to achieve mechanical properties comparable to those of OPC. However, the mechanical properties of geopolymer are significantly affected by its synthesis factors, including chemical composition (e.g., Si/Al and Na/Al ratios) of the raw materials and curing conditions (e.g., curing temperature, humidity and curing time). To fully understand reaction processes and the strength development mechanisms of geopolymer, it is imperative to investigate the formation of geopolymer gel that is largely responsible for gaining strength of this material. In geopolymer gel, silicate and aluminate tetrahedrons are linked by sharing oxygen atoms, with alkaline cations balancing the negative charge of $Al(OH)_4^-$. The structure of geopolymer gel can be simplified as the following chemical formula [6, 141]:

$$M_n\{-(SiO_2)_z - AlO_2 -\}_n$$

Where M is an alkali cation such as potassium (K^+) or sodium (Na^+) that is used for balancing negatives charge of $Al(OH)_4^{-1}$, n is the polycondensation degree; and z is the Si/Al ratio with the value range of 1 to 300. It should be noted that geopolymer shows different mechanical properties with different values of z. Three dimensional and cross-linked molecular structures form when $z<3$, which results in stiff and brittle geopolymer; and two dimensional and linearly linked structures are resulted, giving the synthesized geopolymer adhesive and rubbery properties when z value is larger than 3. Geopolymer gel forms via the geopolymerization that is often simplified into three steps in a conceptual model: (i) the raw materials are dissolved in alkali hydroxide and/or alkali silicate solutions to release reactive Si and Al monomers; (ii) the reactive Si and Al monomers polymerized to form the oligomers in different sizes; and [142] the oligomers further polycondense and form three dimensional aluminosilicate molecules, so called geopolymer gel [143, 144]. These three stages are interactive with each other, and water is extracted in the last two stages.

In general, geopolymers can be synthesized from a wide range of aluminosilicate rich raw materials, such as red mud [32, 141], fly ash [145-147], granulated blast furnace slag[148, 149], rice husk ask [32, 150], natural aluminosilicate minerals, metakaolin [151-153] and the mix of these materials [126, 154]. In this study, red mud slurry (denoted as RMS) and Class F fly ash were chosen to synthesize geopolymers. RMS is the major waste produced in the industrial production of alumina from Bayer process [32-36]. About 1.5-1.6 tons of RMS generated from every ton of alumina produced [37]. The annual production of RMS is estimated about 200 million tons worldwide [34, 35], with an increase of 120 million tons annually and a global inventory of 2.6 billion tons by 2011 [36, 38]. Due to the different bauxite ore sources and refining processes, RMS has different physical, chemical, mineralogical properties with a pH value of ~10-13 [32, 35,

39, 40]. The main compositions of RMS are iron oxide and alumina-silicate oxides. The enormous quantity, high alkalinity, and chemical compositions make RMS (1) occupy large areas of valuable land; (2) be harmful to the environment (especially soil and ground water) and public health [155]; (3) impose serious disposal problems and challenges in the mining industry [33]. In the past, fresh RMS is either transported to waste lakes, following by dewatering, or dried and utilized towards bricks making [156, 157], glass ceramics [158, 159], etc. However, these methods are not sustainable and only consume a small amount of RMS. In recent years, many researchers focus on developing new ways to recycle or reuse RMS at larger scale, one of which is geopolymer synthesis or geopolymerization in civil engineering applications [36]. The high alkalinity and the presence of aluminosilicates make RMS a potential raw material in geopolymerization process. Its high alkalinity can partially replace the alkali reaction solution in geopolymer synthesis, which can reduce the cost of synthesized geopolymer. However, based on previous studies [36, 42], the activity of RMS in geopolymerization is poor or limited. To achieve a better mechanical property of geopolymer, another raw material with higher reactivity in geopolymerization must be added in this study.

Class F Fly ash (denoted as FFA), also known as "coal ash", is a coal combustion product with calcium content less than 20%. Fly ash is generally rich in silicates and aluminates, which can supply enough SiO_2 and AlO_4 required for geopolymerization. Most of the aluminum plants which generate RMS waste also generate fly ash from their captive power plants, which make the two raw materials a good combination for geopolymer synthesis due to the low transportation cost of waste materials [46].

Red mud and fly ash-based geopolymer has been synthesized by other researchers [41, 47], but it still needs to take extra efforts to dry and grind red mud slurry to red mud powder prior to

the synthesis. Therefore, it is worth exploring the feasibility of synthesizing geopolymer with the mixture of fly ash and RMS without any pre-treatment of the latter to save more time and cost. This chapter aims to investigate the influence of synthesis factors (e.g., Si/Al molar ratio, Na/Al molar ratio, curing temperature, and curing time) on mechanical and microstructure properties of RMSFFA geopolymers.

2.2. MATERIALS AND METHODOLOGY

2.2.1 Materials

RMS was used as received from Alcoa World Alumina LLC in geopolymer synthesis. FFA was provided by Headwaters Resources Inc. The physical properties and chemical compositions of RMS and FFA are shown in **Table 2-1** and **Table 2-2**, respectively. The pH value and water content of RMS are ~14 and 74%, respectively. RMS also contains traceable amount of soluble Na, Si, and Al. The main components of FFA are SiO_2 and Al_2O_3, whose amorphous phases are the main reactive constituents in geopolymerization. FFA also contains an appreciable amount of Fe_2O_3 and some trace elements (e.g., K, Na, Mg, and S). In addition, the median particle size (D_{50}) of FFA is 16 μm. A mixture of 50% NaOH and sodium silicate solution was used as the alkaline activator to activate the mixture of FFA and RMS.

Table 2-1 Chemical compositions of Class F fly ash (wt.%) provided by the supplier.

SiO_2	Al_2O_3	Fe_2O_3	SO_3	CaO	K_2O	MgO	Na_2O	Moisture	Loss on ignition
59.74	27.51	4.91	0.16	1.45	2.39	1.18	0.82	0.08	2.66

Table 2-2 Physical and chemical compositions of RMS (wt.%).

Liquid contents	Solid contents	Soluble Na	Soluble Si	Soluble Al
74	26	1.97	0.00555	0.74

2.2.2 Geopolymer Synthesis

While it is desirable to use RMS at a maximum amount to partially replace expensive alkaline solution, too much RMS results in lower strength of the geopolymer sample due to RMS's poor reactivity [155]. In light of the consideration, the mixture of RMS and FFA at a mass ratio of 1:4 was used as the source materials for geopolymer synthesis. Chemical compositions of the source materials have proven to be critical for synthesizing geopolymer with high mechanical strength. Nominal Si/Al molar ratio (1.8, 1.9, and 2.0) and nominal Na/Al molar ratio (0.6, 0.7, and 1.0) were used to prepare RMSFFA geopolymer samples to examine the effect of chemical compositions on the mechanical properties of RMSFFA. Based on the previous studies in the literature and by the authors' group [47, 131], a nominal Si/Al molar ratio of 2.0 and a Na/Al molar ratio of 0.6 were adopted to prepare RMSFFA geopolymer samples to examine the effect of curing temperature on the mechanical properties of RMSFFA geopolymers. In addition, it was found that excessive amount of water present in geopolymer precursor leads to the residual water existing in the form of hydroxyl in the resulting geopolymer [160], which is unfavorable to strength development of geopolymers. Accordingly, a water content of 25% was used in the geopolymer synthesis, which was the lowest possible water content while adequate workability was maintained for sample preparation. The chemical compositions of geopolymer precursor were controlled by adjusting relative proportions of the source materials (e.g., RMS and FFA) and the alkaline

activator solution. Besides the above synthesis factors, the influence of curing conditions, including curing time periods (14 and 28 days) and curing temperature (room temperature, 50^{o}C, and 80^{o}C), on mechanical properties and strength development of RMSFFA geopolymers was also examined. The sample ID, mix design, and curing conditions of RMSFFA geopolymer specimens are listed in **Table 2-3**. The sample set ID was named as follows: raw materials - Si/Al (SA) mole ratio - Na/Al (NA) mole ratio - curing temperature - curing time; RT, 50C, and 80C stand for curing temperatures of room temperature, 50°C, and 80°C, respectively; and 14D and 28D stand for 14 days or 28 days curing time periods.

The alkaline activator solution was pre-prepared and then cooled down to room temperature for later use. RMS and FFA were firstly mixed at the pre-determined ratio with a mechanical mixer, followed with the addition of the alkaline activator solution, and the whole precursor was stirred for 30 minutes to ensure thorough mixing. The slurry was poured into pre-made cylindrical molds with dimensions of 2 inch (diameter) x 4 inch (height), and vibrated for 10 minutes to remove the air bubbles. All the samples were sealed in plastic bags with duct tape. Samples were placed in a chamber at a relative humidity (RH) of 40% - 50% for curing at room temperature. For the samples cured at elevated temperatures (i.e., 50°C and 80°C), they were placed in the oven and taken out after 7 days and 1 day for 50°C and 80°C, respectively, which were further cured at ambient conditions until respective final curing time was reached. All the samples were demolded after 14-day curing, and then the 14-day cured samples were taken out for mechanical property testing while the 28-day cured ones were continuously cured at ambient temperature for another 14 days. Detailed sample preparation process can be referred to a previous study from the authors' group [47]. OPC samples were also prepared and tested for providing a baseline reference.

Table 2-3 Summary of mix design and curing conditions of RMSFFA geopolymer specimens used for mechanical properties tests.

Sample set ID	Curing time	Curing temp	Si/Al (mol)	Na/Al (mol)	L/S (weight	Water Content
RMSFFA-SA2.0-NA0.6	14/28	50	2	0.6	0.53	~25
RMSFFA-SA2.0-NA0.7			2	0.7	0.57	
RMSFFA-SA2.0-NA1.0			2	1	0.7	
RMSFFA-SA1.8-NA0.7			1.8	0.7	0.5	
RMSFFA-SA1.9-NA0.7			1.9	0.7	0.53	
RMSFFA-SA2.0-NA0.7			2	0.7	0.57	
RMSFFA-SA2.0-NA0.6	14/28	RT (~23) 50 80	2	0.6	0.53	~25

2.2.3 Characterization of Mechanical Properties and Microstructure

Unconfined compressive strength (UCS) tests were conducted on RMSFFA geopolymer samples after curing for 14 or 28 days using an Instron loading machine to determine their UCS, failure strain and Young's modulus. A constant loading rate of 0.5 in./min was used, which was relatively high but was chosen for the main purpose of comparing the relative trend in mechanical properties among the samples. In addition, some small pieces were collected from the crushed samples after the strength test for subsequent characterization of their chemical bonding, mineralogy, and pore characteristics, to shed light on the samples' strength development. The external surface of the samples was avoided since they might have been carbonated after being exposed to the air. Prior

to the characterization tests, the selected sample pieces were pre-frozen by liquid nitrogen right after the strength test and then subjected to freeze-drying in order to prevent the samples from any further geopolymerization reactions. Some of the small pieces were ground to powder for FTIR and BET testing. The chemical bonding information was inferred from the FTIR spectra obtained with a BrukerOptics Vetex70 FTIR spectrometer using transmittance mode in the range of 500~1600 cm^{-1} at a resolution of 2 cm^{-1}. Specific surface area, accumulative pore volume and pore characteristics were tested with the instrument ASiQ IQ TPX from Quantachrome Instruments and analyzed with Non-Local Density Functional Theory (NLDFT) method.

2.3. RESULTS AND DISCUSSION

2.3.1 Mechanical Properties of RMSFFA Geopolymers

The mechanical and physical properties (UCS, failure strain ε_f, Young's modulus E, and bulk density ρ.) of OPC and all the RMSFFA geopolymer samples cured for 14 days and 28 days are shown in **Figures 2-1, 2-2, and 2-3**. The values of OPC are listed in each Figure for reference.

Based on **Figure 2-1(a)**, among the geopolymer samples studied in this study, their UCS values increased with the increasing of Si/Al molar ratio regardless of the curing time. The UCS of sample has a dramatically increase when the Si/Al molar ratio increased from 1.9 to 2.0, which can reach 24 MPa for the sample cured for 14 days. Based on **Figure 2-2(a)**, with the increase of Na/Al molar ratio, the UCS decreased with the samples cured for 28 days. For 14-day cured samples, the sample with Na/Al molar ratio of 0.7 has the highest UCS. In general, 28-day cured RMSFFA geopolymer samples achieved higher UCS values than their 14-day counterparts, except

SA2.0-NA0.7. This might have been caused by the formation of cracks during further curing after 14 days.

Based on **Figure 2-3(a)**, the UCS of the samples cured at higher temperatures is higher than the ones cured at room temperature. However, the geopolymer samples cured at 80°C show slightly lower mechanical strength than those cured at 50°C, and strength reduction in geopolymers cured at the temperature higher than 80°C was also reported in the previous studies [147, 161]. This might be caused by more cracks developed at higher temperatures (e.g., 80°C). Higher curing temperature facilitated geopolymerization (faster and higher degree of dissolution of the raw materials; faster processes of geopolymer gel formation; higher earlier strength); on the other hand, elevated curing temperature (>=80°C) often cause more thermal cracking during curing that offset the benefits of high curing temperature.

A similar trend in the Young's modulus of geopolymer samples to that of UCS is shown in (**Figure 2.1(c), Figure 2.2(c), and Figure 2.3(c)**). Geopolymers have a relatively lower Young's modulus compared to OPC. The failure strain, and bulk density of geopolymers with different synthesis factors (e.g., Si/Al molar ratio, Na/Al molar ratio, and curing temperature) are shown in **Figure 2.1(b)(d), Figure 2.2(b)(d), and Figure 2.3(b)(d)**, respectively. Most of the geopolymer samples have either comparable or larger failure strain, especially those with higher UCS values than OPC samples, which means better ductility and more favorable engineering performance. With the increase of Si/Al molar ratios, the failure strain and bulk density increases; however, there is no obvious trend on the changes of Na/Al molar ratio and curing temperature.

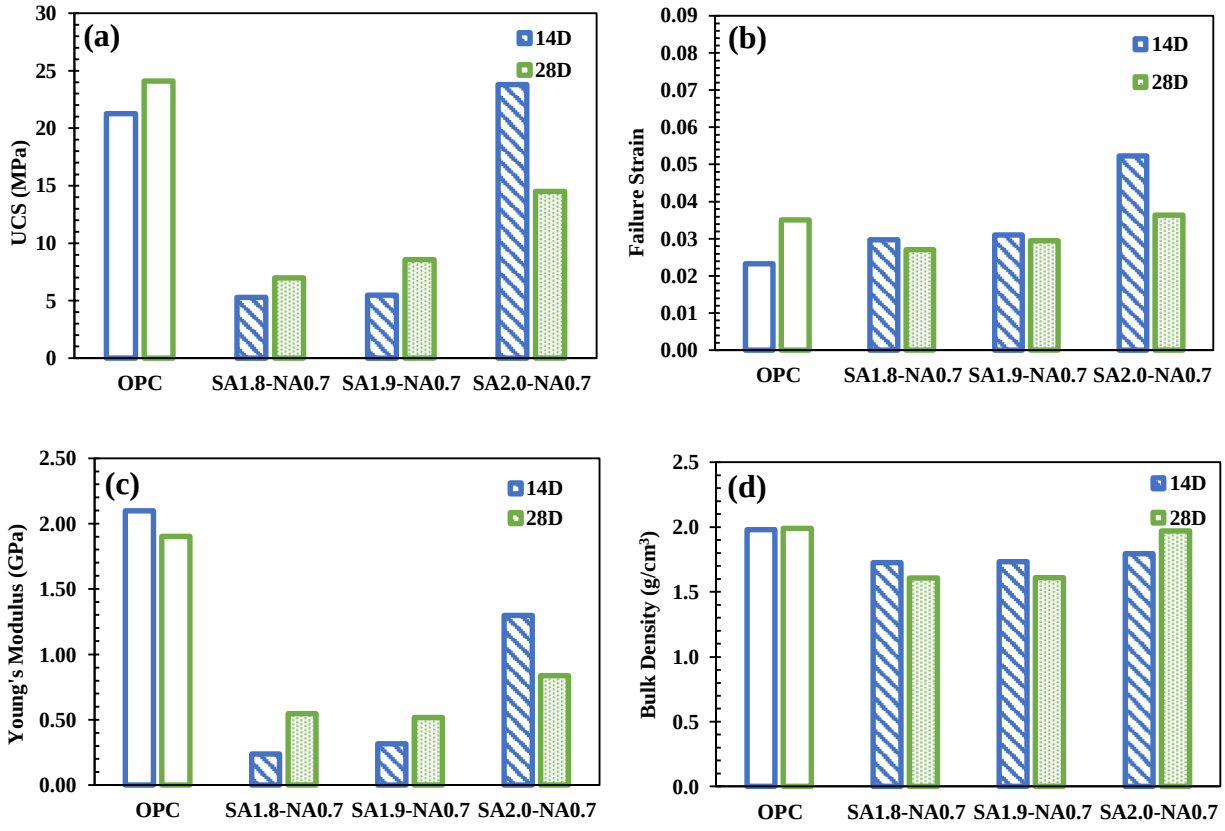

Figure 2-1 Mechanical properties of OPC and RMSFFA geopolymers with different Si/Al molar ratios cured for 14 and 28 days: (a) UCS; (b) ε_f; (c) E; and (d) ρ.

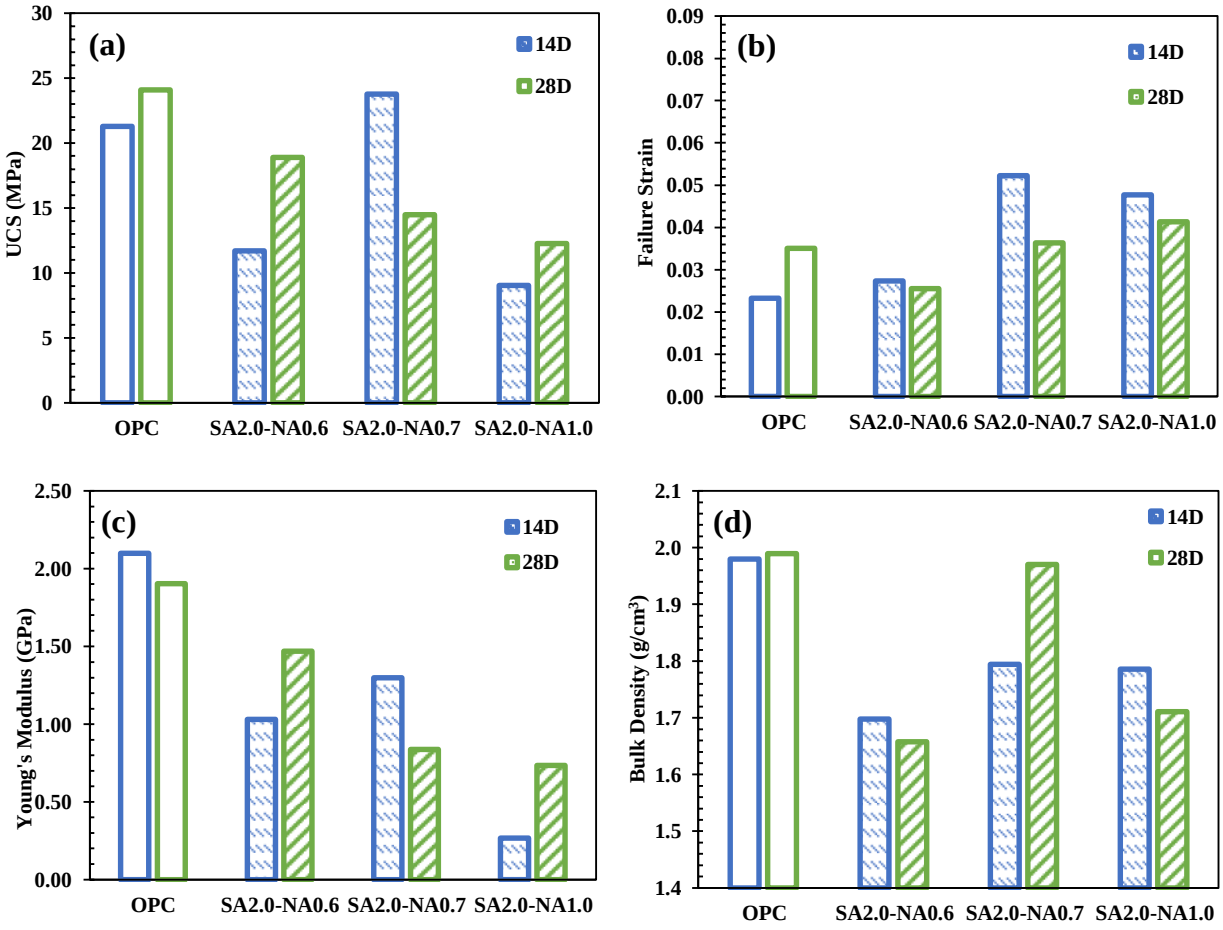

Figure 2-2 Mechanical properties of OPC and RMSFFA geopolymers with different Na/Al molar ratios cured for 14 and 28 days: (a) UCS; (b) ε_f; (c) E; and (d) ρ.

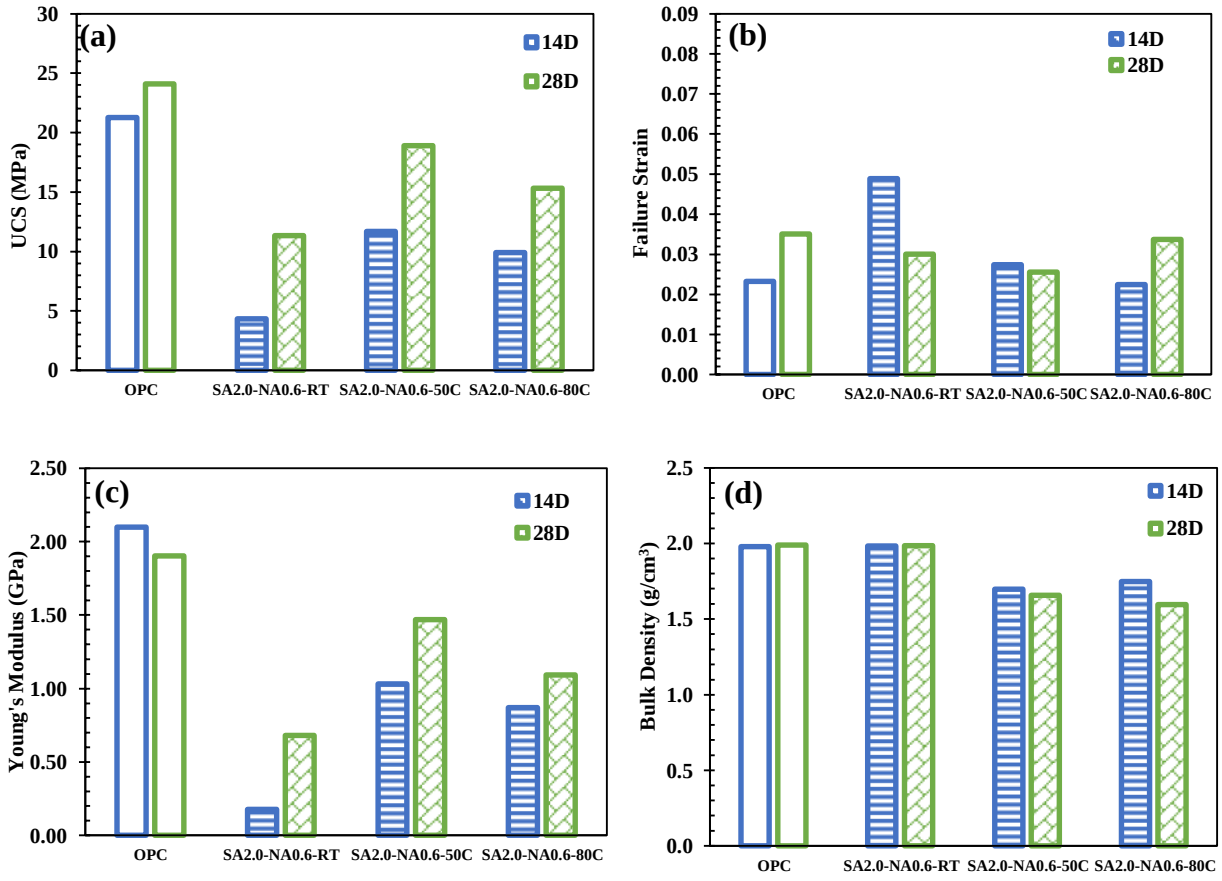

Figure 2-3 Mechanical properties of OPC and RMSFFA geopolymers with different curing temperature cured for 14 and 28 days: (a) UCS; (b) ε_f; (c) E; and (d) ρ.

2.3.2 Microstructural Characterization by FTIR

FTIR spectra of the RMSFFA geopolymer samples were acquired to shed light on the effects of various chemical compositions and curing conditions (curing temperatures and curing time) on the bonding information of RMSFFA geopolymers. **Figures 2-4 (a)** and **(b)** show the variation of FTIR spectra of the samples cured for 14 and 28 days, respectively. The characteristic spectrum of the mixture of raw materials (20% RMS+80%FFA) was also provided as the baseline for better understanding the characteristic bands shift due to geopolymerization processes. As reported by numerous studies in the literature [162-165], the FTIR spectra in the region of 1300-900 cm^{-1} are

often used to characterize geopolymer gels, which represent the Si-O-T (T is Si or Al) asymmetric stretching vibration band, also called the “main band”. The main band of the raw material was centered at 1029.97 cm^{-1}. Then the main band of raw material shifted towards lower wavenumber, which indicates the dissolution of the raw material and the formation of geopolymer gels [164, 166]. The band ~1450 cm^{-1} is assigned to the asymmetric stretching of the O-C-O bonds in CO_3^{2-} formed by the reaction between excessive Na^+ presenting in the geopolymer and the atmospheric CO_2 after the samples were exposed to air [51, 167-169]. The band observed at ~850 cm^{-1} is assigned to the bending vibration of Si-OH [170-172], which does not exist in the raw materials. This band usually appeared in the incompletely formed polymers that can reduce the mechanical properties of the resulting geopolymers, but disappeared upon dehydration [172, 173].

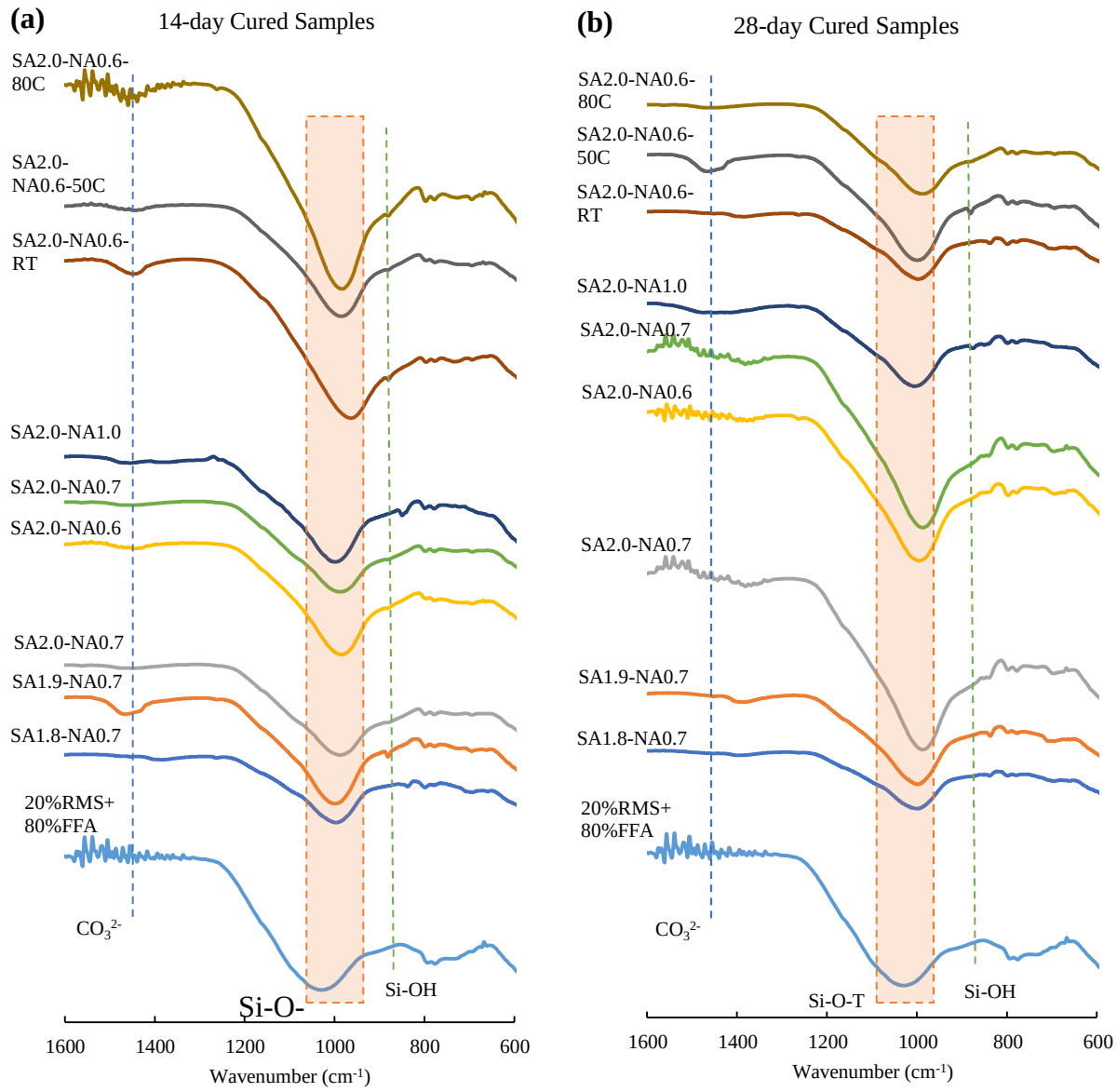

Figure 2-4 Changes in FTIR spectra of 14-day (a) and 28-day (b) cured samples with different chemical compositions and curing conditions (curing temperature and curing time).

2.3.3 Pore Characterization of RMSFFA Geopolymers

The pore size distributions of RMSFFA geopolymers with various Si/Al and Na/Al molar ratios cured for 14 and 28 days are presented in **Figure 2-5**. Due to the unavailability of BET device

when different curing temperatures were studied, the results of different curing temperatures are not available in this section. Based on **Figure 2-5**, the dominant pore size of all the samples is below 15 nm. With the increase of curing time, the dominant pore size slightly shifted to smaller radius regardless of chemical compositions. This is likely due to the higher temperature which facilitates the geopolymerization reaction, thus resulting in smaller pore radius. There is no clear trend of the effects of Si/Al molar ratio on pore size distribution. However, with the increasing of the Na/Al molar ratio, the pore volume increased regardless of the curing time. The total pore volume of all the RMSFFA geopolymers was plotted in **Figure 2-6**. Generally speaking, the total pore volume decreases with the increase of Si/Al molar ratio, and with the decrease of Na/Al molar ratio. This is consistent with the UCS results: lower total pore volume is corresponding to higher UCS. The underlying mechanisms associated with this are: i) more geopolymer gel formed; and ii) denser microstructure; both of which attribute to the strength improvement.

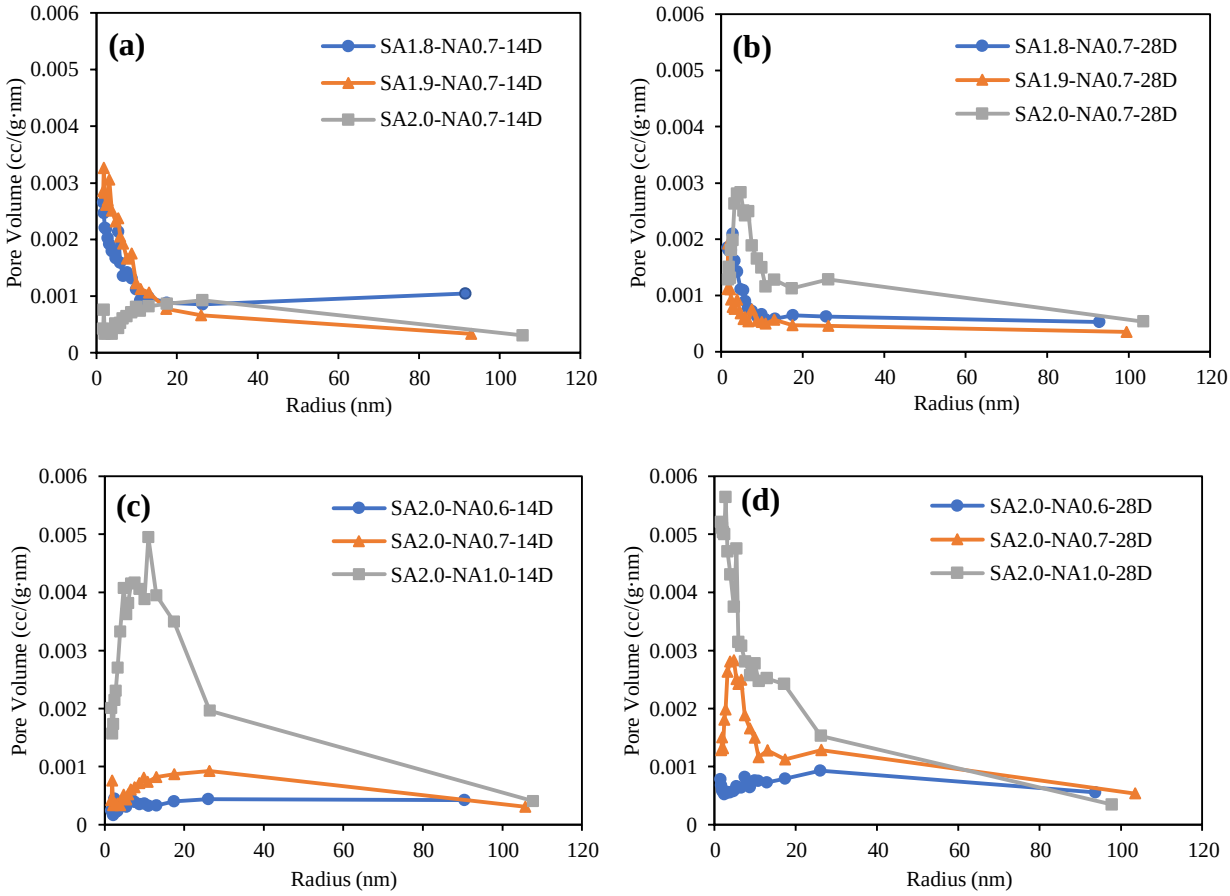

Figure 2-5 Pore size distribution of RMSFFA geopolymers with various Si/Al molar ratios cured for (a)14 days and (b)28 days, and pore size distribution of RMSFFA geopolymers with various Na/Al molar ratios cured for (c)14 days and (d)28 days.

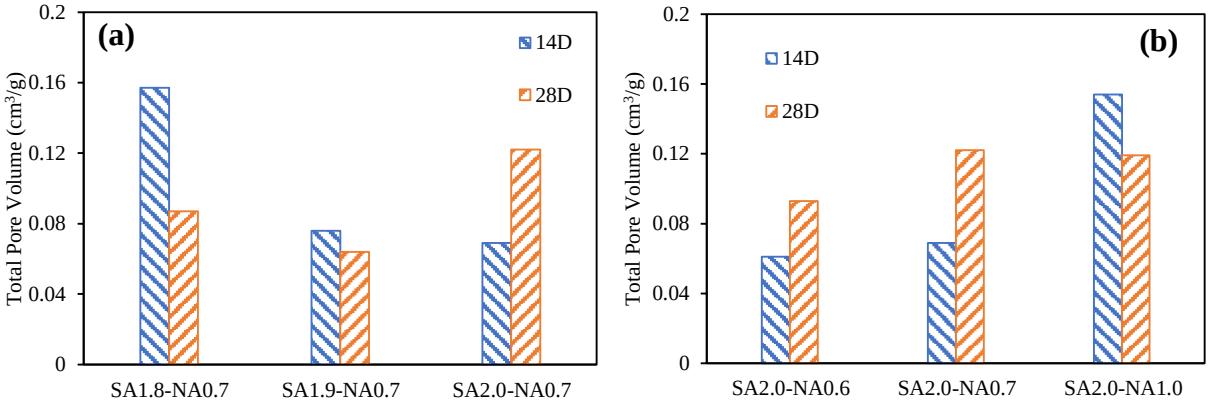

Figure 2-6 Total pore volume of (a) 14-day and 28-day cured RMSFFA geopolymers with various Si/Al molar ratios, and (b) 14-day and 28-day cured RMSFFA geopolymers with various Na/Al molar ratios.

2.4. CONCLUSIONS

In this study, geopolymers were synthesized with the mixture of red mud slurry and Class F fly ash. The effects of chemical molar ratios (Si/Al and Na/Al), curing temperature, and curing time on the mechanical properties, chemical bonding, and porosity of RMSFFA geopolymers were investigated. The following conclusions can be drawn:

- The UCS and Young's modulus of RMSFFA geopolymers increased, with the increase of Si/Al molar ratio and decrease of Na/Al molar ratio within the value ranges of the geopolymer recipes investigated in the current study. The geopolymer gels formation was confirmed by FTIR results.
- Higher curing temperature is more suitable for strength development of RMSFFA geopolymers compared to room temperature. However, elevated curing temperature (>=80^{o}C) might offset the benefit of promoted geopolymerization at high temperature due to more pronounced thermal cracking during curing.

- BET results shows the lower the total pore volume, the higher strength RMSFFA geopolymers, which is consistent with the UCS results and reveals the two mechanisms underlying strength development: cementation by the formation of geopolymer gel and densification by denser and more compact microstructure of geopolymers.

CHAPTER III –VOLUME CHANGE BEHAVIOR OF RED MUD SLURRY AND CLASS F FLY ASH BASED GEOPOLYMERS

3.1 INTRODUCTION

Geopolymers are alkaline-activated aluminosilicates and promising green alternatives to ordinary Portland cement (OPC), for their following advantages: low CO_2 emission during synthesis process [6-8], comparable mechanical strength [9, 10], good resistance to inorganic and organic acid [4, 5], and excellent fire resistance [2, 3]. Geopolymers can be produced by activating aluminosilicate materials with alkaline solutions, such as sodium/potassium silicate, sodium hydroxide, or their mixtures. Common source materials for geopolymer synthesis include natural minerals or industrial wastes that are rich in aluminates or silicates, such as metakaolin [25, 26], red mud [27, 28], fly ash [29, 30], or the mixture of the above [31]. Despite being confirmed as a promising alternative to OPC by numerous laboratory experimental studies [47, 57, 58], geopolymer has not been widely applied in civil engineering mainly because of several main barriers, one of which is the lack of information and knowledge about their long-term performance and volume change behavior during synthesis process. Excessive volume change and the resulting cracking of cementitious materials are often major causes of the deterioration of civil engineering structures, reduced durability, and service life, or even catastrophic failure [59-63].

Chemical volume change of cementitious material is the absolute (or internal) volume change resulting from the volume difference between the formed products and the reactants during the reactions. The change in volume of OPC in sealed environment was firstly observed by Powers in 1935 during a hardening process of a mixture of cement and water [174]. Chemical volume

behavior of OPC during cement hydration process is dominantly reduction in volume (i.e., shrinkage), for which dilatometry method specified in ASTM C 1608 [175] is often used for its simple set-up (see **Figure 3-1(a)**). In the dilatometry method, deionized water is used as the filling solution, and the drop in level of water is regarded as the volume reduction of the hydrated cement [176, 177]. As an emerging cementitious material, geopolymers' volume change behavior during geopolymerization process is much less clear or well understood, for the following reasons: i. there lacks a well-accepted laboratory testing procedure for measuring chemical volume change of geopolymers, particularly the selection of appropriate filling solution and the required monitoring time period; ii. very limited research studies have been performed on the chemical volume change of geopolymers; and iii. underlying chemical processes and their concomitant volume change during geopolymerization is far from well understood. Due to different chemical reactions of geopolymer synthesis (geopolymerization instead of hydration for OPC) and thus potential intervention of using deionized water as the filling solutions on geopolymerization, the standard dilatometry method for measuring chemical shrinkage of OPC might not be directly applicable to geopolymers.

Most of the previous studies focused on autogenous shrinkage or dying shrinkage of the blended geopolymer-related systems. Therefore, very limited data are available regarding the chemical volume change of geopolymer-related systems, even fewer for N-A-S-H geopolymer systems (i.e., the geopolymers without appreciable amount of Ca). Hojati et al. [88] investigated the shrinkage behavior of alkali-activated fly ash-slag binder system, indicating that the binders activated at high pH values experienced larger chemical shrinkage, but lower autogenous and drying shrinkage. Chemical, autogenous, and drying shrinkages of the similar system were determined by Lee et al. [89]. It was reported that higher sodium silicate and slag contents in the

mixture caused more shrinkage but resulted in a higher compressive strength. There is no consensus about which filling solution is suitable for quantifying chemical volume change of geopolymer, nor systematic study on the influence of filling solution on geopolymerization and thus the accuracy of measured volume change. In addition, inconsistent chemical volume changes have been reported in the literature. Hojati et al. [88] and Lee et al. [89] used activator solution to test the chemical volume change of alkali-activated fly ash-slag system; Sakulich et al. [90] utilized distilled water to investigate the chemical volume change of alkali-activated slag system; and Cartwright [91] used a NaOH solution with an equivalent pH of the activator solution as the filling solution to characterize the chemical volume change of alkali-activated slag system. The chemical volume change of metakaolin-based geopolymer (MKG) was first investigated by Li et al. [92], largely following the chemical shrinkage testing procedure developed for OPC but using the activator solution (i.e., a mixture of sodium hydroxide solution and sodium silicate solution) as the filling solution. Unlike OPC, the chemical deformation of MKGs does not show monotonic chemical shrinkage but exhibits three stages of different chemical deformation: chemical shrinkage, chemical expansion, and chemical shrinkage, during 14-day monitoring time. They further linked different volume change stages with geopolymerization processes as follows: the first chemical shrinkage stage was attributed to the dissolution of metakaolin, the chemical expansion stage was due to the formation of Al-rich geopolymer gel, and the formation of Si-rich geopolymer network gel attributed to the second chemical shrinkage. Lolli et al. [93] also studied the volume change behavior of MKGs based on the testing procedure for chemical shrinkage of OPC but using paraffin oil as the filling solution. Lolli et al. [93] reported that the geopolymers undergo early-stage chemical expansion instead of shrinkage.

Despite recent progress made in testing procedure and understanding of chemical volume change of geopolymer, the volume change behavior (shrinkage or expansion) of geopolymer systems and its dependence on the synthesis factors remain poorly understood. In addition, potential intervention of filling solutions (e.g., deionized water or activator solution) on the geopolymerization and the resulting geopolymer gel has not been systematically investigated, which is the main barrier for establishing a well-accepted laboratory testing procedure. To fill in these knowledge gaps, this study aims to examine the influence of filling solutions (deionized water and alkaline activator solution) on chemical volume change of MKGs using the dilatometry method. Ion exchanges, heat flow evolution, chemical under bonding changes, microstructure evolution, and porosity characteristics of MKGs were characterized to shed light on geopolymerization process using different filling solutions. Ion concentrations in filling solutions were obtained by ICP Mass Spectrometer (ICP-MS) to examine the ion exchange between MKGs and filling solutions. The heat release of geopolymer reactions with different filling solutions were monitored by Isothermal Conduction Calorimeter (ICC) to help better understand how the filling solutions might intervene the geopolymerization process. Furthermore, MKG specimens at different curing time were characterized by Scanning Electron Microscopy (SEM), Energy Dispersive X-Ray (EDX), Fourier-transform infrared spectroscopy (FTIR), and the Brunauer-Emmett-Teller method (BET) to examine the changes in their morphology, chemical molar ratios, chemical bonds, and pore volume distribution, respectively. Lastly, the control samples without filling solutions at different curing times were prepared and tested with the same characterization techniques for providing the baseline information.

3.2 VOLUME CHANGE BEHAVIOR OF GEOPOLYMERS

To better understand the volume change behavior of geopolymers, it is very important to verify the feasibility of using the existing chemical shrinkage testing procedure initially developed for cement and to see if any modification to the testing procedure is needed. There are two parts in this section: (i) chemical volume change test procedure development for geopolymer. Metakaolin was used to verify the feasibility of the existing volume change testing procedure of OPC due to the high purity of the raw material; and (ii) using the procedure developed in part (i) to characterize the volume change of the more complicated geopolymer system - RMSFFA geopolymers.

3.2.1 Volume Change Test Procedure Development

3.2.1.1 Materials and Methodology

3.2.1.1.1 Materials

Geopolymer samples were prepared with metakaolin, which was acquired from Advanced Cement Technologies, and its chemical composition is shown in **Table 3-1**. Although MK is not necessarily more cost-effective or greener than other raw materials [49, 50], it is a more preferred raw material for exploratory investigations because MK has high percentages of reactive aluminates and silicates and thus the complexity and uncertainties associated with impurity present in other raw materials (e.g., fly ash) can be limited. Its average particle size, density, and pH value at 20˚C are 3.9 μm, 2.1-2.6 g/cm^3, and 4-8, respectively. A mixture of sodium silicate solution and 50% NaOH was prepared as the alkaline activator for MKG synthesis. Two filling solutions were used in chemical volume change tests: deionized water (DIW) and the same activator solution (AS) that was used to synthesize MKGs.

Table 3-1 Chemical composition of metakaolin used for synthesizing MKG samples.

SiO_2	Al_2O_3	Fe_2O_3	CaO	MgO	Na_2O	K_2O	SO_3	Moisture Content	Loss on Ignition
52.20	43.11	1.53	0.07	0.06	0.07	0.22	0.09	0.33%	0.18%

3.2.1.1.2 Geopolymer Synthesis and Sample Preparation of Chemical Volume Change Test

Nominal Si/Al ratio of 1.68 and nominal Na/Al ratio of 1.0 were used for synthesizing MKGs in this study for: i. achieving high mechanical strength based on the authors' previous studies [178]; and ii. its relative quicker final setting time compared to other recipes tested by the authors' group, which can minimize the potential influences of filling solutions on geopolymerization [179]. The nominal chemical ratios of the MKG precursors were calculated based on the chemical compositions of both metakaolin and the alkali activator solution. The liquid/solid ratio and water content used for synthesizing geopolymer were 1.72 and 40%, respectively. The activator solution was premixed, cooled down to ambient temperature, and then added to the pre-weighed metakaolin. The whole precursor was thoroughly mixed for 30 minutes at ambient conditions (around 23˚C and atmospheric pressure) with the aid of a kitchen mixer and then vibrated on a shaking table for five minutes to get rid of air bubbles trapped inside the slurry. The unconfined compression strength (UCS) testing data of MKG samples with the same synthesis recipe and cured at 6 hours, 2 days, 7 days, 14 days, and 28 days are presented in **Figure 3-1** as the complementary information that is imperative for synthesizing geopolymer with satisfactory performance, with 6 hours being the final setting time of MKGs. The compressive strength of this MKG recipe reached 12 MPa and remained stable after curing for 7 days.

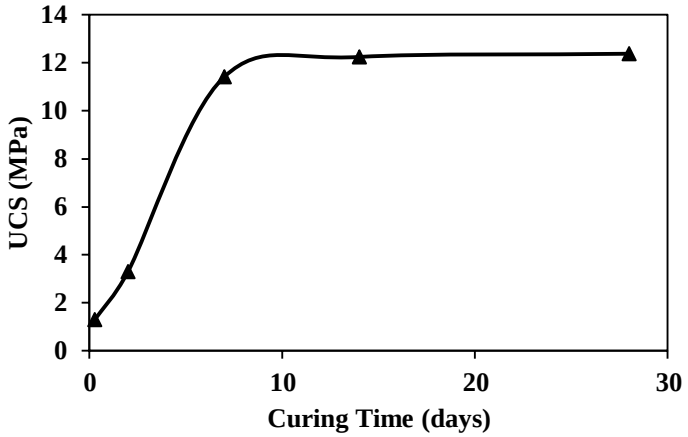

Figure 3-1 UCS results of MKGs cured for 6 hours, 2 days, 7 days, 14 days, and 28 days.

Two groups of MKG samples were prepared: Group I was prepared for the chemical volume change test; Group II was prepared for investigating the influences of the filling solutions on geopolyermerization processes under the same curing conditions as Group I. The detailed sample preparation is described below:

- Group I: Chemical volume change samples were prepared according to ASTM C1608. Two sample sets, designated as DIW (DIW as the filling solution) and AS (AS as the filling solution), respectively, were prepared. Well-mixed geopolymer precursor slurry was poured into glass vials up to 1 cm thickness to maintain the consistency (see **Figure 3-2(a)**). Then the filling solution was slowly poured onto the geopolymer paste along the vial wall without affecting the paste surface. Finally, a drop of paraffin oil was added to the top of the filling solution to prevent the evaporation of the filling solution during the monitoring time. All the MKG samples were placed within a water bath with a constant temperature of 25˚C and their volume changes were continuously measured for 20 days (shown in **Figure 3-2(b)**). To get more representative measurements, 20 MKG duplicates

were prepared for each sample set. The dilatometry method (shown in **Figure 3-2(a)**) was used to monitor the chemical volume change by taking readings on the graduated tube at different time intervals. The expansion or shrinkage caused by the chemical reaction was calculated as the reading differences with respect to the initial reading and more calculation details are presented in **Section 3.2.3.1**.

- Group II: The second group was prepared in the same way as Group I. Three sample subgroups, Group II-Control (without filling solutions), Group II-DIW, and Group II-AS were prepared for further characterizing the changes in ion concentration in the filling solutions and micro-structure of MKG samples at different time instants during chemical volume monitoring. Group II-Control was added to provide the baseline micro-structural for investigating the influence of filling solutions on the resulting geopolymers. To this end, seven sub-sets were prepared for each sample subgroup to track their pH value of the filling solution, ion centration of the filling solution, and microstructure changes at seven corresponding curing time instants (4 hours, 8 hours, 1 day, 3 days, 7 days, 14 days, and 18 days). Three duplicates were prepared for each sub-set, with the sample IDs and curing conditions summarized in **Table 3-2**.

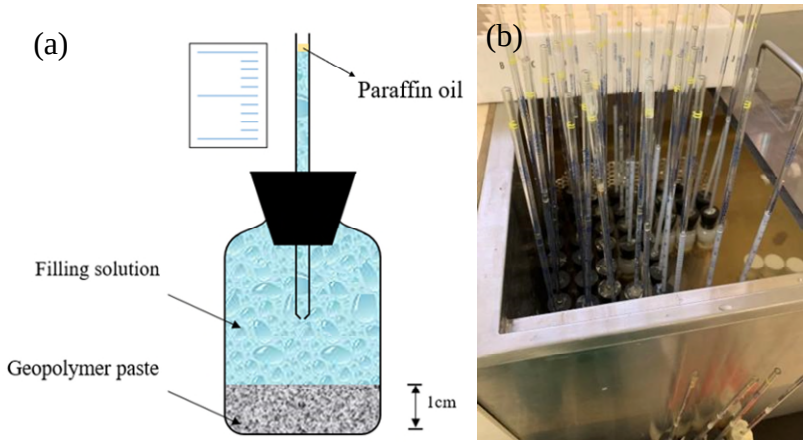

Figure 3-2 Experimental set up of chemical volume change test: (a) enlarged glass vial part, and (b) whole experimental set up in the water bath of a constant temperature.

Table 3-2 Sample IDs and curing conditions of Group II MKG specimens.

Sample ID	Filling solution	Curing time
C-4h	-	4 hours after mixing
C-8h		8 hours after mixing
C-1D		1 day after mixing
C-3D		3 days after mixing
C-7D		7 days after mixing
C-14D		14 days after mixing
C-18D		18 days after mixing
DIW-4h	DIW	4 hours after mixing
DIW-8h		8 hours after mixing
DIW-1D		1 day after mixing
DIW-3D		3 days after mixing
DIW-7D		7 days after mixing
DIW-14D		14 days after mixing
DIW-18D		18 days after mixing
AS-4h	AS	4 hours after mixing
AS-8h		8 hours after mixing
AS-1D		1 day after mixing
AS-3D		3 days after mixing
AS-7D		7 days after mixing
AS-14D		14 days after mixing
AS-18D		18 days after mixing

3.2.1.1.3 Calculation Method and Sample Characterizations

3.2.1.1.3.1 Calculation Method for Chemical Volume Change of MKGs

Chemical volume change measurements were taken by reading the values on capillary tube of each sample every hour over the first 7 hours, and every day afterwards until 20 days. The first reading was taken one hour (including half-hour mixing time, 5-minute vibration time, and other preparation time) after the mixing started. Based on the ASTM standard C1608 [175], chemical volume change per unit mass of geopolymer slurry at time t is calculated as:

$$CS(t) = \frac{[h(t) - h(t_0)]}{M_{geopolymer}} \quad (3\text{-}1)$$

Where $CS(t)$ is the chemical volume change at time t (mL/g), $h(t)$ is the filling solution level in the glass tube at time t [87], $h(t_0)$ is the initial reading [87] at t_0 , and $M_{geopolymer}$ is the mass of geopolymer paste. $CS(t) > 0$ means that the sample expands while the sample shrinks with a negative value.

3.2.1.1.3.2 Sample Preparations for Examining the Influence of Filling Solutions on Geopolymerization

Group II specimens were taken out from the water bath at seven different times (4 hours, 8 hours, 1 day, 3 days, 7 days, 14 days, and 18 days) to probe the influences of filling solutions on geopolymerization, by measuring pH values and ion concentrations in the filling solutions and examining microscopic morphology, chemical ratios, chemical bonding, and pore characteristics of Group II MKGs. After the samples were taken out, the filling solution (the liquid part) and the resulting geopolymer (solid part) were directly separated. The filling solution was tested for pH

value immediately, and then sealed in plastic vials and saved for chemical concentration testing. To examine whether any ion diffusion takes place between the MKG precursor and the filling solutions, or the MKG precursor is dissolved by the filling solutions during the monitoring time period, Na and Al concentrations in the filling solutions were measured with a PerkinElmer NexION 350X ICP Mass Spectrometer (ICP-MS). To prepare for the ICP-MS test, the filling solutions from AS sample group were filtered and diluted by 10,000 times with deionized water manually due to their high concentrations of Na and Al ions. The filling solution from DIW sample group was filtered and diluted by 1,000 times with the same procedure.

Based on the visual inspection, the resulting geopolymer has clearly three different portions with thickness of the surface and bottom parts of around 2 mm shown in **Figure 3-3**. To better investigate the influence of filling solutions on resulting geopolymers, each MKG sample was paper dried and cut into three portions (surface, middle, and bottom part, denoted as Surf, Mid, and Bot, respectively, in the rest of the dissertation) right at the layer boundaries with an Isomet 1000 precision saw. Pictures were taken for each of the sample portions right after the cut. All the sample parts were subsequently crushed into small pieces (the side surface was avoided to limit any influences caused by the glass vial walls) and then vacuum-dried for overnight immediately to prevent any further geopolymerization within remaining pore liquids. In addition, small chunks of these samples were saved for SEM-EDX and BET tests, and the rest of them were further ground to powder for FTIR test.

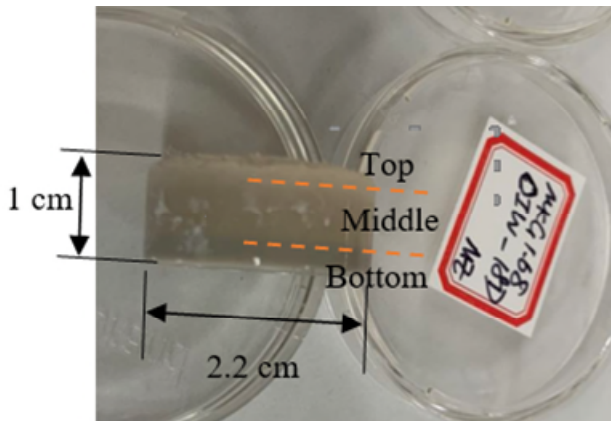

Figure 3-3 MKG sample cured for 18 days (filling solution of DIW) with clearly layered surface, middle, and bottom portions.

The heat release of the control, DIW, and AS sample groups was measured using the intermixing mode with a TAM Air isothermal conduction calorimeter (ICC) at 25°C, to investigate the influence of the filling solutions (i.e., AS or DIW) on the rate and degree of geopolymerization of MKG samples. The temperature was set as the same as that in chemical volume change test. One-gram metakaolin powder was placed in an ampoule, which was sealed by a rubber stopper with a mixer and three syringes. One syringe contained the premixed activator solution and the other two contained 2 ml respective filling solutions. The amount of testing materials was calculated based on the heat capacity of each component of the geopolymer precursor. The whole set-up was placed inside the testing chamber until the system reached thermal equilibrium. The activator solution was gradually injected into metakaolin powder and mixed slowly by the attached mixer. Signals were collected immediately at a 50 s interval. Then the filling solution was gradually injected onto the surface of the slurry one hour after the mixing, which is roughly the same time interval as that between mixing geopolymer ingredients and adding the filling solution

in the chemical volume change test. To maintain consistency, the amount of metakaolin and the filling solution was kept the same for all three samples.

3.2.1.1.3.3 Micro-structural Characterizations

To investigate the evolution of micro-structure, chemical ratios, chemical bonding, and pore characteristics of MKG samples during volume change test, SEM-EDX, FTIR, and BET tests were conducted. The micro-structure of samples was acquired by SEM with a JEOL JSM-7000F in secondary electron scatter mode. Chemical ratios at selected sample spots were detected by EDX using an OXFORD INCA X-act instrument. Chemical bonding information was inferred from FTIR spectra obtained with a BrukerOptics Vetex70 FTIR spectrometer using transmittance mode in the range of 400~1600 cm^{-1} at a resolution of 2 cm^{-1}. Specific surface area, accumulative pore volume and pore size distributions were determined with an instrument ASiQ IQ TPX from Quantachrome Instruments and analyzed with Non-Local Density Functional Theory (NLDFT) method.

3.2.1.2 Results and Discussion

3.2.1.2.1 Chemical Volume Change of MKGs

According to the calculation method described in **Section 3.2.3.1**, chemical volume changes of MKGs (DIW and AS groups) are shown in **Figure 3-4**, with the data between 0 and 1 day enlarged in the inset of **Figure 3-4**. The positive and negative values indicate volume expansion and shrinkage, respectively. Each of values was averaged over 20 duplicate samples, and the standard deviation bars are presented. The curves reached a steady state on the 15th day, and the volume change tests were ended after 20 days.

Different from the monotonic chemical shrinkage of OPC, the chemical volume change of MKGs is more complicated with more uncertainties and variations. Both DIW and AS group curves indicate the samples underwent four different stages, which in turn were affected by the different filling solution. Stage I is shrinkage (0 to 1 hour for both filling solutions), shown in the inset of **Figure 3-4**, while the other three stages are presented in **Figure 3-4**. For AS group, Stages II (expansion), III (shrinkage), and IV (stable) were between 1 hour to 4 days, 4 days to 7 days, and 7 days -20 days, respectively, while for DIW group, the stages were between 1 hour to 1 day (expansion), 1 day to 15 days (shrinkage), and 15 days to 20 days (stable), respectively. These volume change stages are summarized in **Table 3-3** with comparison of Li et al. and Lolli et al.'s work.

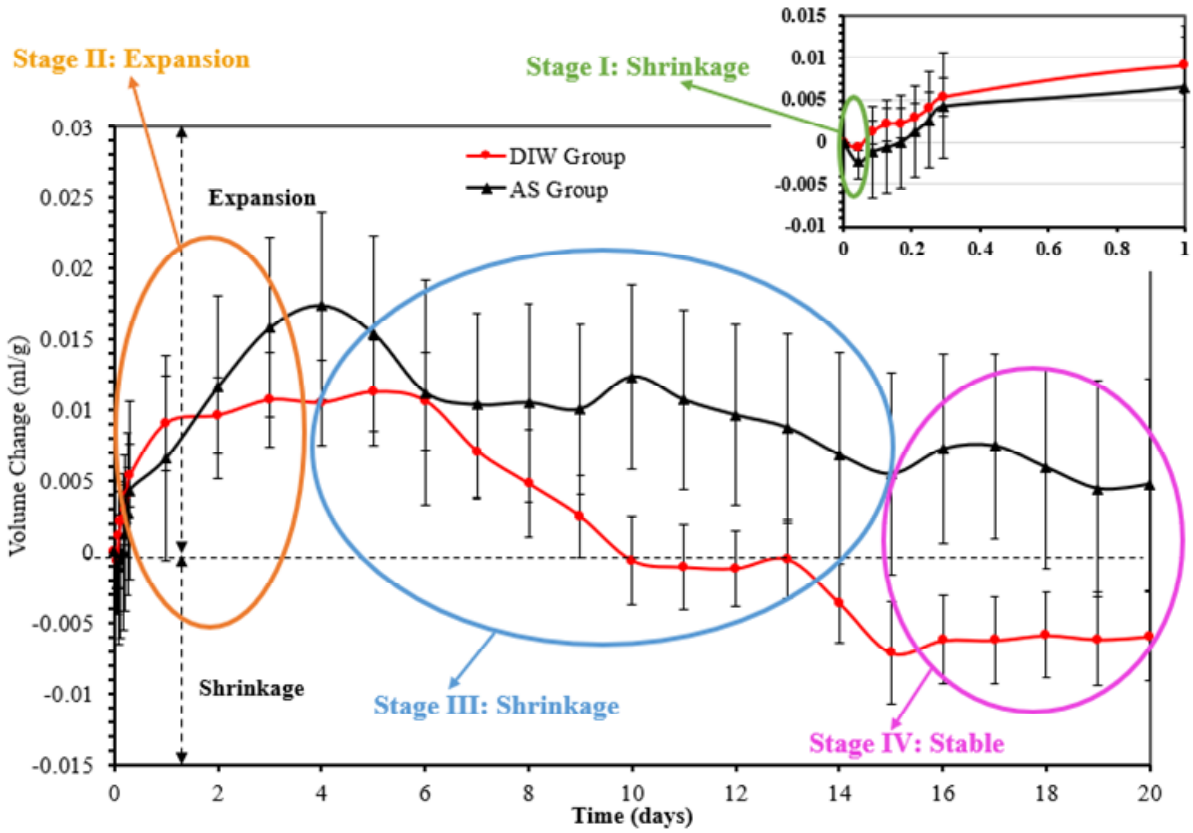

Figure 3-4 Chemical volume changes of MKG samples with DIW and AS filling solutions (above dashed line: Expansion; below dashed line: Shrinkage; the volume change data between 0-1 days are enlarged in the inset; four stages are labeled in the Figure; and all the data were averaged over 20 samples, with their standard deviation bars included.

Table 3-3 Summary of chemical volume change stages of MKGs and relevant literature data.

	This Study		Li et al. [92]	Holli et al. [93]
Si/Al molar ratio	1.68		1.15	1.44/1.75/1.99
Na/Al molar ratio	1.00		1.16	1.00
Filling Solution	AS	DIW	AS	Paraffin oil
Stage I: Shrinkage	0-1 hour	0-1 hour	0 - 8 hours	-
Stage II: Expansion	1 hour - 4 days	1 hour - 1 day	8 hours - 2 days	0 - 3 days
Stage III: Shrinkage	4 days - 7 days	1 day - 15 days	2 days - 14 days	-
Stage IV: Stable	7 days - 20 days	15 days - 20 days	-	-

The volume decrease (shrinkage) of Stage I was attributed to the dissolution of metakaolin, during which smaller species were produced. Similar initial volume change of MKG was also observed and verified by Li et al. through their physical experiments and theoretical calculations. Stage II (expansion) was attributed to the formation of Al-rich geopolymer gel and reaction products, such as lower density compounds (e.g., monomers or small oligomers), zeolites precursors, and secondary building units/fragments of zeolites that cause moderate expansion. Stage III (shrinkage) was related to the formation of the amorphous Si-rich geopolymer gels with higher density (e.g., Si-rich geopolymer gels) [180-182]. The chemical volume change became stable during Stage IV, which indicates that most of the geopolymerization process was finished. The first three stages of this study are in good agreement with Li et al's work [92], and the difference in stage timeframe is likely caused by the difference in geopolymer synthesis recipes (e.g., different Si/Al and Na/Al ratios used in the current study and Li et al.). Comparing the MKG samples with AS filling solution in the current study and in Li et al. [92], higher Si/Al molar ratio with the similar Na/Al molar ratio will result in more rapid reaction rate. This conclusion is only

valid in the relatively “pure” geopolymer system, which might be changed with other impurities presented in the reaction of other geopolymer systems derived from waste materials (e.g., fly ash or red mud-fly ash mixtures).

On the other hand, this study had longer Stage II and shorter Stage III, compared to those in Li et al. [92]. Beside the difference in time duration of different stages, the current study shows overall expansion behavior of MKG samples except the first stage during the testing time period, while Li et al.’s work shows overall shrinkage behavior. The different volume change behavior of the MKG samples between the two studies was likely due to different geopolymerization process of different recipes. Holli et al.’s work showed only the expansion of MKGs with the large Si/Al ratio range, which was likely attributed to the choice of filling solution (i.e., paraffin oil) whose molecular size might be too large to diffuse through the pores of resulting geopolymer gels. Note that the first three stages of volume change are also consistent with those of the geopolymerization processes proposed by Duxson et al. [183]: Dissolution, Gelation, and Reorganization, respectively.

The chemical volume change of DIW group shows overall expansion from 1 hour to 10 days and overall shrinkage from 10 days to the end of the testing. Compared to AS group, DIW group experienced shorter Stage II. This implies the AS group has more Al-rich geopolymer gel formed because more Al was dissolved by the AS filling solution. DIW group has a similar Stage III to that of AS group in terms of the time duration, while DIW group experienced more volume reduction during this stage. Therefore, the choice of filling solution in chemical volume change test is critical for accurately capturing and quantifying chemical volume change of geopolymer. Inappropriate ones can intervene the geopolymerization process during the testing and thus mask the real volume change behavior. For MKGs investigated in the current study, monitoring time

period of 20 days is adequate since their chemical volume change has reached steady-state and geopolymerization has been largely completed, but it will depend on the geopolymerization rate and specific geopolymer synthesis recipe for other geopolymers.

3.2.1.2.2 Visual Observation of MKG Samples

Representative images of surface, middle, and bottom parts of the control, AS, and DIW group samples cured at 8h, 1D, 7D, and 18D are shown in **Figure 3-5**. The diameter of each sample is around 22 mm. The color of DIW samples is very close to that of control samples at each curing time interval. The AS group samples are generally darker than the other two groups throughout the whole monitoring time, regardless of the location of the sample. This is likely due to the fact that the AS filling solution promoted geopolymerization process (more discussions in the following sections). Visual observations also indicate that all the surface parts of DIW group samples are much more porous, weaker, and crumblier. This is likely attributed to the fact that the addition of DIW filling solution intervened geopolymerization of the surface portion of samples and thus not much geopolymer gel formed within this layer. Since visual observation is qualitative at best and can be misleading, further characterizations on different parts of MKG samples are detailed in the following sections.

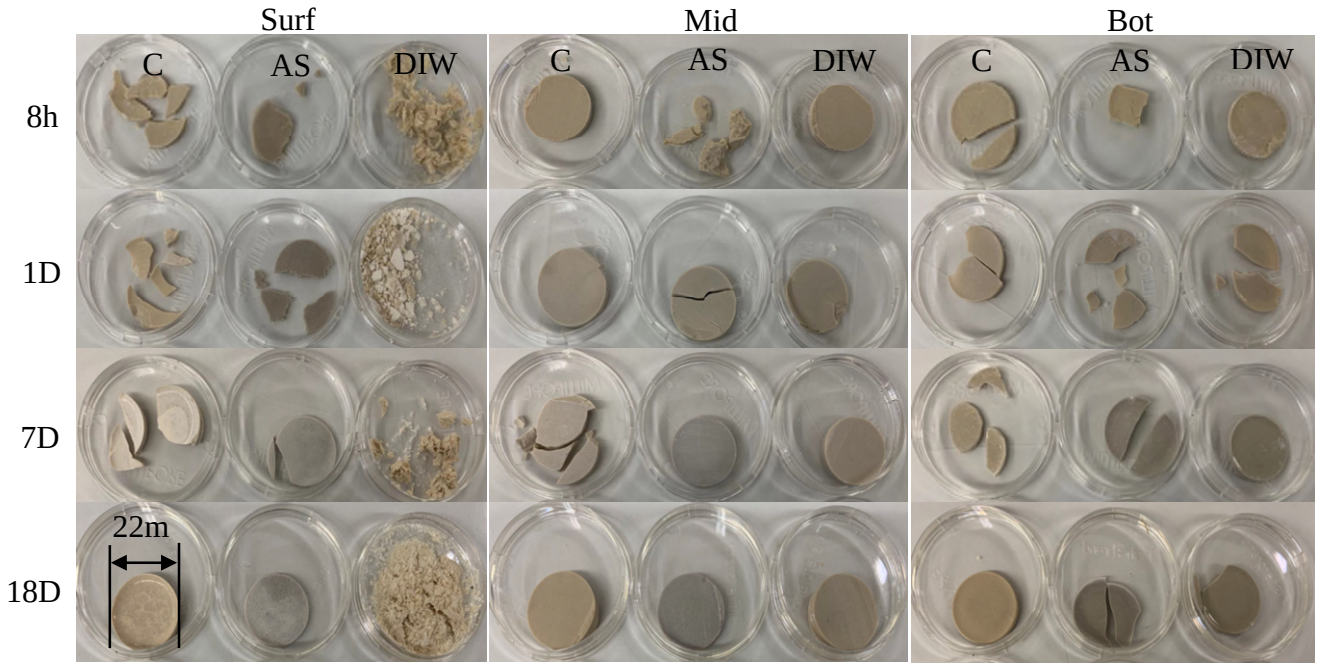

Figure 3-5 Representative photos of the surface, middle, and bottom part of MKG samples (control, AS, and DIW groups) cured at 8h, 1D, 7D, and 18D. The scale bar is shown in left bottom image.

3.2.1.2.3 pH Values and Ion Concentrations in Filling Solutions

The pH values of the filling solutions at different elapsed time instants during volume change test were monitored and its changes relative to the respective initial values were plotted in **Figure 3-6,** to shed light on any potential ion exchange between geopolymer precursors and the filling solutions. The initial values were tested when the geopolymer precursor just was in contact with the filling solution. The change in pH values of AS group samples fluctuated within a small range (~ 0.1). On the other hand, the increase in pH values of DIW filling solution went from 0 up to 1.5 shortly after the filling solution contacted with the geopolymer precursor. This indicates that the concentration of OH^- ions did not change much in the AS group, but appreciable amount of OH^-

ions diffused from the geopolymer precursor to DIW filling solution that was attributed to a large concentration gradient between the geopolymer slurry and DIW filling solution. It is well known that alkali concentration is a key factor controlling the dissolution of aluminates and silicates from the raw materials, geopolymerization and mechanical properties of hardened geopolymer [24, 184, 185]. Therefore, the diffusion of OH^- ions from the DIW geopolymer precursor to the filling solution intervened the geopolymerization of DIW group by dampening the degree of dissolution of metakaolin, which is consistent with visual observations discussed earlier and ICC and FTIR results presented later in **Sections 3.4** and **3.6**.

Na^+ and Al^{3+} ion concentrations were also measured in the filling solutions of all the samples at different elapsed time to further investigate other ion exchanges between the geopolymer precursor and the filling solutions. The changes in ion concentrations are plotted in **Figure 3-7(a)** and **(b)**, relative to their respective initial values, with the initial values tested in the pure filling solution (i.e., DIW or AS). Si ion concentration was not tested because of the limitation of the device. In the DIW group, a small amount of Al ions and a relatively large amount of Na ions diffused into the filling solution due to the large ion concentration gradient. All the ions came from the geopolymer precursor, since there was no Al or Na in the initial DIW filling solution. The fluctuation of Na and Al ion concentrations measured in the filling solutions was attributed to the complex, dynamic chemical ion exchanges between the being-cured geopolymer slurry and the filling solutions that are controlled by competing processes of geopolymerization and diffusion, as reported in the literature [184]. Such competing processes in turn depend on multiple factors such as the rate and kinetics of geopolymerization, the chemical composition and concentration of filling solutions. In AS group, Al ion concentration in the filling solution progressively increased as time elapsed. Since there was no Al in the initial AS filling solution and its pH value did not

change much (see Figure 3-6), Al ions came from the continuously dissolved raw materials (i.e., metakaolin) the diffusion process of the being-cured geopolymer precursor, and the diffusion of hardened geopolymer and even partial dissolution of geopolymer gel. Compared to DIW group, AL ion concentration in the AS filling solution is much higher than that of DIW filling solution throughout the monitoring period. Such differences were likely attributed to two different underlying mechanisms: i. more Al ions dissolved from the geopolymer precursor in high alkaline AS filling solution that diffused from the geopolymer precursor to AS filling solution at the early monitoring stage (up to 3 days); ii. Al concentration in the pore solution of being-cured geopolymer precursor increased as Si-rich geopolymer gel formed from Al-rich gel during Stage III of chemical volume change and more Al ions were freed (i.e., after 7 days), which is consistent with the observed chemical volume change behavior of AS group described earlier. On the other hand, weaker Al-rich gel with DIW group formed relatively quickly such that very limited Al ion diffused to DIW filling solution. Na ion concentration initially increased in the filling solutions of both DIW and AS groups (at 4 h), which was likely attributed to more dissolved Na ions in the geopolymer precursor that was not solidified yet (prior to the final setting time of 6 h). After the geopolymer precursor solidified (i.e., after 6h), Na ion concentration further increased in the filling solution of DIW group while the opposite took place in AS group. Such a different trend in Na concentration in the filling solutions between DIW and AS groups is due to change in relative Na concentration between the geopolymer precursors and their respective filling solutions. As the geopolymer precursor solidified and hardened, Na ions were consumed to form geopolymer gel and became fewer in the porewater of the precursor; consequently, different Na concentration gradients were resulted in DIW and AS filling solutions and thus diffusions occurred in different directions: more Na ions further diffused from the geopolymer precursor to DIW filling solution

while Na ions diffused from AS filling solution into the geopolymer precursor. This is consistent with the EDX results (i.e., a much higher Na/Al ratio in the AS-Surf while a lower Na/Al ratio in the DIW-Surf throughout the monitoring period) in **Section 3.6**. Given the critical roles (e.g., balancing the negative charge of aluminum site of alumina-silicate network consisting of tetrahedral coordinated SiO_4 and AlO_{4-} groups and thus affecting Si/Al ratio of the resulting geopolymer gel and its microstructure and overall mechanical properties of the geopolymer) of Na during geopolymerization [50, 184, 186, 187], it is expected that the diffusion of Na would have affected the geopolymerization of DIW and AS groups, particularly their surface portions. Different diffusion behavior of Na in DIW and AS groups is consistent with other characterization testing results (e.g., visual observations, ICC results, FTIR and EDX results).

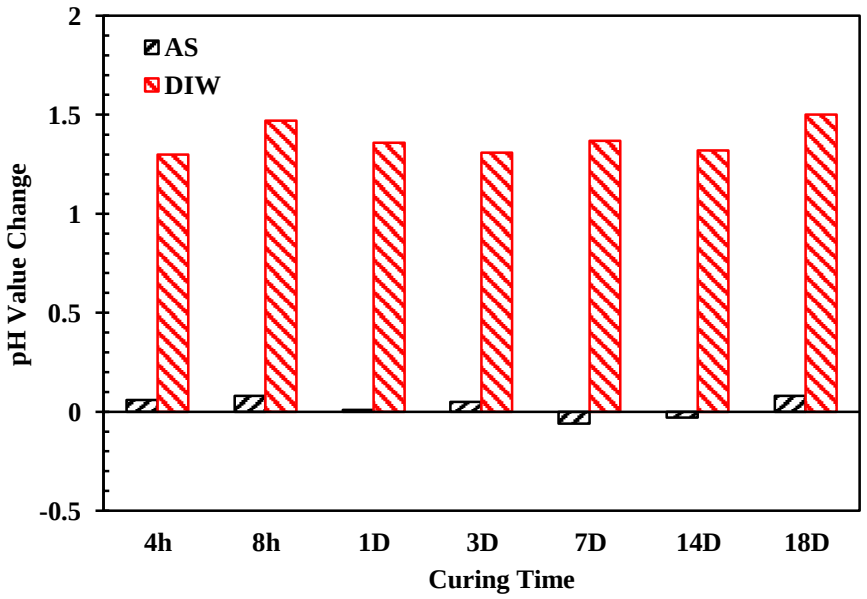

Figure 3-6 pH values change of filling solutions at elapsed time instants during volume change test monitoring compared to the respective initial values. Initial values were tested when the paste just contacted with filling solution.

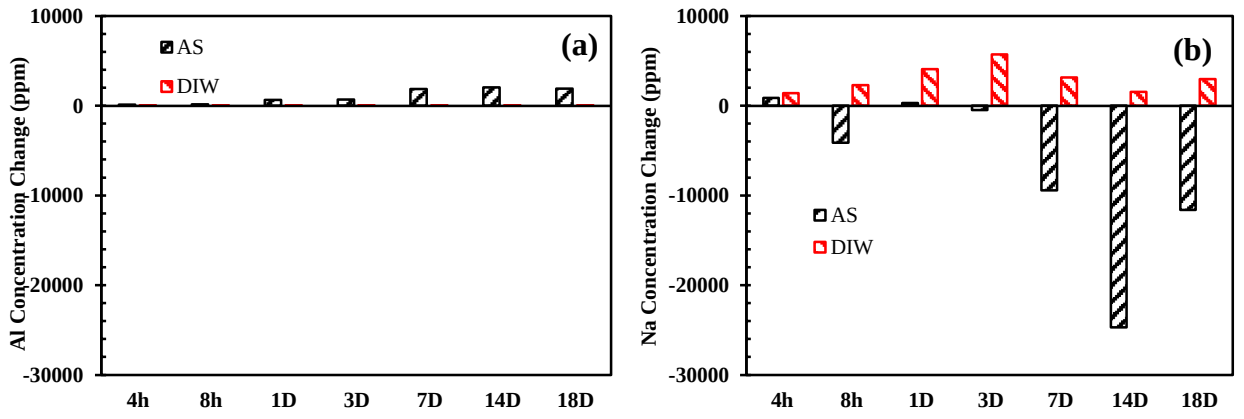

Figure 3-7 Changes in (a) Al and (b) Na ion concentration in the filling solutions at different elapsed time instants during chemical volume change testing compared to their respective initial values. Initial values were tested in the pure filling solution (i.e., DIW or AS).

3.2.1.2.4 ICC results

The heat flow of reactions in control, AS, and DIW group samples at 25°C was measured with ICC to investigate how the filling solutions affect the rate and kinetics of geopolymerization. The normalized heat flows over time are plotted in **Figure 3-8(a)**, and the portion between 0-10 hours is enlarged in **Figure 3-8(b)**. In **Figure 3-8(b)**, the time instants when the activator solutions and the filling solutions (either AS or DIW) added to respective geopolymer samples are marked with vertical solid lines, respectively, while the representative peaks and hump are labeled by arrows in Figure 3-8(a). For all the samples, a sharp peak (Peak I) appeared right after the activator solution was added, which corresponded to the heat release associated with the dissolution of metakaolin and the initiation of geopolymer gel formation. For slower geopolymerization reactions, there would have been two separate peaks, with the first one attributed to raw material dissolution while the second one associated with the initiation of geopolymer gel formation [188, 189]. In this study,

the single peak is attributed to the overlap of the two heat releasing peaks because of rapid reaction of metakaolin.

For the AS group, a new peak (Peak II) appeared almost immediately after the AS filling solution was added, followed with a broad hump. This indicates that the addition of AS filling solution promoted further geopolymerizations. On the other hand, for the DIW group, the heat flow was suddenly dropped to negative and then went back to zero after adding the DIW filling solution. This indicates that the addition of DIW filling solution significantly dampened or even halted geopolymerization within the surface portion of DIW sample group where the filling solution imposed most influence. The occurrence of the seemingly strongly "endothermic reaction" was most likely due to the temperature difference between the added water and geopolymer precursor, which does not present any chemical reaction. This is consistent with porous and weak surface part of DIW group samples, as discussed in the previous sections.

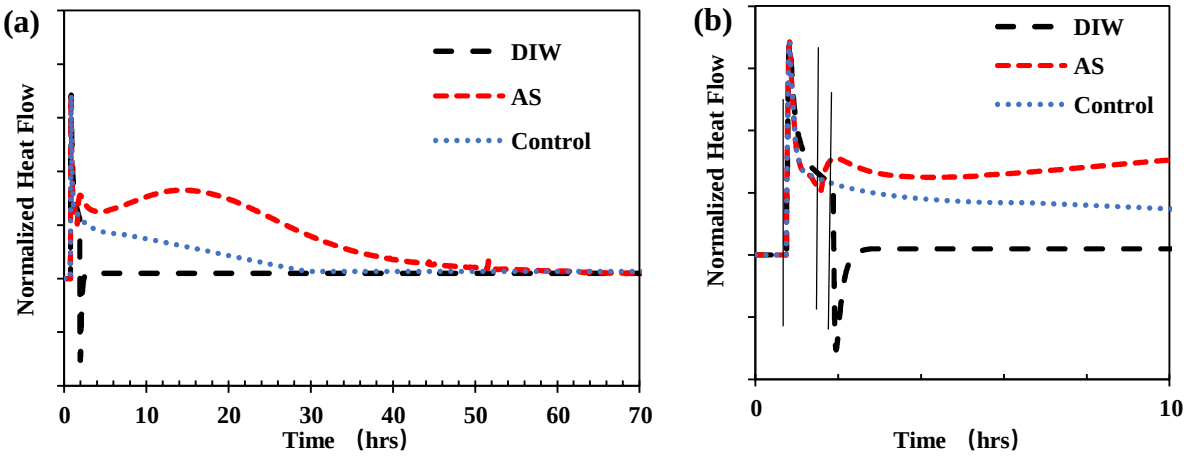

Figure 3-8 (a) Normalized heat flow with time of MKG control group and MKGs filled by DIW and AS, and the portion between 0-10 hours are enlarged in (b).

3.2.1.2.5 BET Results

To investigate the influences of filling solutions on resulting geopolymer samples, pore size distribution and pore volume of different parts of MKG specimens were examined by BET. The pore size distribution of the middle part of control, AS, and DIW sample groups at different elapsed time (e.g., 4h, 8h, 1 day, 3 days, 7 days, 14 days, and 18 days) are shown in **Figure 3-9 (a), (b)**, and **(c)**, respectively. The pore volume is plotted over the half pore width in nm.

For the control group, the dominant pore size evolved from 1.4 nm to 3.7 nm as the time elapsed. The dominant pore size evolution and pore size distribution pattern of DIW group are close to that of the control group. While AS group samples show relatively lower total pore volume, and their dominant pore size shifted to very small size (e.g., ~1.2 nm) after 7 or 14 days. This is likely attributed to the further geopolymerization reactions promoted by the AS filling solution, which results in more geopolymer gels, and thus smaller pore volume and smaller dominant pore size.

The total pore volume of 14-day cured control, AS, and DIW samples is presented in **Figure 3-9 (d)**. Only the 14 day-cured sample data are presented for the sake of brevity. The total volume of 14 day-cured control, AS, and DIW group samples are 0.639 cm^3/g, 0.241 cm^3/g, and 0.633 cm^3/g, respectively. The 14-day cured control group sample has similar total volume in each part (i.e., Surf., Mid., and Bot.). The pore volume of the surface part in DIW sample is “apparently” smaller because modern non-local density functional theory (NLDFT) method can only detect the pore sizes smaller than 50 nm; however, the surface part of DIW group is much more porous and easy to crumble into powder, as shown in pictures in **Figure 3-5,** which implies that the actual pore volume in the DIW’s surface part is largely underestimated by the BET method. Therefore,

the total pore volume cannot be compared between the control group and DIW group, although the total detected pore volume of the DIW sample is “seemingly” much closer to that of the control group. The AS group has much smaller total pore volume compared to the other two groups, which is consistent with the previous results on the influence of AS filling solutions on geopolymerization (i.e., relatively smaller total volume of AS group sample compared to the control group attributed to the formation of more geopolymer gels promoted by the AS filling solution that fill in more pores). Furthermore, since a significant amount of Al was dissolved from geopolymer precursor or the raw materials by the AS filling solution, more Si-rich geopolymer gels formed. The local density of amorphous Si-geopolymer gels is larger than that of Al-geopolymer gels [92], which also resulted in smaller pore volumes.

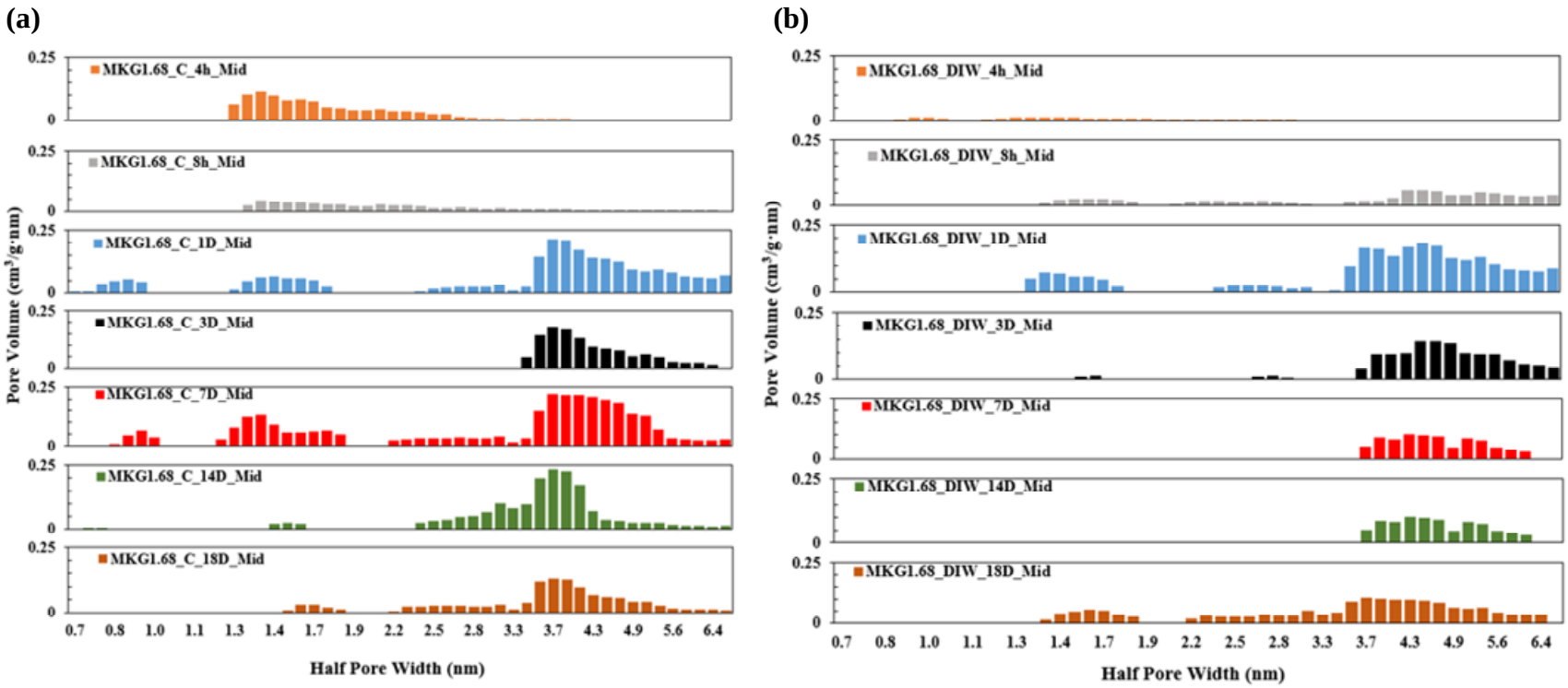
(a)
MKG1.6S_C_4h_Mid
MKG1.6S_C_8h_Mid
MKG1.6S_C_1D_Mid
MKG1.6S_C_3D_Mid
MKG1.6S_C_7D_Mid
MKG1.6S_C_14D_Mid
MKG1.6S_C_18D_Mid
Pore Volume (cm³/g·nm)
0.25
0
0.7 0.8 1.0 1.1 1.3 1.4 1.7 1.9 2.2 2.5 2.8 3.3 3.7 4.3 4.9 5.6 6.4
Half Pore Width (nm)
(b)
MKG1.6S_DIW_4h_Mid
MKG1.6S_DIW_8h_Mid
MKG1.6S_DIW_1D_Mid
MKG1.6S_DIW_3D_Mid
MKG1.6S_DIW_7D_Mid
MKG1.6S_DIW_14D_Mid
MKG1.6S_DIW_18D_Mid
Pore Volume (cm³/g·nm)
0.25
0
0.7 0.8 1.0 1.1 1.3 1.4 1.7 1.9 2.2 2.5 2.8 3.3 3.7 4.3 4.9 5.6 6.4
Half Pore Width (nm)

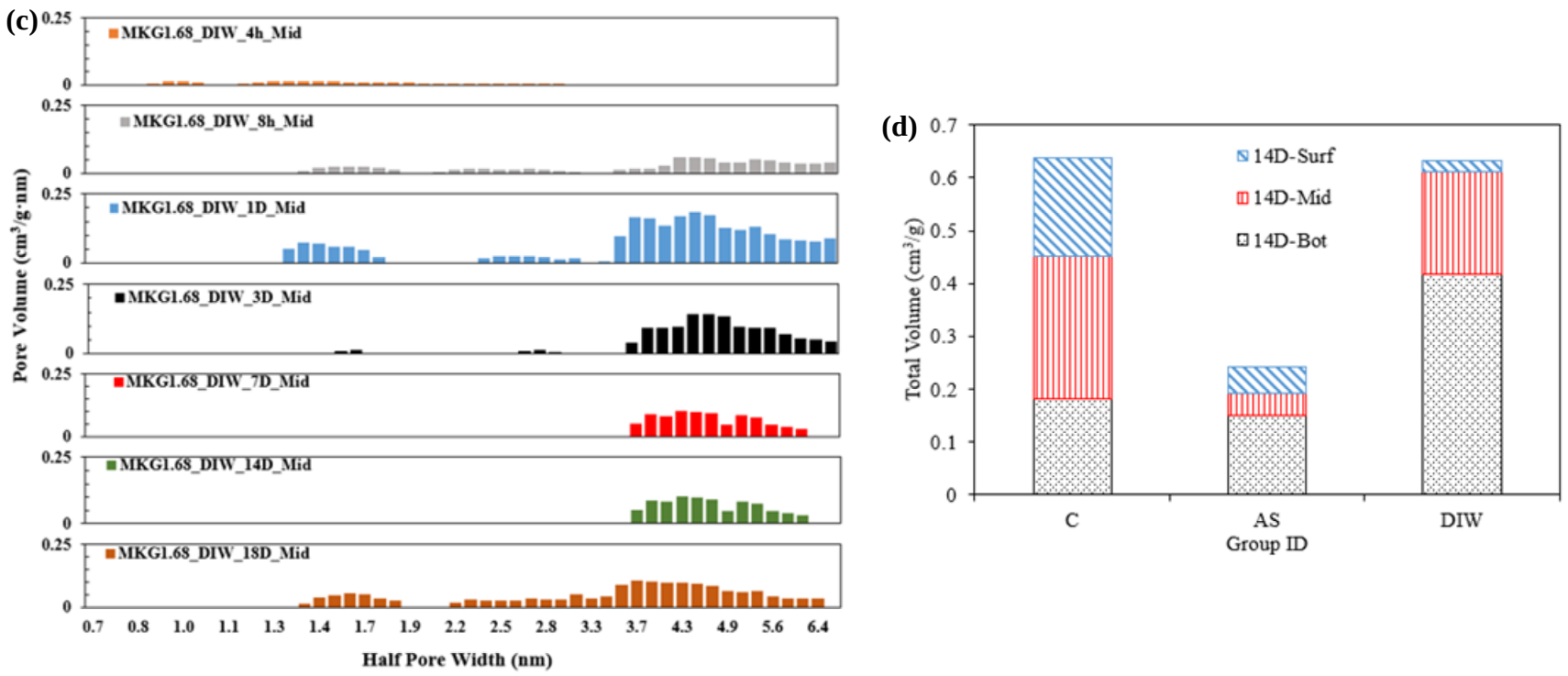

Figure 3-9 Pore size distribution of the middle part of (a) control group, (b) AS group, and (c) DIW group samples at different curing time, with total pore volume of 14 day-cured control, AS, and DIW group samples with adding all three parts together presented in (d).

3.2.1.2.6 FTIR and SEM-EDX Results

To further illustrate the influences of filling solutions on geopolymerization during chemical volume change testing, chemical bonding, chemical ratios, and microscopic morphology of different layers of these sample groups (Control, DIW, and AS groups) were examined by FTIR and SEM-EDX, respectively.

FTIR spectra of surface and middle parts of three sample groups are presented in **Figure 3-10 (I)** and **(II),** along with the spectrum of metakaolin as the baseline. FTIR spectra of bottom parts of the three sample groups were also acquired, whose results were not presented here for brevity since they have the similar trends to middle parts. The FTIR spectra in the range of 1200-900 cm^{-1} are attributed as the 'main band' of geopolymer gels, which corresponds to the Si-O-T (T is Si or Al) asymmetric stretching vibration band [162, 163, 190]. The band at 1080 cm^{-1} (Si-O-T) and the hump at 800 cm^{-1} representing asymmetric stretching vibration of Si-O-Si in raw material became gradually less apparent and the main band shifted to the range of 1030-940 cm^{-1} in all the testing samples, which confirmed the dissolution of raw materials and the formation of geopolymer gels.

For the control group, in general, the shift of the main band of all the parts are highly consistent with each other, as shown in **Figure 3-10(a-I)** &**(a-II)**. The main band was shifted from wavenumber 1080 cm^{-1} to 969 cm^{-1}, from 969 cm^{-1} to 988 cm^{-1}, and then from 988 cm^{-1} to 985 cm^{-1}, and then stabilized with some fluctuations. The main band shift is corresponding to the dissolution, Al-rich gel formation, and Si-rich gel formation, respectively, as verified by previous studies [162, 191]. The spectra of the surface part of 4h cured samples, regardless of the sample group, have relatively low intensity compared with those of the middle part, suggesting that the

degree of geopolymerization at early stage is different at different layer within the sample. Besides the 4h-cured sample, the geopolymer gels development was similar to each other at different layers.

The humps located at around 870 cm^{-1}, 680 cm^{-1}, and 570 cm^{-1}, shown in all the samples regardless of the layer, are corresponding to bending vibration of Si-OH bonds [188, 192], vibration of Al-O bonds [92], and bending vibration of Si-O-Al bonds, respectively [193]. A weak hump at around 1400 cm^{-1} is assigned to O-C-O bond, which possibly caused by the atmospheric carbonation [193, 194]. Compared to the control group, the AS group has a similar geopolymer gel evolution (shown in **Figure 3-10 (b-I)** and **(b-II)**) except the 14-day cured sample. However, the Si-OH bending vibration bonds, Al-O vibration bonds, and Si-O-Al bending vibration bonds are less obvious than the control group, as well as the middle part of AS group samples. These non-obvious Si-OH bending vibration bonds suggest the higher degree of geopolymer gel condensation [192], which means that the surface part of AS group samples have higher condensation degree than its own middle part and the counterpart (i.e., the surface part) of the control group. The non-obvious Al-O vibration bonds and Si-O-Al bending vibration bonds possibly caused by the absence of Al in the geopolymer gels, which were dissolved by the AS filling solution from the surface part. This is consistent with the ICP-MS results presented earlier in **Section 3.3**.

For DIW group (shown in **Figure 3-10 (a-III)** and **(b-III)**), two differentiable bands shown in the ‘main band’ area, the band around 1015 cm^{-1} is assigned to be Si-O-Si asymmetric stretching vibration bond, and the band around 1025 cm^{-1} is assigned to be Si-O-Al asymmetric stretching vibration bond. A new band located at around 790 cm^{-1} appeared in the DIW surface part samples, which is attributed to the AlO_4 vibrations [195]. The differentiable Si-O-Si and Si-O-Al bonds not

overlapped as the case in other two groups and the presence of AlO_4 vibrations indicate that the lower geopolymerization degree than the samples cured at the same time of the other groups. This is consistent with the ICC results (see **Section 3.3.4**): the addition of DIW filling solution intervened or dampened the reaction process. Such a band is not shown in the middle part of DIW samples, which indicates that the influence of DIW filling solution on geopolymerization was largely confined to the surface part.

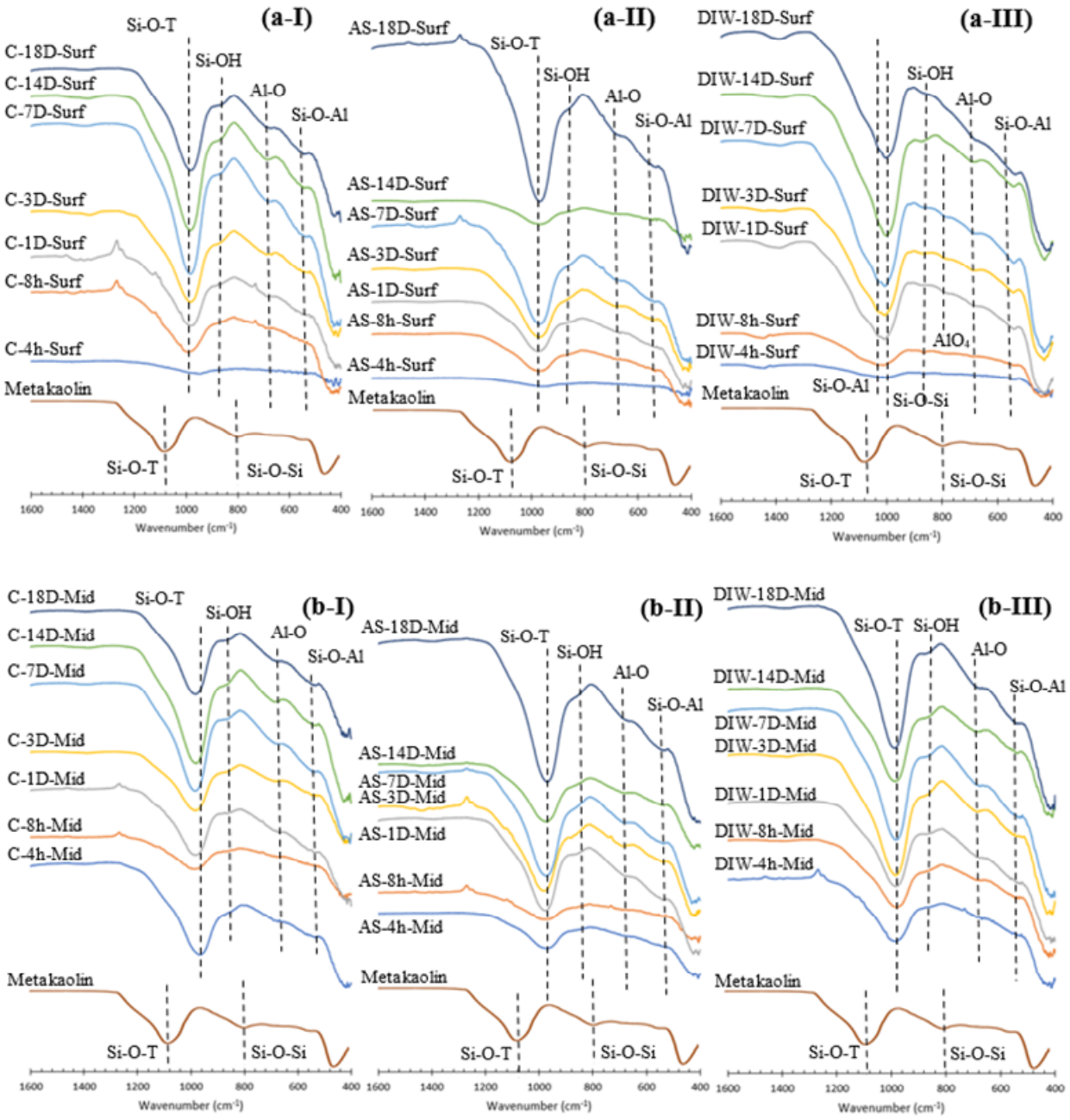

Figure 3-10 FTIR spectra of (a) Surface parts, and (b) Middle parts of (I) control samples, (II) AS samples and DIW samples at curing time 4h, 8h, 1D, 3D, 7D, 14D, and 18D.

The centers of the geopolymer gel 'main band' of surface, middle, and bottom parts of all three groups were plotted over the elapsed time in **Figure 3-11 (a-I)**, **(b-I)**, and **(c-I)** to further

reveal the influence of filling solutions on geopolymerization. The center of the 'main band' of raw material is also included in the Figures as a reference, which is 1080 cm^{-1}. The Si/Al and Na/Al molar ratio of geopolymer gels of all the samples parts were approximated from the EDX measurements. The detected spots with Si/Al molar ratio in the range of 1-3, and Na/Al molar ratio around 1 are considered as typical ranges for geopolymer gels [151, 196, 197]. The Si/Al and Na/Al molar ratios are also plotted in **Figure 3-11 (a-II)**, **(b-II)**, **(c-II)**, and **Figure 11 (a-III)**, **(b-III)**, **(c-III)**, respectively, which were averaged over ten spots considered as geopolymer gels of each sample. As expected, the filling solution has a larger influence on the surface part of both DIW and AS groups based on FTIR and EDX results. The main band shifted to smaller wavenumber represents the formation of more geopolymer gels. DIW group surface part has highest main band wavenumber and lowest Si/Al and Na/Al molar ratios compared to the other two groups, which indicates that the surface part of DIW group contains fewer geopolymer gels. This was likely attributed to: i. the intervention of the geopolymerization process of this part by the filling solution; and ii. some of the geopolymer gels might be partially dissolved by the filling solution. This is consistent with the visual inspection of surface part of DIW group samples and diffusions of Na^+ and OH^- between DIW filling solution and the geopolymer precursor discussed earlier in **Section 3.3** (see **Figure 3-5**).

The AS group has the lowest main band wavenumber and relatively highest Si/Al and Na/Al molar ratios for all their three different parts. The main band shifted to lower wavenumber compared to the control group suggests more geopolymer gels formation. Relatively higher Si/Al and Na/Al molar ratios compared to the other groups also implies the higher degree of geopolymerization or polycondensation into higher oligomers and polymeric 3D-networks, which agree well with diffusions of Na^+ and OH^- between AS filling solution and the geopolymer

precursor discussed earlier in **Section 3.3**. The much higher Na/Al ratio for the bottom part was likely caused by the precipitation of Na ions from the filling solution in AS group, which was captured by the SEM images (the flower-like feature) shown in **Figure 3-12**. From the EDX results, the chemical ratios of the flower-like features can be summarized as three categories: (i) O/Na ~1.3; (ii) O/Na~1.5, C/Na~0.6, and [142] O/Na~2. All these might belong to (i) NaOH crystal, (ii) NaOH crystal mixed with Na_2CO_3, and [142] Monohydrate, $NaOH \cdot H_2O$. Since this feature is only shown in samples of AS group, this might be corresponding to the precipitation of the extra Na cations in the AS filling solution, which is consistent with ICP-MS results shown in **Figure 3-7(b)**, which can explain the decrease of Na concentrations in the filling solutions.

The SEM images of surface part of 18-day cured samples are presented in **Figure 3-13**, which is the most differentiable part from the morphology perspective. The microscopic morphologies of the surface part in control and AS group are similar (i.e., dense and compact); however, the surface part of DIW sample is much more porous and easier to crumble. This is consistent with the visual inspection (**Figure 3-5**), diffusions of chemical ions (**Section 3.3**), and FTIR and EDX results (**Figure 3-11**).

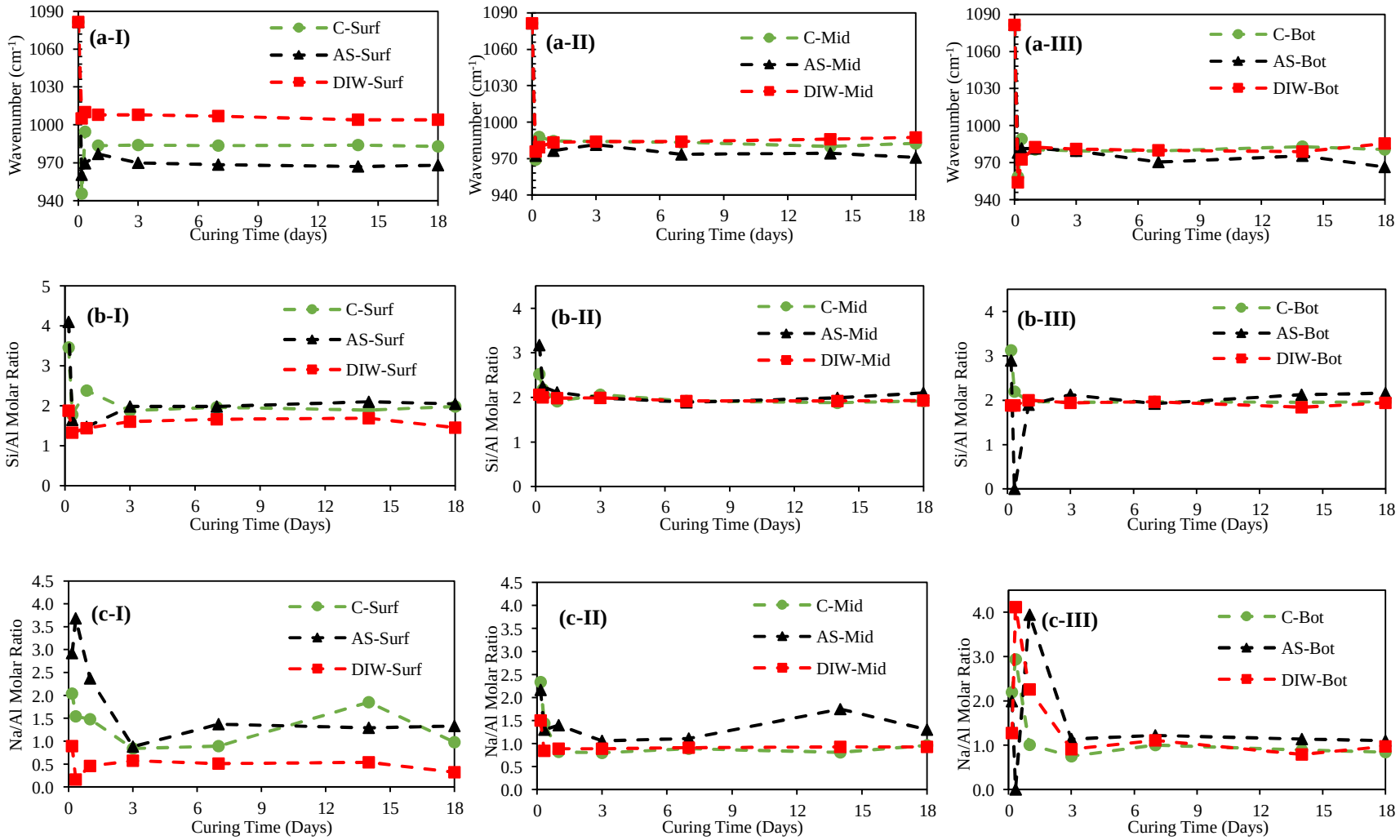

Figure 3-11 (a) Si-O-T band wavenumber, (b) averaged Si/Al molar ratio, and (c) averaged Na/Al molar ratio of (I) Surface part, (II) Middle part, and (III) Bottom part of geopolymer gels in different sample groups. Each figure is plotted over curing time.

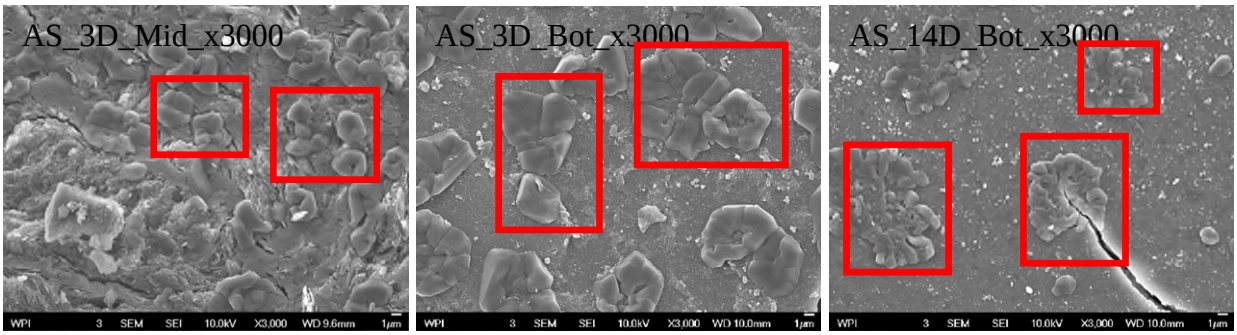

Figure 3-12 SEM images of AS samples with the flower-like features. The magnification is 3000.

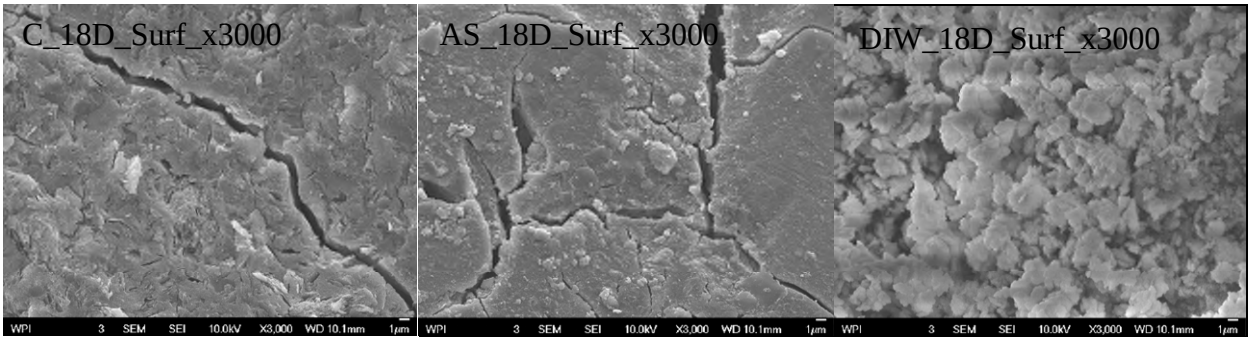

Figure 3-13 SEM images of surface part of 18-day cured control, AS, and DIW samples. The magnification is 3000.

3.2.2 Volume Change Properties of Red Mud Slurry and Class F Fly Ash Based Geopolymers

3.2.2.1 Materials and Methodology

3.2.2.1.1 Materials

A mixture of FFA and RMS, a mass ratio of 1:4 was used to synthesize geopolymers. RMS was used in geopolymer synthesis as received from Alcoa World Alumina, LLC. FFA was provided

by Headwaters Resources Inc. The physical properties and chemical compositions of RMS and FFA are shown in **Table 3-4** and **Table 3-5**, respectively. The pH value and water content of RMS are ~14 and 74%, respectively. RMS also contains traceable amount of soluble Na, Si, and Al. The main components of FFA are SiO_2 and Al_2O_3, whose amorphous phases are the main reactive constituents in geopolymerization. FFA also contains an appreciable amount of Fe_2O_3 and some trace elements. In addition, the median particle size (D_{50}) of FFA is 16 μm. A mixture of 50% NaOH and sodium silicate solution was used as the alkaline activator to synthesize geopolymer.

Table 3-4 Chemical compositions of Class F fly ash (wt.%) provided by the supplier.

SiO_2	Al_2O_3	Fe_2O_3	SO_3	CaO	K_2O	MgO	Na_2O	Moisture	Loss on ignition
59.74	27.51	4.91	0.16	1.45	2.39	1.18	0.82	0.08	2.66

Table 3-5 Physical and chemical compositions of RMS (wt.%).

Liquid contents	Solid contents	Soluble Na	Soluble Si	Soluble Al
74	26	1.97	0.00555	0.74

3.2.2.1.2 Geopolymer Synthesis and Sample Preparation

While it is desirable to use RMS at a maximum amount to partially replace expensive alkaline solution, too much red mud will result in lower strength of the resulting geopolymer sample due to its poor reactivity [155]. In light of the consideration, a 1:4 mass ratio of RMS to FFA was used as the source materials for geopolymer synthesis. Chemical compositions of the source materials proved critical to synthesizing geopolymer with high mechanical strength. The synthesis recipe was used based on Chapter II results.

The alkaline activator solution was pre-prepared and then cooled down to room temperature for later use. RMS and FFA were firstly mixed at the pre-determined ratio with a mechanical mixer, followed with the addition of the alkaline activator solution, and the whole precursor was stirred for 30 minutes to ensure thorough mixing. The slurry was vibrated for 10 minutes to remove the air bubbles. Well-mixed geopolymer precursor slurry was poured into glass vials up to 1 cm thickness to maintain consistency. Based on the conclusions made in **Section 3.2.1**, DIW was used in this study as the filling solution. Then DIW was slowly poured onto the geopolymer paste along the vial wall without affecting the paste surface. Finally, a drop of paraffin oil was added to the top of the filling solution to prevent the evaporation of the filling solution during the monitoring time. All the RMSFFA samples were placed within a water bath with a constant temperature of 50˚C and their volume changes were continuously measured for 20 days. To get more representative measurements, ten duplicates were prepared for each sample set. The dilatometry method (shown in **Figure 3-2(a)**) was used to monitor the chemical volume change by taking readings on the graduated tube at different time intervals. The expansion or shrinkage caused by the chemical reaction was calculated as the reading differences with respect to the initial reading and more calculation details followed the same rules presented in **Section 3.2.3.1**.

Table 3-6 Summary of mix design of RMSFFA geopolymer specimens used for volume change tests.

Sample set ID	Si/Al (mol)	Na/Al (mol)	L/S (weight ratio)	Water Content (wt.%)	Objectives
RMSFFA-SA2.0-NA0.6	2	0.6	0.53	~25	Effect of Na/Al molar ratio
RMSFFA-SA2.0-NA0.7	2	0.7	0.57		
RMSFFA-SA2.0-NA1.0	2	1	0.7		
RMSFFA-SA1.8-NA0.7	1.8	0.7	0.5		Effect of Si/Al molar ratio
RMSFFA-SA1.9-NA0.7	1.9	0.7	0.53		
RMSFFA-SA2.0-NA0.7	2	0.7	0.57		

3.2.2.2 Sample Micro-structural Characterizations

To investigate the evolution of pore characteristics of MKG samples during volume change test, BET tests were conducted. Specific surface area, accumulative pore volume and pore size distributions were determined with an instrument ASiQ IQ TPX from Quantachrome Instruments and analyzed with Non-Local Density Functional Theory (NLDFT) method.

3.2.2.3 Results and Discussions

According to the calculation method described in **Section 3.2.1.1.3.1**, chemical volume changes of RMSFFA geopolymers are shown in **Figure 3-14 (a)** with different Si/Al molar ratios and **(b)** with different Na/Al molar ratios, with the data between 0-1 day enlarged in the inset of **Figure 3-14 (a)** and **(b).** The positive and negative values indicate volume expansion and shrinkage,

respectively. Each of the values was averaged over 10 duplicate samples. All the RMSFFA geopolymers have overall expansion behavior regardless of the chemical compositions.

Unlike the four chemical volume change stages of MKGs, the RMSFFA geopolymers shows only three stages regardless of the chemical compositions: Expansion (0-2 hours), Shrinkage (2 hours to 7 days), and Stable stage (7 days to 20 days). There is no clear trend can be found on the effects of different chemical compositions (Si/Al or Na/Al molar ratio) on the chemical volume change of RMSFFA geopolymers. The shrinkage and stable stages have some fluctuations, which might be caused by the process of water evaporation and cold water been added to the water bath.

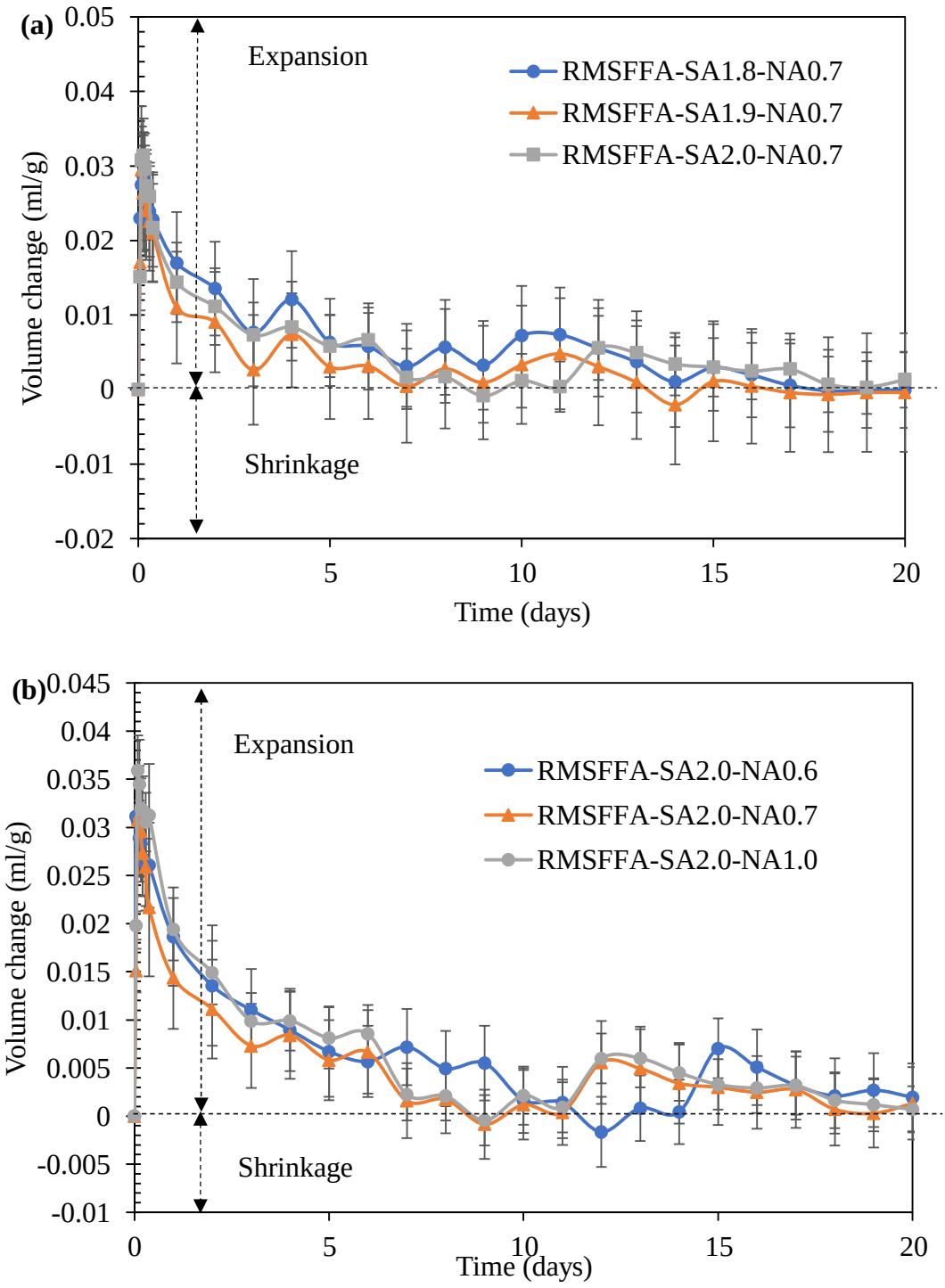

Figure 3-14 Chemical volume changes of RMSFFA geopolymers with (a) different Si/Al molar ratios and (b) different Na/Al molar ratios. The volume change data between 0-1 day are enlarged in the inset, and all the data were averaged over 10 samples.

3.3 CONCLUSIONS

A comprehensive experimental study was performed to investigate the chemical volume change behavior of geopolymers. Two different aspects are evaluated in this Chapter: (i) to verify the feasibility of the existing volume change testing procedure of OPC in the volume change test of geopolymers by using Metakaolin as the raw material, and (ii) to characterize the volume change of the more complicated geopolymer system - RMSFFA geopolymers. The following conclusions can be drawn:

For the chemical volume change behavior of MKGs:

- There are four stages: Shrinkage, expansion, shrinkage, and stable stages, which reflected different chemical reaction processes during geopolymerization. The main findings are summarized below:

- For the geopolymer synthesis recipe used in this study, the AS group showed an overall expansion behavior except the first shrinkage stage, while the DIW group presented shrinkage behavior (i.e., its final chemical volume is reduced).

- Visual inspection indicates the similar color of DIW group to that of the control group besides the surface part, while the AS group is much darker.

- The ICC results show that AS filling solution caused further geopolymerization reactions and DIW filling solution dampened the geopolymerization process of the surface portion of the precursor.

- The FTIR and SEM-EDX results also indicate that the AS group samples exhibit relatively lower main band wavenumber, high Si/Al molar ratios and high Na/Al molar ratios, which implies higher geopolymerization/polycondensation degrees that promoted by the diffusion of Na ion from AS filling solution to being-cured geopolymer precursor. The center of the main band and the Si/Al and Na/Al molar ratios of AS group are closer to these of control group for middle and bottom parts.

- Given that the much more porous DIW surface part with much larger size pores cannot be accurately characterized by the BET techniques, the total pore volume of DIW cannot be compared to the control group, although the total detected pore volume of the DIW sample is "seemingly" much closer to that of the control group. The AS group has much smaller total pore volume compared to the other two groups and shows relatively smaller pore size distribution, largely attributed to further geopolymerization by the diffusion of Na ion from AS filling solution.

- The filling solutions affect the geopolymerization of MKGs and thus their micro-characteristics and chemical volume change, largely through complex, dynamic chemical exchanges between the filling solutions and geopolymer slurry, particularly diffusion-based leaching or ingress of Na^+ and OH^-. Such chemical exchanges are governed by competing processes of geopolymerization and diffusion, which is affected in turn by the type of raw materials, chemical composition of synthesis recipe, and chemical composition of filling solutions.

- Although an appropriate filling solution for characterizing chemical volume change of geopolymer has not been identified, this study sheds light on the fundamental processes of

how a filling solution affects geopolymerization and thus provides guidance for selecting filling solution. Ideally, an appropriate filling solution for geopolymers would be inert, non-volatile, with small molecular size, etc., for characterizing chemical volume change of geopolymer. Furthermore, an appropriate filling solution should suppress potential ion exchanges between filling solutions and geopolymer precursor.

- For MKGs investigated in this study, a total monitoring time of 20 days is adequate to capture their chemical volume change; different monitoring time is likely required for other geopolymer systems that have different rate and kinetics of geopolymerization.

For the chemical volume change behavior of RMSFFA geopolymers:

- There are three stages: expansion, shrinkage, and stable stages. The main findings are summarized below:

- The RMSFFA geopolymers have no the initial shrinkage stage as detected on the MKGs, which might be caused by the different geopolymerization process of different raw materials.

- All the RMSFFA geopolymers experienced overall expansion regardless of the geopolymer synthesize recipes. All the recipes studied in this investigation show pretty close chemical volume change behavior. There is no clear trend of the effects of chemical compositions on the chemical volume change behavior of RMSFFA geopolymers.

- To investigate the effects of chemical compositions on the chemical volume change behavior in the future, a bigger chemical compositions range is recommended.

- For RMSFFA geopolymers investigated in this study, a total monitoring time of 20 days is adequate to capture their chemical volume change; different monitoring time is required for other geopolymer systems that have different rate and kinetics of geopolymerization.

CHAPTER IV - DURABILITY PROPERTIES OF GEOPOLYMERS

4.1. INTRODUCTION

Geopolymers have emerged as promising green alternatives to Ordinary Portland cement (OPC) because of their following advantages: low CO_2 emission during synthesis process [198, 199], mechanical strength comparable to OPC [23, 143], low shrinkage [200, 201], good resistance to acid [131, 202], and excellent fire resistance [148, 203]. Geopolymers can be produced by activating aluminosilicate materials with alkaline solution [201], such as sodium/potassium silicate, sodium hydroxide, or their mixtures. The source materials for geopolymerization are usually natural minerals and industrial wastes rich in aluminates or silicates, such as red mud [32, 141], fly ash [145-147], rice husk ask [32, 150], and the mixture of the above [126, 154].

Geopolymerization also presents a viable economic and environmentally friendly approach to recycling and reusing various industrial wastes. Red mud slurry (denoted as RMS) is the major waste in the production of alumina from the Bayer process [32-36]. The annual production of red mud slurry is estimated about 200 million tons worldwide [34, 35, 37], with an increase of 120 million tons annually [36, 38]. Due to different bauxite ore sources and refining processes, RMS has variable physical, chemical, and mineralogical properties, with a pH value of ~10 to 13 [32, 35, 39, 40]. The main compositions of RMS are iron oxide and alumina-silicate oxides. The management and reuse of RMS have been challenging because of its enormous quantity, high alkalinity, high water content, presence of various heavy metals [41], and serious disposal problems in the mining industry [33]. In recent years, many researchers focus on developing a new

way to recycling or reusing RMS, one of which is geopolymerization [36] by taking advantage of its high alkalinity and the presence of aluminosilicates. The high alkalinity can partially replace the alkaline solution in geopolymer synthesis, and aluminosilicates present in RMS can participate in and act as fillers in geopolymerization reactions. In addition, the application of geopolymerization technology in civil engineering can consume RMS in large quantities. However, based on previous studies [36, 42], the reactivity of RMS in geopolymerization at ambient conditions is poor or limited. To achieve better mechanical properties of geopolymer products, other raw materials with high reactivity in geopolymerization must be added, such as metakaolin or fly ash. Class F Fly ash (denoted as FFA) is a coal combustion by-product with calcium content less than 20%. More than 750 million tons of fly ash are generated all over the world each year. Fly ash is rich in silicate and aluminates, both of which are main reactants in geopolymerization processes. Most of the aluminum plants which generate red mud also generate fly ash from their captive power plants, which make these two industrial wastes a good combination for geopolymer synthesis due to low transportation costs [46]. Red mud and fly ash-based geopolymer has been synthesized by a number of researchers in recent years [41, 47]; however, RMS still needs to be dried and ground to powders prior to geopolymer synthesis, which costs more than directly using RMS in geopolymer synthesis.

Although mechanical properties of geopolymers synthesized from the mixture of red mud and FFA have been confirmed in the laboratory by a number of researchers [47, 126-130], their durability under different conditions needs to be investigated before it can be used in civil engineering applications. Generally speaking, geopolymers are usually more durable compared to conventional Portland cement concrete. However, the durability of specific geopolymer is not always ensured for the following reasons: 1. For geopolymers synthesized from industrial wastes,

their variable chemical compositions might have negative effect on their durability; and 2. different synthesis conditions (e.g., chemical composition of raw materials and curing conditions) can result in different mechanical properties and durability of the resulting geopolymers. The durability of red mud-fly ash based geopolymer in sulfuric acid and deionized water was studied by the authors' group [131], which confirmed that red mud-FFA based geopolymer has a good resistance to sulfuric acid and deionized water and is comparable to cement. However, its F-T resistance has not been systematically investigated. F-T often causes damages to concrete structures in cold areas and undermines their long-term performance [132]. When the critically saturated concrete is subjected to temperature fluctuating above and below freezing, the freezing front continuously sucks water from the adjacent region and makes the ice lens get bigger and bigger, which results in repeated loss of concrete surface and deterioration of its mechanical properties [133]. Good F-T resistance of various geopolymers was confirmed by few laboratory studies [132, 134-139]. Sun and Wu [134] and Li et al. [138] investigated the F-T durability of fly ash-based geopolymer mortar and geopolymer paste. Compared to OPC, both of the geopolymer paste and geopolymer mortar have good F-T resistance, in light of the small deterioration in their mechanical strength in the range of 5% to 20% relative to their respective initial strength after subjected to 15 and 300 F-T conditioning cycles, respectively. F-T resistance of fluidized bed combustion bottom ash-based geopolymers and coal bottom ash-based geopolymers were investigated by Slavik et al. [135] and Topcu et al. [136], respectively. Almost all of the samples were reported to have good F-T resistance after subjected to 50 and 100 F-T conditioning cycles, respectively, with less than 20% reduction in compressive strength compared to the unconditioned specimens. A similar study conducted by Topcu et al. in 2014 [137] indicates that coal bottom ash-based geopolymer lost only 6.77% of its initial strength after 30 F-T cycles. Zhang et al. [140] reported that the PVA short

fiber reinforced metakaolin and fly ash-based geopolymer mortar composites have excellent F-T resistance, based on their high remaining impact resistance after subjected to 20 F-T cycles. In most of the above studies, F-T durability is inferred from the changes in mechanical properties of geopolymer specimens before and after F-T conditioning cycles. However, the changes in microstructure, chemical bonding, and pore characteristics of geopolymers during F-T conditioning processes have not been systematically examined, neither are the fundamental processes underlying the deterioration of mechanical properties of geopolymer samples during the conditioning. In addition, the effects of synthesis factors (e.g., curing conditions, Si/Al and Na/Al molar ratios, water content, and pH values) on F-T durability of geopolymers have not been studied.

In this study, F-T durability of RMSFFA geopolymers was investigated, with emphasis on understanding the deteriorating mechanisms and processes underlying F-T conditioning. RMSFFA geopolymer specimens were prepared under different chemical compositions and different curing conditions. then subjected to 50 F-T conditioning cycles. F-T durability of RMSFFA samples was evaluated based on the changes in their mechanical properties (unconfined compressive strength (UCS), Young's modulus, and failure strain) at various F-T cycles. The changes in their chemical bonding, mineralogy, and pore characterization were also investigated with Fourier transform infrared spectroscopy (FTIR), X-ray diffractometer (XRD), and Brunauer–Emmett–Teller (BET) testing, respectively, to shed light on the mechanisms underlying F-T conditioning induced damage to RMSFFA samples.

4.2. MATERIALS AND METHODOLOGY

4.2.1 Materials

A mixture of FFA and RMS was used to synthesize geopolymers. RMS was used in geopolymer synthesis as received from Alcoa World Alumina, LLC. FFA was provided by Headwaters Resources Inc. The physical properties and chemical compositions of RMS and FFA are shown in **Table 4-1** and **Table 4-2**, respectively. The pH value and water content of RMS are ~14 and 74%, respectively. RMS also contains traceable amount of soluble Na, Si, and Al. The main components of FFA are SiO_2 and Al_2O_3, whose amorphous phases are the main reactive constituents in geopolymerization. FFA also contains appreciable amount of Fe_2O_3 and some trace elements. In addition, the average particle size (D_{50}) of FFA is 16 μm. A mixture of 50% NaOH and sodium silicate solution was used as the alkaline activator to synthesize geopolymer.

Table 4-1 Chemical compositions of Class F fly ash (wt.%) provided by the supplier.

SiO_2	Al_2O_3	Fe_2O_3	SO_3	CaO	K_2O	MgO	Na_2O	Moisture Content	Loss on ignition
59.74	27.51	4.91	0.16	1.45	2.39	1.18	0.82	0.08	2.66

Table 4-2 Physical and chemical compositions of RMS (wt.%).

Liquid contents	Solid contents	Soluble Na	Soluble Si	Soluble Al
74	26	1.97	0.00555	0.74

4.2.2 Geopolymer synthesis

While it is desirable to use RMS at a maximum amount to partially replace expensive alkaline solution, too much red mud will result in lower strength of the resulting geopolymer sample due to its poor reactivity [155]. In light of the consideration, a mass ratio of 1:4 between RMS and FFA was used as the source materials for geopolymer synthesis. Chemical compositions of the source materials proved critical to synthesizing geopolymer with high mechanical strength. Based on the previous studies in the literature and by the authors' group [47, 131], a nominal Si/Al molar ratio of 2.0 and a Na/Al molar ratio of 0.6 were adopted to prepare RMSFFA geopolymer samples to examine the effect of curing conditions on the F-T durability of RMSFFA (curing temperature and curing time). Nominal Si/Al molar ratio (1.8, 1.9, and 2.0) and nominal Na/Al molar ratio (0.6, 0.7, and 1.0) were used to prepare RMSFFA geopolymer samples to examine the effect of chemical compositions on the F-T durability of RMSFFA. In addition, it was found that too much water present in geopolymer precursor leads to the residual water existing in the form of hydroxyl in the resulting geopolymer [160], which is unfavorable to strength development of geopolymers. Accordingly, a water content of 25% was used in the geopolymer synthesis, which was the lowest possible water content while adequate workability was also maintained for sample preparation. The chemical compositions of geopolymer precursor were controlled by adjusting relative proportions of the source materials and the alkaline activator solution. The sample ID, mix design, and curing conditions of RMSFFA geopolymer specimens are listed in **Table 4-3** and **Table 4-4**. The sample set ID was named as follows: raw materials - Si/Al (SA) mole ratio - Na/Al (NA) mole ratio - curing temperature - curing time; RT, 50C, and 80C stand for curing temperatures of room temperature, 50°C, and 80°C, respectively; and 14D and 28D stand for 14 days or 28 days curing time periods.

The alkaline activator solution was pre-prepared and then cooled down to room temperature for later use. RMS and FFA were firstly mixed at the pre-determined ratio with a mechanical mixer, followed with the addition of the alkaline activator solution, and the whole precursor was stirred for 30 minutes to ensure thorough mixing. The slurry was poured into pre-made cylindrical molds with dimensions of 2 inch (diameter) x 4 inch (height), and vibrated for 10 minutes to remove the air bubbles. All of the samples were sealed in plastic bags with duct tape. Samples were placed in a chamber at a relative humidity of 40% - 50% for curing at room temperature. For the samples cured at elevated temperatures (i.e., 50°C and 80°C), they were placed in the oven and taken out after 7 days and 1 day for 50°C and 80°C, respectively, which were further cured at ambient conditions until respective final curing time was reached. All the samples were demolded after 14-day curing, and then the 14-day cured samples were taken out for mechanical property testing while the 28-day cured ones were continuously cured at ambient temperature for another 14 days. Detailed sample preparation process can be referred to a previous study from the authors' group [47]. 15 specimens were prepared for each sample set, 12 of which underwent F-T conditioning which is detailed in the following section, while three of which were tested without F-T conditioning as the control group.

Table 4-3 Summary of mix design and curing conditions of RMSFFA geopolymer specimens used for F-T durability tests (the effects of curing conditions on F-T durability).

Sample set ID	Curing time (days)	Curing temp (°C)	Si/Al (mol)	Na/Al (mol)	L/S (weight ratio)	Water Content (wt.%)
RMSFFA-SA2.0-NA0.6-RT-14D	14	RT(~23)	2.00	0.60	0.53	25
RMSFFA-SA2.0-NA0.6-RT-28D	28					
RMSFFA-SA2.0-NA0.6-50C-14D	14	50				
RMSFFA-SA2.0-NA0.6-50C-28D	28					
RMSFFA-SA2.0-NA0.6-80C-14D	14	80				
RMSFFA-SA2.0-NA0.6-80C-28D	28					

Table 4-4 Summary of mix design and curing conditions of RMSFFA geopolymer specimens used for F-T durability tests (the effects of chemical compositions on F-T durability).

Sample set ID	Curing time	Curing temp	Si/Al (mol)	Na/Al (mol)	L/S (weight	Water Content	Objectives
RMSFFA-SA2.0-NA0.6	14/28	50	2.0	0.6	0.53	25	Effect of Na/Al molar ratio
RMSFFA-SA2.0-NA0.7			2.0	0.7	0.57	25	
RMSFFA-SA2.0-NA1.0			2.0	1.0	0.70	27	
RMSFFA-SA1.8-NA0.7			1.8	0.7	0.50	25	Effect of Si/Al molar ratio
RMSFFA-SA1.9-NA0.7			1.9	0.7	0.53	25	
RMSFFA-SA2.0-NA0.7			2.0	0.7	0.57	25	

4.2.3 F-T conditioning

In each sample set, the three specimens without undergoing F-T conditioning were the control group and denoted as F-T ‘cycle 0’. The other twelve samples were immersed in deionized water for 30 minutes at RT, and then all the samples underwent F-T conditioning for various cycles (up to 50). According to ASTM C666, F-T conditioning was carried out in two incubators, with their temperatures kept at -10°C and 4°C for the freezing and thawing processes, respectively. An F-T cycle comprises the following two steps: i. freezing the samples in the air at -10°C incubator for two and a half hours; and ii. thawing the samples by soaking in the deionized water at 4°C incubator for one and a half hours. Diameter, height, and weight of the samples before and after the conditioning were measured throughout the conditioning process.

4.2.4 Mechanical and Microstructural Characterization

Unconfined compressive strength (UCS) tests were conducted on RMSFFA geopolymer samples after various F-T conditioning cycles using an Instron loading machine to determine their UCS, failure strain and Young’s modulus. A constant loading rate of 0.5 in./min was used, which was relatively high but was chosen for the main purpose of comparing the relative trend in mechanical properties among the samples. In addition, some small pieces were collected from the crushed samples after the strength test for subsequent characterization of their chemical bonding, mineralogy, and pore characteristics. The external surface of the samples was avoided since they might be carbonated during exposing to the air. Prior to the characterization tests, the selected sample pieces were pre-frozen by liquid nitrogen right after the strength test and then subjected to freeze-drying in order to prevent the samples from any further geopolymerization reactions. Some of the small pieces were ground to powder for FTIR, XRD, and BET testing. The chemical bonding

information was inferred from the FTIR spectra obtained with a BrukerOptics Vetex70 FTIR spectrometer using transmittance mode in the range of 500~1600 cm^{-1} at a resolution of 2 cm^{-1}. The mineralogical compositions were determined with a Rigaku Geigerflex X-ray powder diffractometer (XRD) using a CuKα radiation with a voltage of 37.5 kV and a current of 25 mA at 1 sec/step to obtain the XRD spectra. The XRD spectra were collected from 5° to 90° 2θ at 0.02 °/step and analyzed with MDI Jade 5.0. Specific surface area, accumulative pore volume and pore characteristics were tested with the instrument ASiQ IQ TPX from Quantachrome Instruments and analyzed with Non-Local Density Functional Theory (NLDFT) method.

4.3. RESULTS AND DISCUSSION

4.3.1 Effect of Curing Conditions

4.3.1.1 Changes in Physical and Mechanical Properties of RMSFFA Geopolymer during F-T Conditioning

Changes in weight of the samples after F-T conditioning are presented in **Figures 4-1 (a) and (b)**, which is normalized by their respective initial values prior to F-T conditioning and is plotted versus the number of F-T conditioning cycles. **Figures 4-1 (a)** and **(b)** indicate that both curing time and curing temperature affect the change in weight during F-T conditioning. For the sample set cured at RT, both 14- and 28-day cured samples lost weight during the F-T conditioning, especially those cured for 28 days losing much more weight (over 20%) and collapsed at the 44^{th} F-T cycle. Therefore there was no data collected for this sample set afterward. On the other hand, the normalized weight of the samples cured at higher temperatures (i.e., 50 and 80 °C) increases regardless of the curing time. The difference in the weight variation among the conditioned

samples might be attributed to the difference in their strength development at different curing temperatures, with the latter being discussed in the following sections.

The variation of UCS for the samples after various F-T conditioning cycles is presented in **Figures 4-1 (c)** and **(d)**, for 14 and 28 days of curing, respectively. For the sake of clarity, the influence of curing time period is discussed first, followed by the effect of curing temperature. Influence of curing time period: For samples cured for 14 days (**Figure 4-1(c)**), there is no strong or obvious trend of mechanical strength of the samples vs. F-T conditioning cycles, except that the UCS values of the conditioned samples fluctuate by different magnitudes. Yet, the remaining mechanical strength of all the conditioned samples after 50 F-T cycles was close to their respective initial values or did not deteriorate appreciably, which indicates a good F-T resistance. Compared to their 14-day cured counterparts, the 28-day cured samples had higher initial strength values and experienced a more pronounced strength decrease in general, especially from 5 to 20 F-T cycles, regardless of the curing temperature, as shown in **Figure 4-1(d)**. Although more strength decrease was observed on the 28-day cured samples, the sustained strength values of 50°C and 80°C cured samples after 50 F-T cycles were still high and around 9 MPa. The samples cured for 14 days had less strength decrease than their 28-day cured counterparts during F-T conditioning, except RT cured samples, which even had a strength increase compared to the original value. This is likely to be because 14-day cured samples still had strength development during the F-T conditioning which offset to some extent the negative effects caused by the F-T conditioning, whereas the 28-day cured samples might have already finished most of the strength development prior to F-T conditioning, with the strength decrease likely being caused by the micro-cracks formation introduced during the F-T cycling and the partial geopolymer gel dissolution during the soaking [131]. Influence of curing temperature: Because of relatively lower reaction rate and higher

remaining water content, RT cured samples for both 14 and 28 days had relatively low initial strength, and thus their sustained UCS values after the F-T conditioning are also low. The samples cured at 50°C had a better F-T resistance compared to the other two groups, due to their overall relatively higher average UCS values (all above 10 MPa). This is probably because 50°C is a more favorable curing temperature that facilitated both the dissolution of the raw materials and geopolymerization processes during sample synthesis, which promotes the strength development. However, at the even higher temperature of 80°C, the samples had lower compressive strength compared to the 50°C counterpart. This might be caused by the formation of internal cracks during the curing process and the faster moisture evaporation, which results in lacking enough water content to support geopolymerization processes at later stages. Similar findings were reported in other studies [121, 161, 204]. Therefore, 14 days and 50°C are more favorable curing conditions for synthesizing RMSFFA geopolymers to achieve both higher initial mechanical strength and better F-T durability.

Mechanical properties, including UCS, failure strain, and Young's modulus of 14- and 28-day cured samples before and after 50 F-T conditioning cycles are replotted in **Figures 4-2(a)-(c)** to better illustrate the sustained mechanical properties and thus the F-T resistance. In general, the higher temperature (i.e., 50 and 80 °C) cured samples had a higher average Young's modulus than that of RT cured samples. Similar to the change in UCS (**Figure 4-2(a)**), the average Young's modulus of the samples without F-T conditioning is higher than that of the samples after 50 F-T cycles, except RT and 80°C cured samples for 14 days (**Figure 4-2(c)**). In light of the average failure strain (see **Figure 4-2(b)**), no appreciable changes in 50°C and 80°C cured samples for 28 days, and 14-day cured samples became more ductile after 50 F-T conditioning cycles compared to the one without F-T conditioning. Under the same curing temperature (i.e., 50°C), the 14-day

cured samples are more ductile than their counterparts cured for 28 days, except the samples cured at 80°C. Additionally, samples cured at RT became more brittle after F-T conditioning cycles, regardless of the curing time.

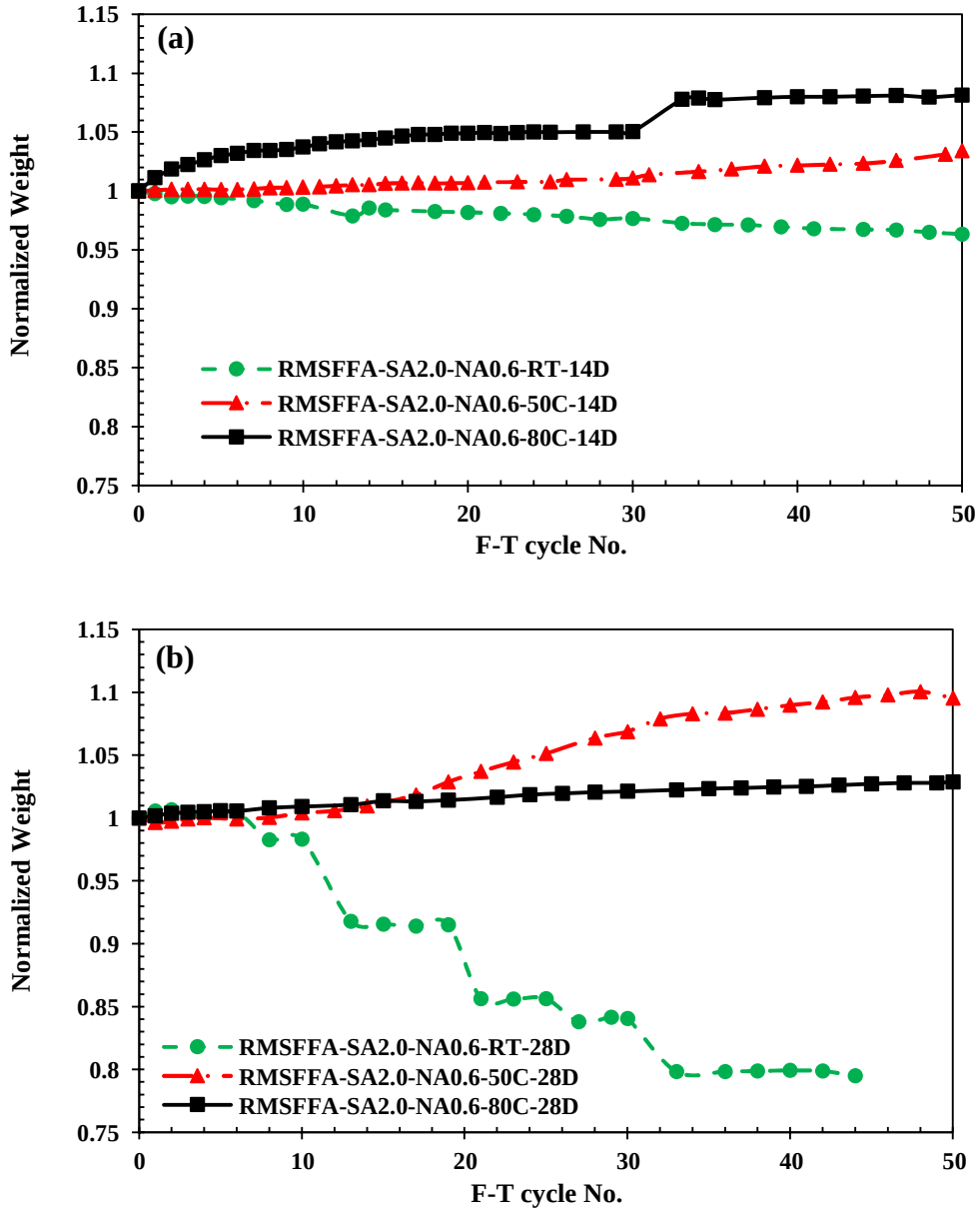

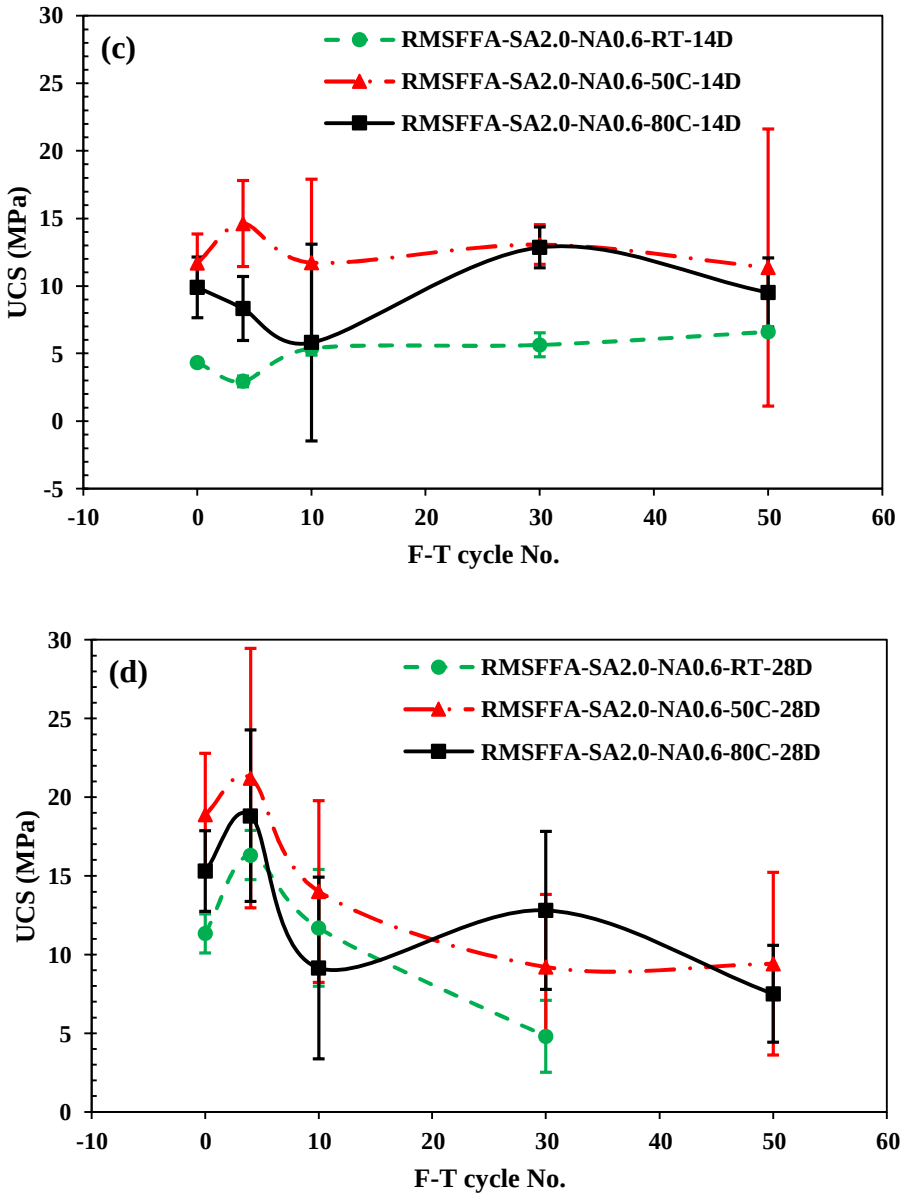

Figure 4-1 Variation of normalized weight and UCS of 14-day cured (a) (c) and 28-day cured (b) (d) RMSFFA geopolymers with different curing temperature during F-T conditioning.

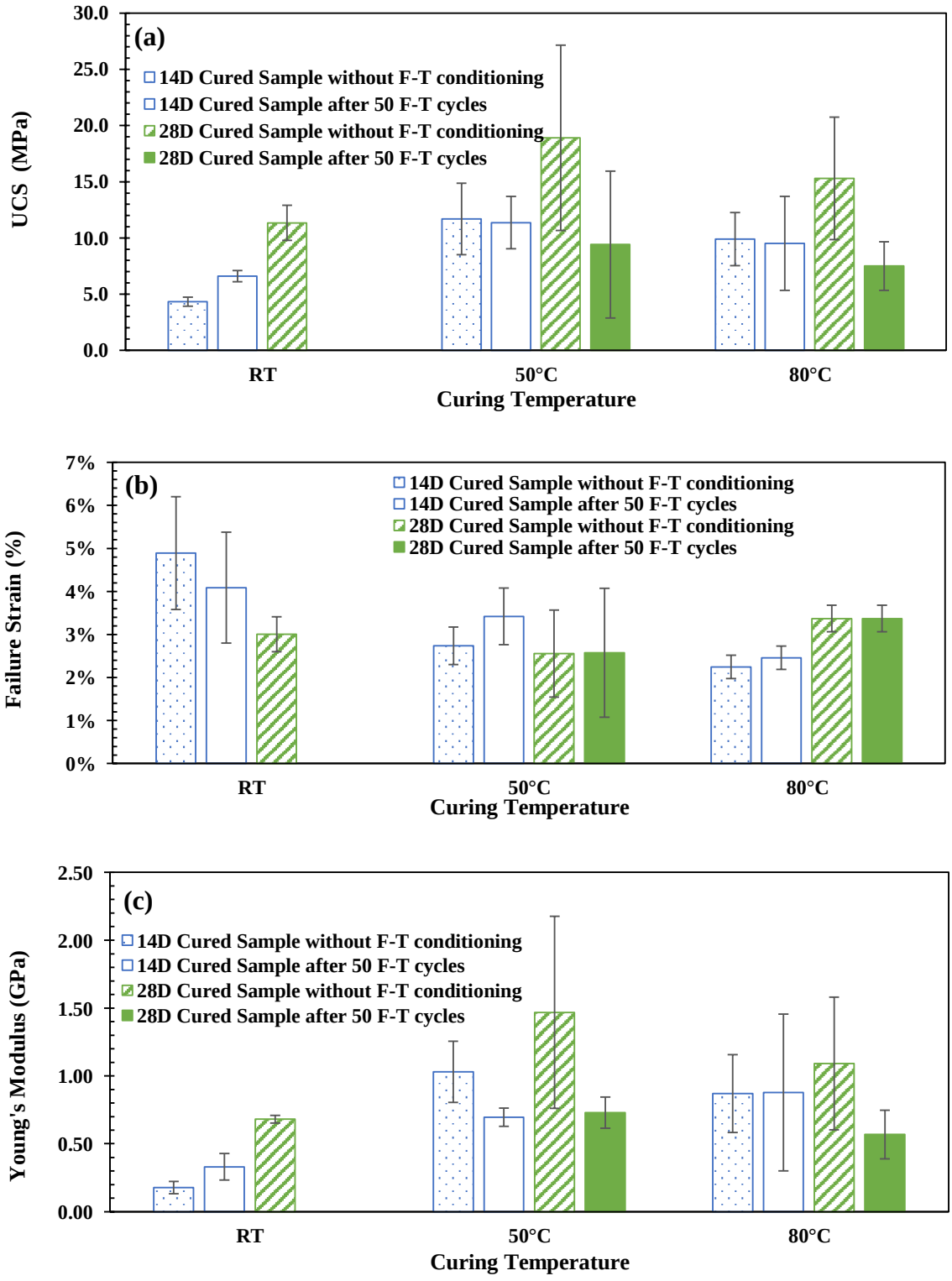

Figure 4-2 Comparison of mechanical properties of RMSFFA geopolymer samples before and after 50 F-T conditioning cycles: (a) UCS (b) ε_f (c) E

4.3.1.2 Chemical Bonding, Mineralogy, and Pore Characteristics Changes of RMSFFA Geopolymers during F-T Conditioning

FTIR spectra of the geopolymer samples after subjected to various F-T conditioning cycles were acquired to shed light on the mechanisms underlying the deterioration during F-T conditioning. **Figures 4-3(a)** and **(b)** show the variation of FTIR spectra of the samples cured for 14 and 28 days, respectively, after various F-T conditioning cycles. As reported by numerous studies in the literature [162-165], the FTIR spectra in the region of 1300-900 cm-1 are often used to characterize geopolymer gels, which represent the Si-O-T (T is Si or Al) asymmetric stretching vibration band, also called the "main band". From **Figure 4-3(a)**, the main band of 14-day cured samples became narrower with the increase in F-T cycles. This is likely caused by the continuous increase of silicates or substitution of tetrahedral Al in the gel structure [205-208]. The main band also slightly shifted to a relatively higher wavenumber, which might be attributed to (i) more Si inclusions were formed and joined into the geopolymer gels, which was also observed in Catauro's study [209]; or/and (ii) dealumination and [164] depolymerization processes caused by F-T conditioning [131]. Then the main band shifted back to a lower wavenumber a little bit after 10 F-T cycles. This shifting of the main band indicates (i) the increasing substitution of tetrahedral Al in the silicate network and thus more geopolymer gels formed [165, 210]. The formation of geopolymer gels are also confirmed by the increase in intensity after 10 F-T cycles, which is also reported by Bakharev [202]; or/and (ii) the increase in nonbridging oxygens on silicate sites [131, 165, 206-208, 211-214]. However, the spectra of 28-day cured samples (**Figure 4-3(b)**) exhibit a different trend throughout F-T conditioning processes. Compared to the counterparts cured for 14 days, the main band of the samples cured for 28 days is narrower prior to F-T conditioning, which means higher extent of geopolymerization and is consistent with the fact that higher unconfined compressive

strength was achieved in 28-day samples (see **Figures 4-1(c)** and **(d)**) prior to F-T conditioning. As the F-T conditioning continued, the peak of the main band fluctuated by a very small range of 7 cm^{-1}, while the peak of 14-day cured samples changed by a range of 12 cm^{-1} and started with a lower wavenumber of 985 cm^{-1}. This is mainly due to the partial dissolution and rearrangement of geopolymer gel structure. Similar trends in FTIR spectra were observed in samples cured at RT and 80°C (Figures are not shown here for clarity). Besides the main band, the bands around 790 cm^{-1}, 760 cm^{-1} and 670 cm^{-1} are attributed to AlO_4 vibrations [202], crystalline phase of quartz [215], and the structural units (i.e., aluminosilicate ring and cage structures) [163], respectively. For 14-day cured samples at F-T 'cycle 30', the band around 790 cm^{-1} disappeared and a new band around 670 cm^{-1} was observed, indicating the formation of geopolymer gels. Then the band at 670 cm^{-1} disappeared and the band at 790 cm^{-1} reappeared at 'cycle 50', illustrating the partial dissolution of geopolymer gels at the later stage of the conditioning. Both bands were observed in all the 28-day cured samples, which suggests that the 28-day cured samples have finished most of the geopolymerization process before the F-T conditioning, and no appreciable geopolymerization reactions taking place during the F-T conditioning.

To investigate whether the changes in chemical bonding and mechanical properties of the samples during F-T conditioning correlate with each other, the main band peak of the samples is re-plotted versus F-T conditioning cycles, along with the corresponding unconfined compressive strength (see **Figures 4-3(c)** and **(d)**). From both **Figures 4-3 (c)** and **(d)**, the UCS was changing in an opposite way to the change of the main band (i.e., UCS decreases as the main band shifts to higher wavenumber and vice versa) except between F-T conditioning cycles 0-4 and 30-50 in 14-day cured samples. This is because that the 14-day cured samples likely underwent the combined effect of continuing geopolymerization and structural deterioration during F-T conditioning, while

the 28-day cured samples were most likely subjected to deteriorating effect during F-T conditioning. Similar trends were also found in the samples cured at RT and 80°C, with some differences that might be attributed to the sample variations.

Partial geopolymer gel dissolution and further geopolymer gel development during F-T conditioning were also observed with the XRD spectra. XRD spectra of F-T conditioned geopolymer samples are shown in **Figure 4-4**, which include samples cured at 50°C for 14 days (**Figure 4-4(a)**) and 28 days (**Figure 4-4(b)**), respectively. The spectra in the range of 10°-50° 2θ are presented since no characteristic peaks were detected in the rest of diffraction angles. The main crystals detected in F-T conditioned geopolymer samples are quartz and mullite. Overall, there were no minerals generated or disappeared, indicating that there were no crystals dissolved during the F-T conditioning. The hump in the range of 15° - 40° 2θ is the typical XRD pattern of the amorphous gel in geopolymer, which can be observed in all the XRD spectra of geopolymer samples in this study and is specifically indicated by two dashed lines on each spectrum in Figure 4-4. For 14-day cured samples, the hump of spectra at F-T 'cycle 0' between 15° and 33° 2θ, shifted to lower 2θ value at F-T 'cycle 4' and 'cycle 10', which implied the partial dissolution of geopolymer gels [131]. Then the hump slightly shifted to a higher 2θ degree at F-T 'cycle 30' and went broader at F-T 'cycle 50', which elucidated that there were geopolymer gels forming during the F-T conditioning. For 28-day cured samples, the hump shifted back and forth within a very small range and did not follow any clear trend, which is due to the partial dissolution and rearrangement of geopolymer gel structure. This is generally consistent with UCS and FTIR results described in previous sections.

The pore size distributions and total pore volume of RMSFFA geopolymers vs. F-T conditioning cycles are plotted in **Figure 4-5**. Due to the limited access to the BET testing device,

only one representative sample of each batch was tested for its pore size distribution. The pore size distribution of 14-day cured sample at 'cycle 0' is in the range of 1.51 – 17.99 nm, with a dominant pore size (i.e., the pore size with the largest pore volume) of around 7.66 nm (**Figure 4-5 (a)**). The pore size distribution did not change much at F-T 'cycle 4', however, it shifted to smaller pores with no dominant pore size at F-T 'cycle 10' and 'cycle 30'. Concomitantly, the 14-day cured samples exhibited appreciable decrease in total pore volume. This was likely attributed to the formation of geopolymer gel during this early stage of F-T conditioning. However, after the samples subjected to more than 10 F-T conditioning cycles, their total pore volume started to increase and exceeded the initial pore volume without F-T conditioning. At F-T 'cycle 50', the pore size distribution shifted back to larger pores with a dominant pore size of 7.66 nm. This change in pore volume during the later stage of F-T conditioning was likely attributed to partial gel dissolution caused by F-T conditioning. For 28-day cured samples (**Figure 4-5 (b)**), the pore size distributions of samples did not have appreciable changes in pore size range or dominant pore size before 30 F-T conditioning cycles. However, a tendency to form a bimodal pore size distribution was observed, especially after 10 F-T cycles. The bimodal distribution was explained as the formation of larger volume of interconnected pores, as reported by P. Duxson et al. [23]. Then the pore size distribution shifted into larger pore size at F-T 'cycle 50'. The 28-day cured samples had higher total pore volume (higher air-content) (see **Figure 4-5(c)**), which was likely due to the cracking formation during longer curing period. In the meantime, the 28-day cured samples exhibited relatively smaller change in total pore volume, which indicates that there was no geopolymer gel formation during F-T conditioning, and the micro-cracks formation and the partial dissolution of geopolymer gel caused by F-T conditioning likely resulted in the interconnection of smaller pore into larger ones. The variation of pore volume and pores size

distribution of both 14- and 28-day cured samples is consistent with the variation of their mechanical strength and the shift of the main band's wavenumber during F-T conditioning.

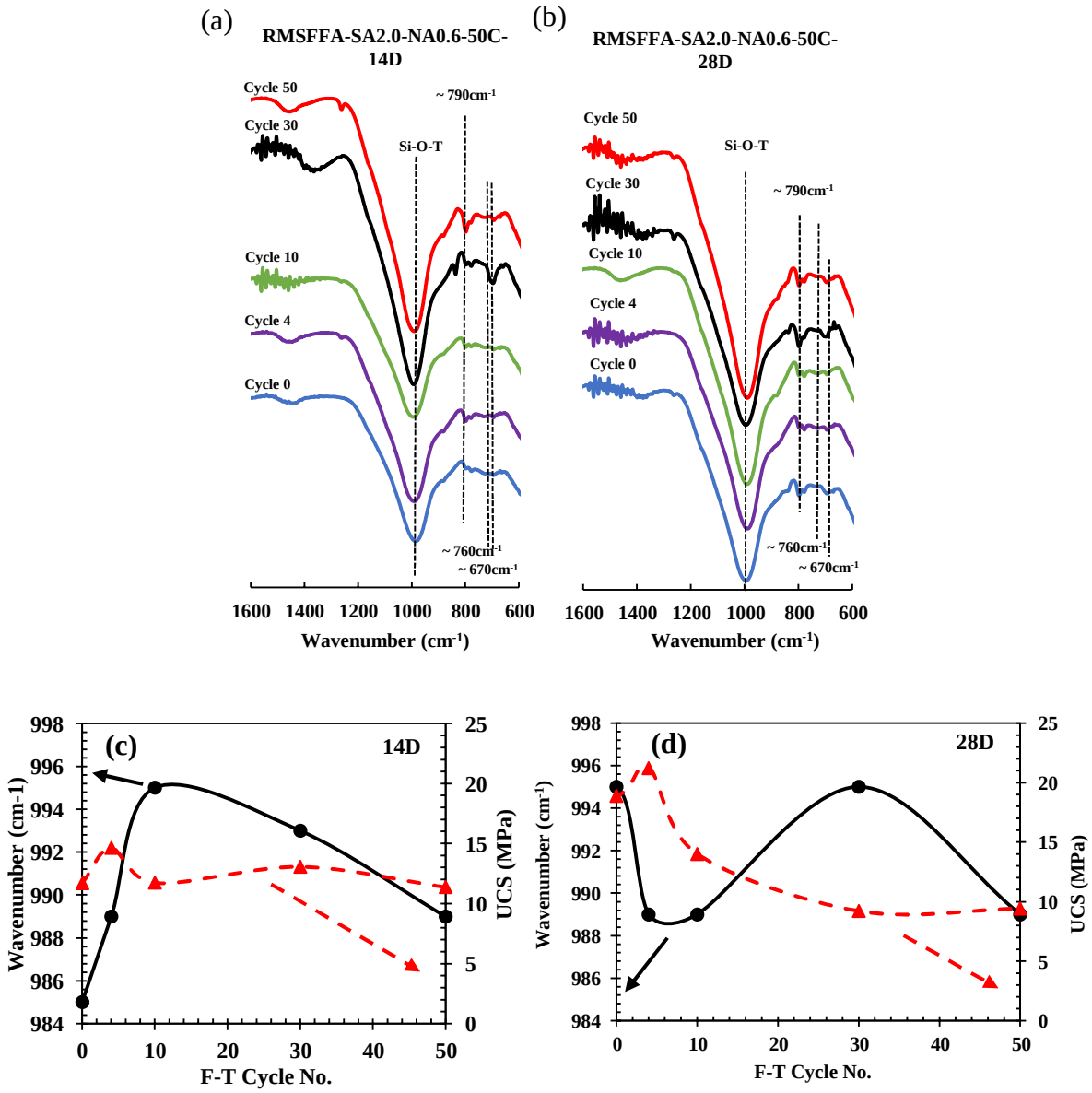

Figure 4-3 Changes in FTIR spectra of 14-day (a) and 28-day (b) after subjected to various F-T conditioning cycles; Wavenumber of asymmetric stretching vibration band (Si-O-T band (T is Si or Al)) and UCS versus F-T cycle number of (c) 14-day and (d) 28-day cured geopolymer samples at various F-T cycle (up to 50).

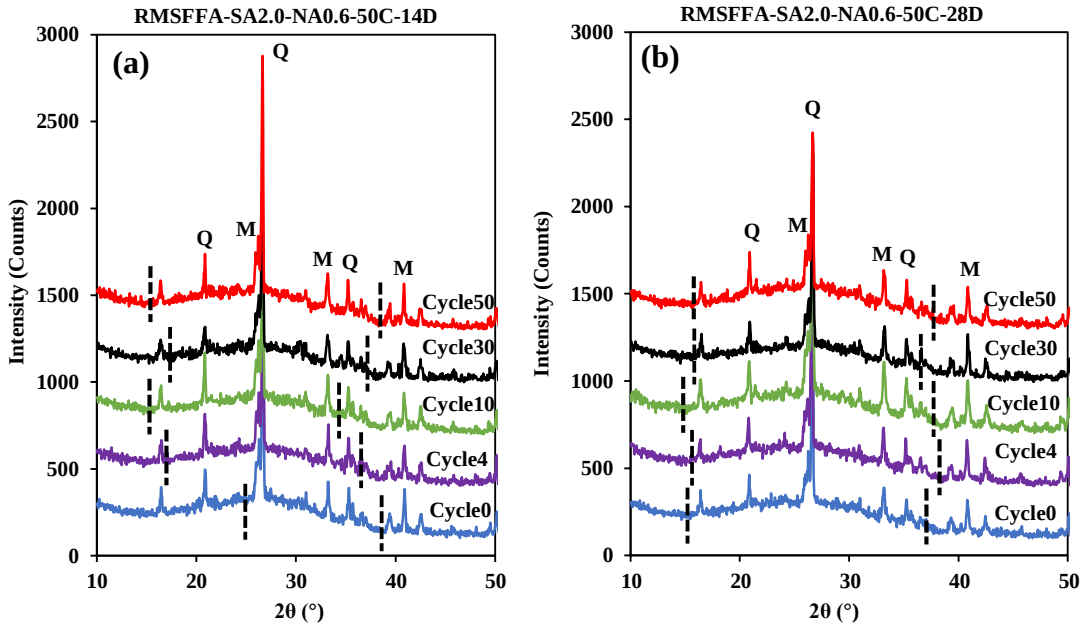

Figure 4-4 XRD spectra of 14-day (a) and 28-day (b) cured RMSFFA geopolymer samples cured at 50°C after various F-T conditioning cycles in the range of 10-50° 2θ (Q: Quartz, and M: Mullite)

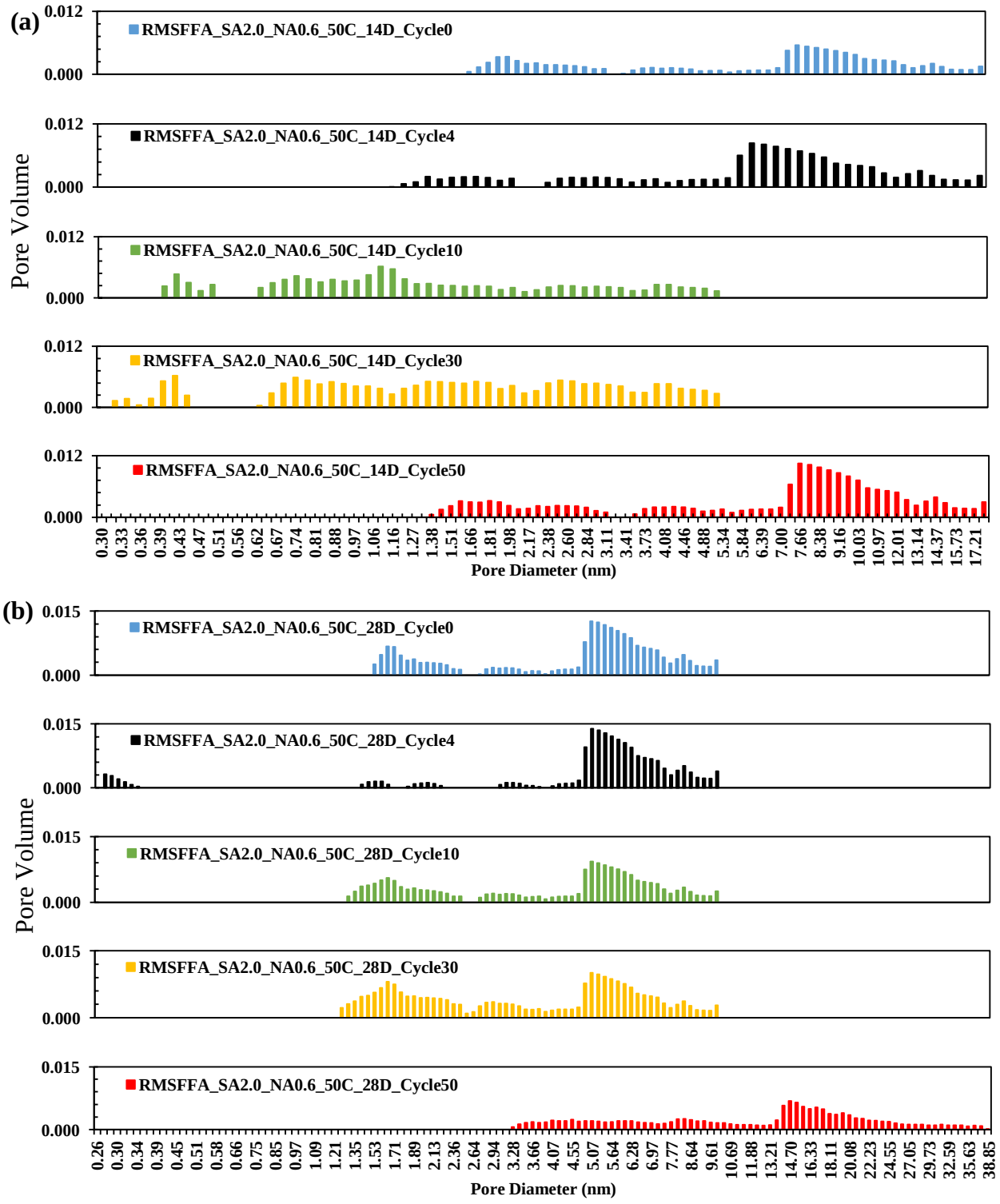
(a)
RMSFFA_SA2.0_NA0.6_50C_14D_Cycle0
RMSFFA_SA2.0_NA0.6_50C_14D_Cycle4
RMSFFA_SA2.0_NA0.6_50C_14D_Cycle10
RMSFFA_SA2.0_NA0.6_50C_14D_Cycle30
RMSFFA_SA2.0_NA0.6_50C_14D_Cycle50
0.012
0.000
Pore Volume
0.30 0.33 0.36 0.39 0.43 0.47 0.51 0.56 0.62 0.67 0.74 0.81 0.88 0.97 1.06 1.16 1.27 1.38 1.51 1.66 1.81 1.98 2.17 2.38 2.60 2.84 3.11 3.41 3.73 4.08 4.46 4.88 5.34 5.84 6.39 7.00 7.66 8.38 9.16 10.03 10.97 12.01 13.14 14.37 15.73 17.21
Pore Diameter (nm)
(b)
RMSFFA_SA2.0_NA0.6_50C_28D_Cycle0
RMSFFA_SA2.0_NA0.6_50C_28D_Cycle4
RMSFFA_SA2.0_NA0.6_50C_28D_Cycle10
RMSFFA_SA2.0_NA0.6_50C_28D_Cycle30
RMSFFA_SA2.0_NA0.6_50C_28D_Cycle50
0.015
0.000
Pore Volume
0.26 0.30 0.34 0.39 0.45 0.51 0.58 0.66 0.75 0.85 0.97 1.09 1.21 1.35 1.53 1.71 1.89 2.13 2.36 2.64 2.94 3.28 3.66 4.07 4.55 5.07 5.64 6.28 6.97 7.77 8.64 9.61 10.69 11.88 13.21 14.70 16.33 18.11 20.08 22.23 24.55 27.05 29.73 32.59 35.63 38.85
Pore Diameter (nm)

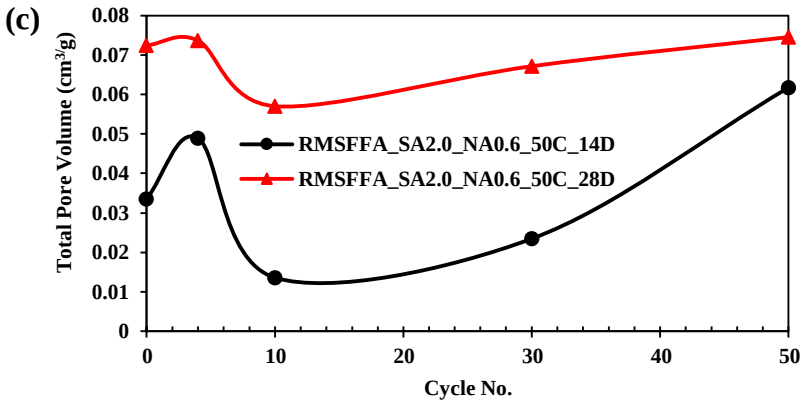

Figure 4-5 Pore size distributions of RMSFFA geopolymers cured for (a) 14 and (b) 28 days at 50°C, and (c) change in total pore volume of 14- and 28-day cured samples at 50°C with various F-T conditioning cycles.

4.3.2 Effect of Chemical Compositions of RMSFFAs

As discussed in the previous section, the 14-day (curing time) and 50°C (curing temperature) are the more favorable curing conditions used in this study. Therefore, different RMSFFAs with different chemical composition cured at 50°C were prepared to study on the effect of chemical composition on the F-T performance of RMSFFA geopolymers. Although 14-day is a more favorable curing time, the results of 28-day cured samples are listed below to shed light on the effect of curing time on the F-T performance of RMSFFA geopolymers.

4.3.2.1 Changes in Physical and Mechanical Properties of RMSFFA Geopolymer during F-T Conditioning

For the sake of clarity, the influence of Si/Al molar ratio is discussed first, followed by the effect of Na/Al molar ratio.

Influence of Si/Al molar ratio: Changes in weight of the samples with different Si/Al molar ratios after F-T conditioning are presented in **Figures 4-6 (a)** and **(c)**, which are normalized by their respective initial values prior to F-T conditioning and are plotted versus the number of F-T conditioning cycles. **Figures 4-6 (a)** and **(c)** indicate that Si/Al molar ratio has not much influence on the change in weight of RMSFFA geopolymers regardless of the curing time. The normalized weight of all the samples increased regardless of the curing time; however, there is no clear trend of the weight change with the Si/Al molar ratio changes. The sample with Si/Al molar ratio of 2.0 experienced the smallest weight change regardless of the curing time. The weight gain of 28-day cured samples (<10%) is larger than the ones cured for 14 days (<5%), which might be due to the strength development in 14-day cured sample as discussed in **Section 4.3.1**. The variation of UCS for the samples after various F-T conditioning cycles is presented in **Figures 4-6 (b)** and **(d)**, for 14 and 28 days of curing, respectively. In general, there is no strong or obvious trend of mechanical strength of the samples vs. F-T conditioning cycles, except that the UCS values of the conditioned samples fluctuate by different magnitudes regardless of the curing time. The sample with Si/Al molar ratio of 2.00 is much higher than the other two groups for both initial and the sustained strength after 50 F-T cycles, which is more obvious for 14-day cured samples. Mechanical properties, including UCS, failure strain, and Young's modulus of 14- and 28-day cured samples with different Si/Al molar ratios before and after 50 F-T conditioning cycles are replotted in **Figures 4-7(a)-(c)** to better illustrate the sustained mechanical properties and thus the F-T resistance. In general, with increasing the Si/Al molar ratios, both initial strength and sustained strength after 50 F-T cycles increased regardless the curing time (**Figure 4-7(a)**). However, with higher Si/Al ratio, the samples experienced more strength loss after F-T conditioning. This might be attributed to the higher geopolymerization reaction rate with high Si/Al molar ratios, which

finished the strength development much faster and there is no further strength development to offset the strength loss caused by F-T conditioning. The change in average Young's modulus of 14-day cured samples (**Figure 4-7(c)**) are similar to the change in UCS, in which the Young's modulus after 50 F-T cycles is higher than the ones without F-T conditioning except the sample with Si/Al molar ratio of 2.0. The Young's modulus of Si/Al molar ratio of 2.0 decreased after 50 F-T cycles; however, the sustained Young's modulus is still high compared to other groups. The average Young's modulus of 28-day cured samples after 5- F-T cycles doesn't have appreciable change compared to the samples without F-T conditioning. In light of the average failure strain (see **Figure 4-7(b)**), samples became less ductile after 50 F-T cycles regardless of the curing time except the sample with Si/Al molar ratio of 1.8, which slightly increased in ductility after the F-T conditioning.

In conclusion, with increasing the Si/Al molar ratio, the samples have less weigh change during the F-T conditioning, higher initial and sustained UCS and Young's modulus, and become more ductile regardless of the curing time except the ductility of 28-day cured samples after 50 F-T cycles. For the samples with Si/Al molar ratio of 1.8 and 1.9, the UCS, failure strain, and Young's modulus might increase in some cases, which correspond to the lower reaction rate thus the strength development still taking place during the F-T conditioning which offset to some extent the negative effects caused by the F-T conditioning, whereas the samples with Si/Al molar ratio of 2.0 might have already finished most of the strength development prior to F-T conditioning, with the strength decrease likely being caused by the micro-cracks formation introduced during the F-T cycling and the partial geopolymer gel dissolution during the soaking.

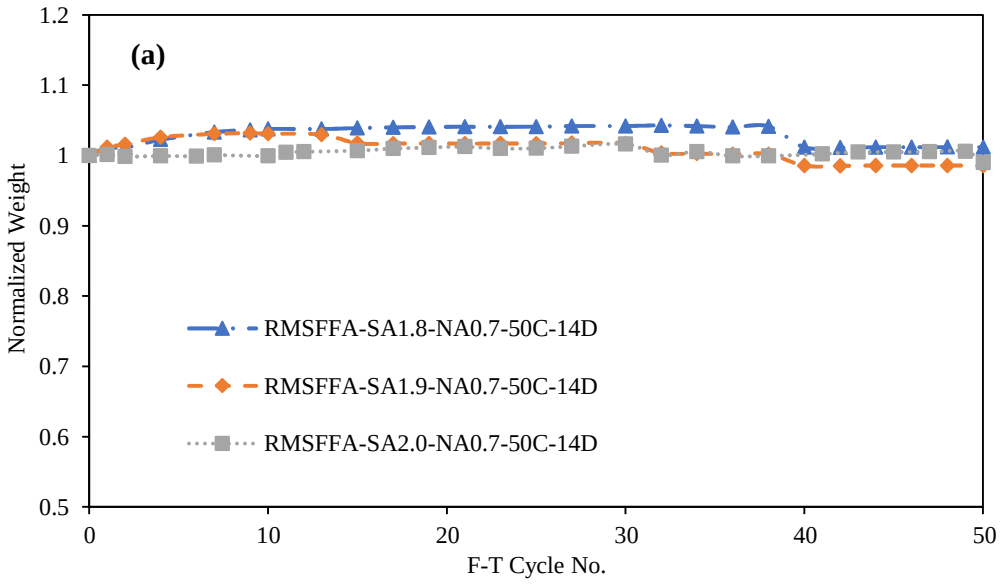
(a)
Normalized Weight
F-T Cycle No.
RMSFFA-SA1.8-NA0.7-50C-14D
RMSFFA-SA1.9-NA0.7-50C-14D
RMSFFA-SA2.0-NA0.7-50C-14D

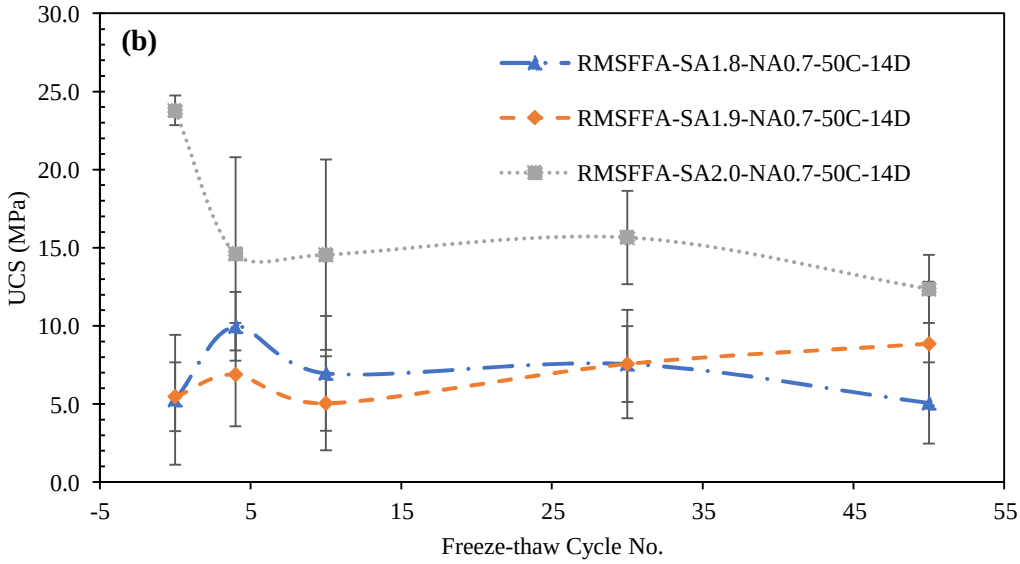
(b)
UCS (MPa)
Freeze-thaw Cycle No.
RMSFFA-SA1.8-NA0.7-50C-14D
RMSFFA-SA1.9-NA0.7-50C-14D
RMSFFA-SA2.0-NA0.7-50C-14D

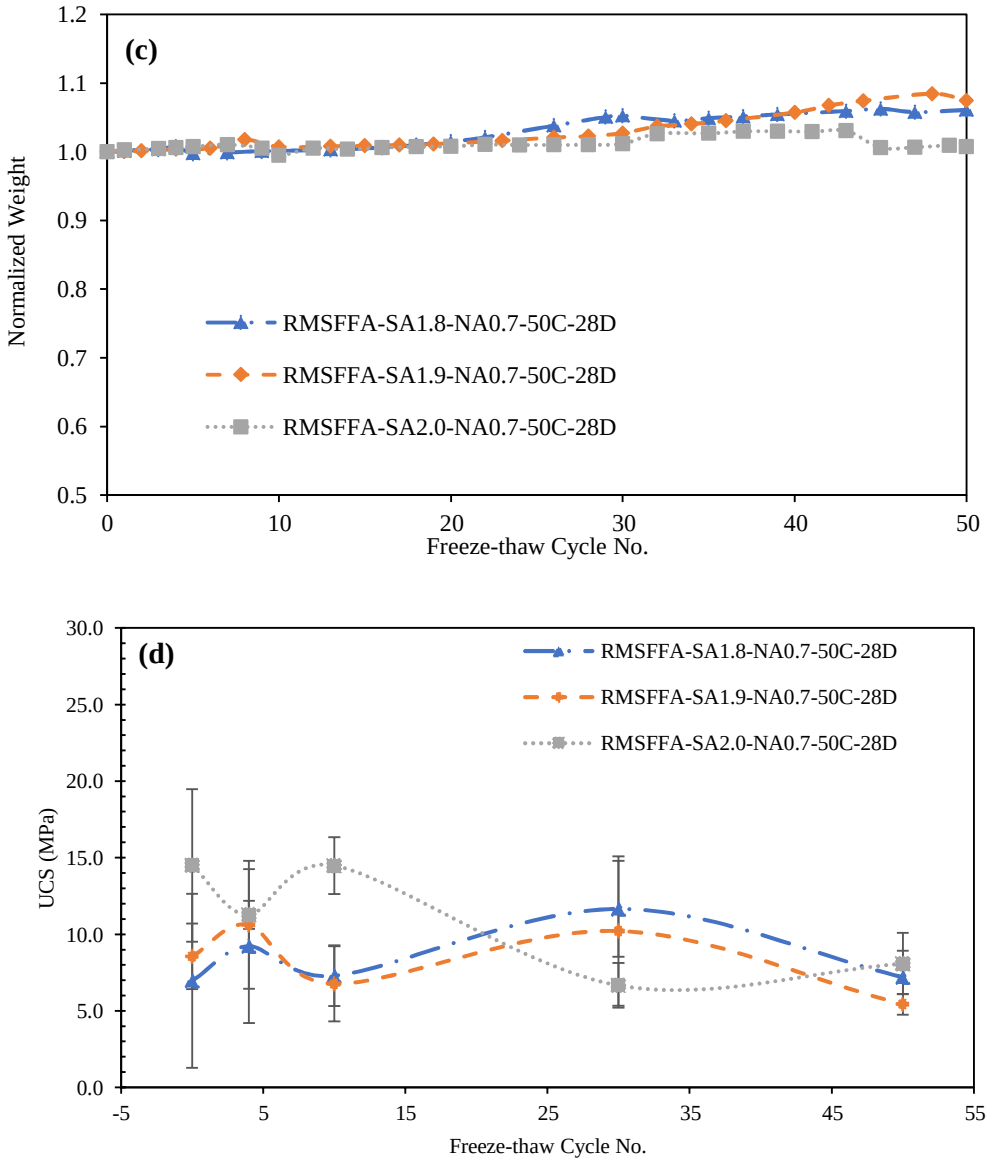

Figure 4-6 Variation of normalized weight and UCS of 14-day cured (a) (b) and 28-day cured (c) (d) RMSFFA geopolymers with different Si/Al molar ratio at 50°C during F-T conditioning.

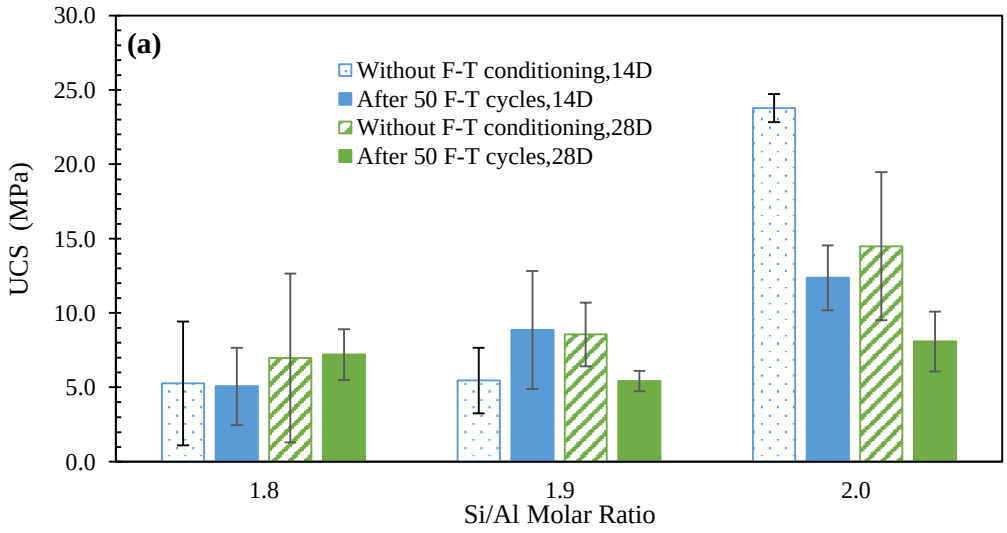
(a)
Without F-T conditioning,14D
After 50 F-T cycles,14D
Without F-T conditioning,28D
After 50 F-T cycles,28D
UCS (MPa)
30.0
25.0
20.0
15.0
10.0
5.0
0.0
1.8
1.9
2.0
Si/Al Molar Ratio

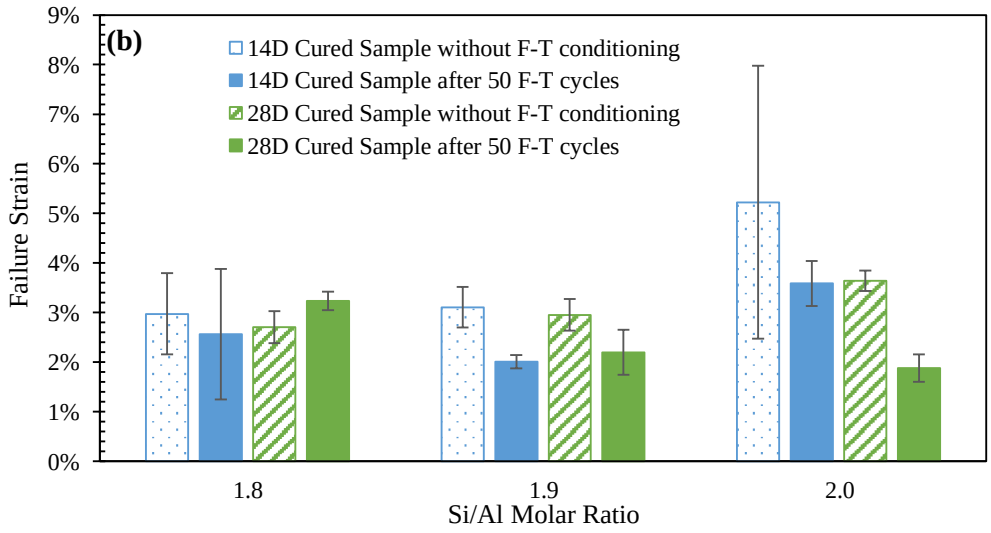
(b)
14D Cured Sample without F-T conditioning
14D Cured Sample after 50 F-T cycles
28D Cured Sample without F-T conditioning
28D Cured Sample after 50 F-T cycles
Failure Strain
9%
8%
7%
6%
5%
4%
3%
2%
1%
0%
1.8
1.9
2.0
Si/Al Molar Ratio

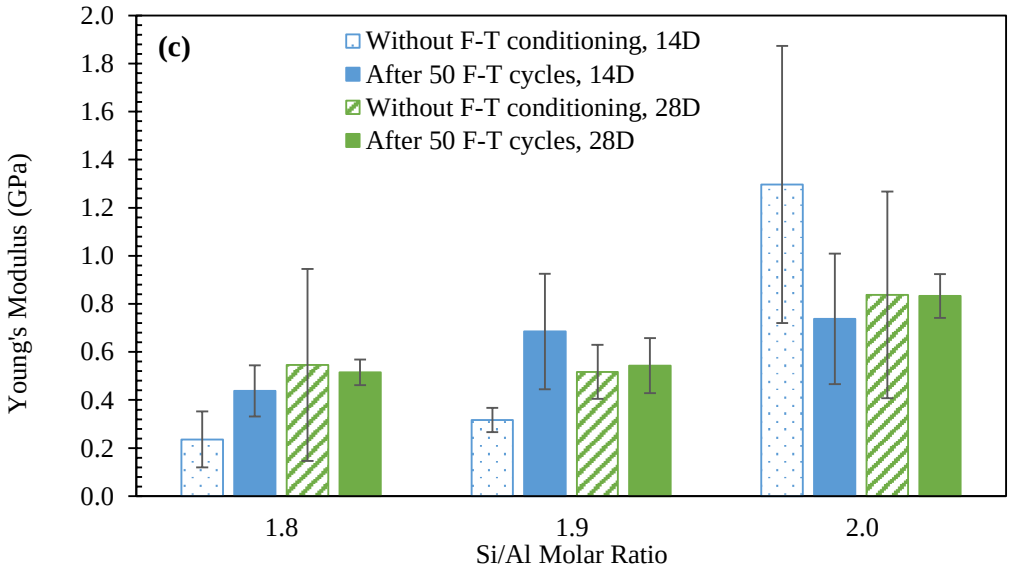

Figure 4-7 Comparison of mechanical properties in (a) UCS, (b) ε_f, and (c) Young's Modulus of RMSFFA geopolymers cured at 14 and 28 days with different Si/Al molar ratios during F-T conditioning before and after 50 F-T conditioning.

Influence of Na/Al molar ratio: Changes in weight of the samples with different Na/Al molar ratios after F-T conditioning are presented in **Figures 4-8 (a)** and **(c)**, which are normalized by their respective initial values prior to F-T conditioning and is plotted versus the number of F-T conditioning cycles. **Figures 4-8 (a)** and **(c)** indicate that Na/Al molar ratio has significant influence on the weight change of RMSFFA geopolymers. With increasing of Na/Al molar ratios, the weight loss changes from negative to positive regardless of the curing time. The samples with Si/Al ratio of 0.7 is more stable in weight change than the other two groups. The 14-day cured sample with Na/Al molar ratio of 1.0 has weight loss up to 50% after 45 F-T cycles, while the weight loss is only up to 12% for its 28-day cured counterpart. The variation of UCS for the samples after various F-T conditioning cycles is presented in **Figures 4-8 (b)** and **(d)**, for 14 and 28 days of curing, respectively. In general, there is no strong or obvious trend of mechanical

strength of the samples vs. F-T conditioning cycles, except that the UCS values of the conditioned samples fluctuate by different magnitudes regardless of the curing time. Mechanical properties, including UCS, failure strain, and Young's modulus of 14- and 28-day cured samples with different Na/Al molar ratios before and after 50 F-T conditioning cycles are replotted in **Figures 4-9(a)-(c)** to better illustrate the sustained mechanical properties and thus the F-T resistance. In general, there is no clear trend of all the mechanical properties with Na/Al molar ratios change. Samples with Na/Al molar ratios of 0.6 and 0.7 have relatively higher initial and sustained compressive strength and Young's modulus (**Figure 4-9(a) and (c)**). In light of the average failure strain (see **Figure 4-9(b)**), sample with Na/Al molar ratio of 1.0 is more ductile after 50 F-T cycles regardless of the curing time compared to other two groups.

In conclusion, there is no appreciable trend in mechanical properties change with increasing the Na/Al molar ratio. Samples with Na/Al molar ratios of 0.6 and 0.7 have relatively higher compressive strength and Young's modulus, while samples with Na/Al molar ratio of 1.0 have relatively higher ductility after 50 F-T cycles regardless of the curing time.

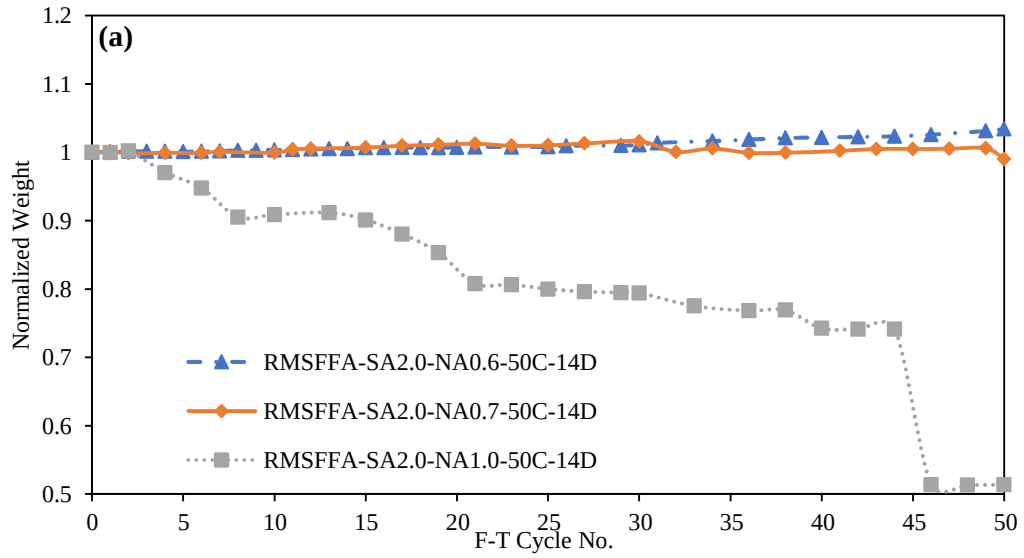
(a)
Normalized Weight
F-T Cycle No.
RMSFFA-SA2.0-NA0.6-50C-14D
RMSFFA-SA2.0-NA0.7-50C-14D
RMSFFA-SA2.0-NA1.0-50C-14D

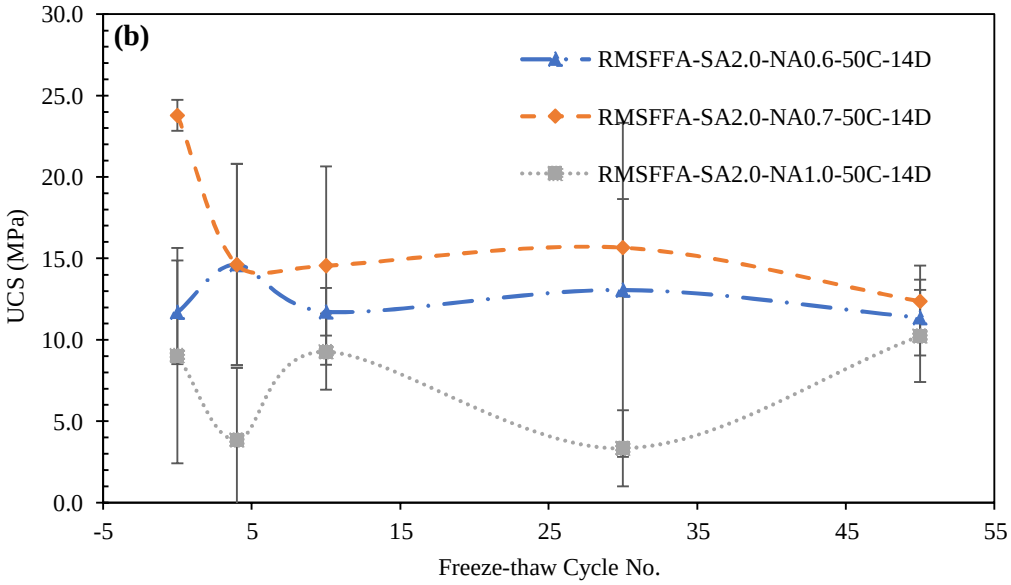
(b)
UCS (MPa)
Freeze-thaw Cycle No.
RMSFFA-SA2.0-NA0.6-50C-14D
RMSFFA-SA2.0-NA0.7-50C-14D
RMSFFA-SA2.0-NA1.0-50C-14D

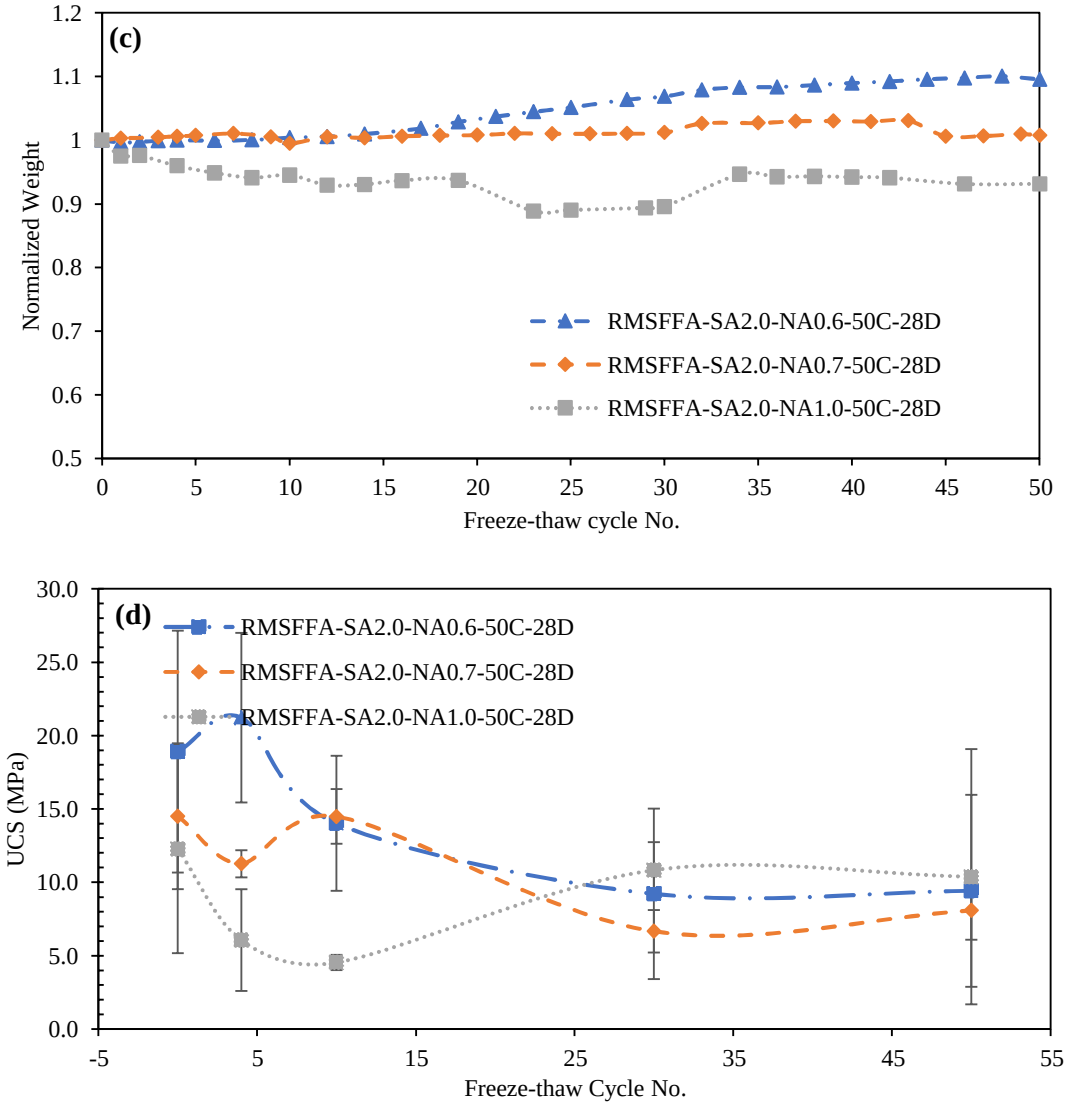

Figure 4-8 Variation of normalized weight and UCS of 14-day cured (a) (b) and 28-day cured (c) (d) RMSFFA geopolymers with different Na/Al molar ratio at 50°C during F-T conditioning.

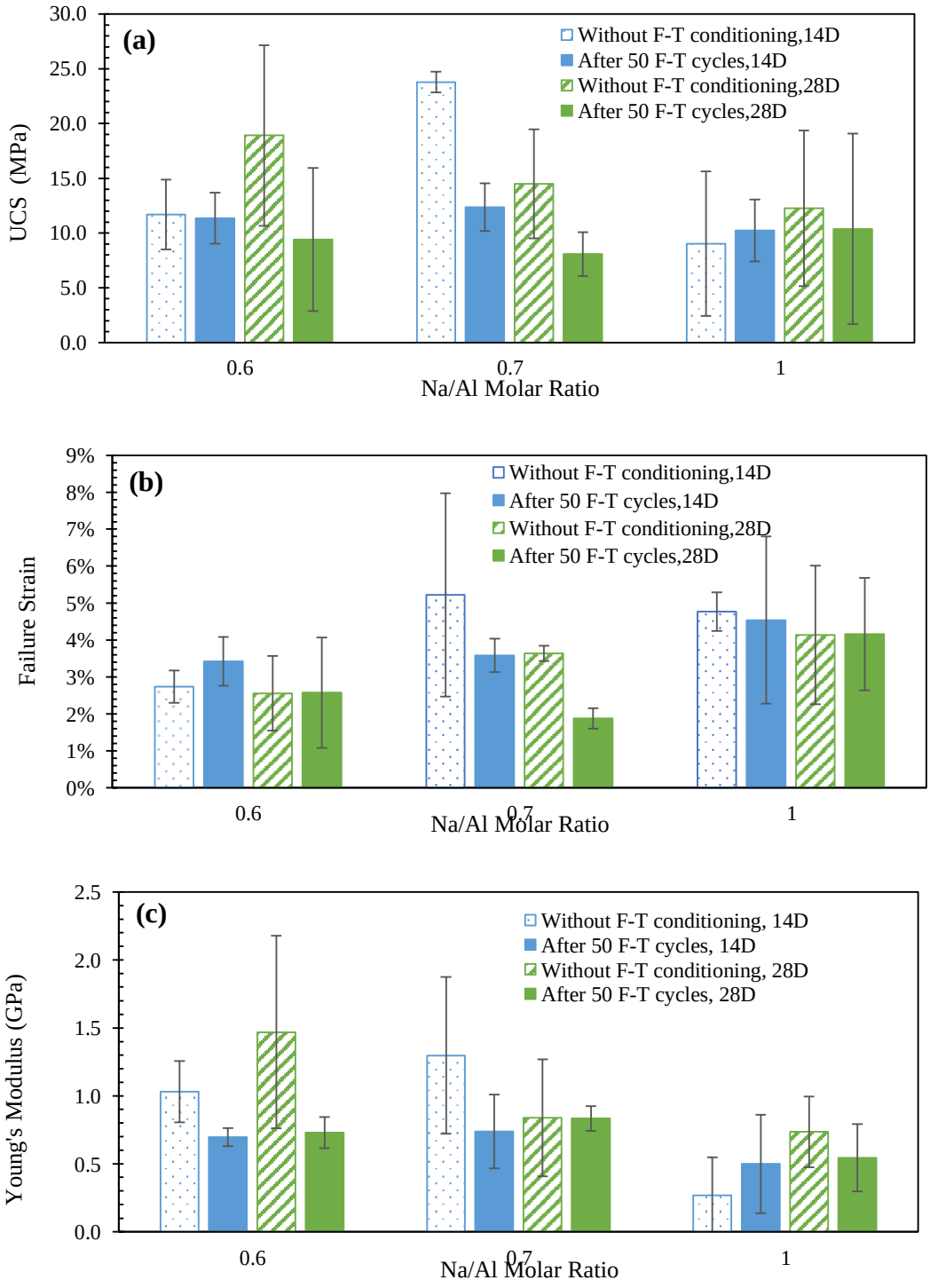

Figure 4-9 Comparison of mechanical properties in (a) UCS, (b) ε_f, and (c) Young's Modulus of RMSFFA geopolymers cured at 14 and 28 days with different Na/Al molar ratios during F-T conditioning before and after 50 F-T conditioning.

4.3.2.2 Chemical Bonding and Pore Characteristics Changes of RMSFFA Geopolymers during F-T Conditioning

The pore size distributions of RMSFFA geopolymers with different Si/Al and Na/Al molar ratios vs. F-T conditioning cycles are plotted in **Figure 4-10** and **Figure 4-11**, respectively. Due to the limited access to the BET testing device, only one representative sample of each batch was tested for its pore size distribution. Based on **Figure 4-10**, different Si/Al molar ratios don't have appreciable trend in the changes of pore size distributions. Based on **Figure 4-11**, it is obvious that the general pore volumes increased with the increase of Na/Al molar ratios. The changes in pore volumes of 14- and 28-day cured RMSFFA samples with different Na/Al and Si/Al molar ratios after subjected to various F-T conditioning cycles (up to 50) is shown in **Figure 4-12**. The pore volume change of 28-day cured samples and the 14-day cured samples with Si/Al molar ratio of 2.0 are highly consistent with UCS change. The lower total pore volumes, the higher UCS values. This is consistent with the UCS testing results, 28-day cured samples already finished the geopolymerization process, and the 14-day cured sample with Si/Al molar ratio of 2.0 has higher reaction rate thus finished the geopolymerization process much quicker than other groups. The other 14-day cured samples still have geopolymerization development during the F-T conditioning, so the total pore volumes cannot correlate the UCS values.

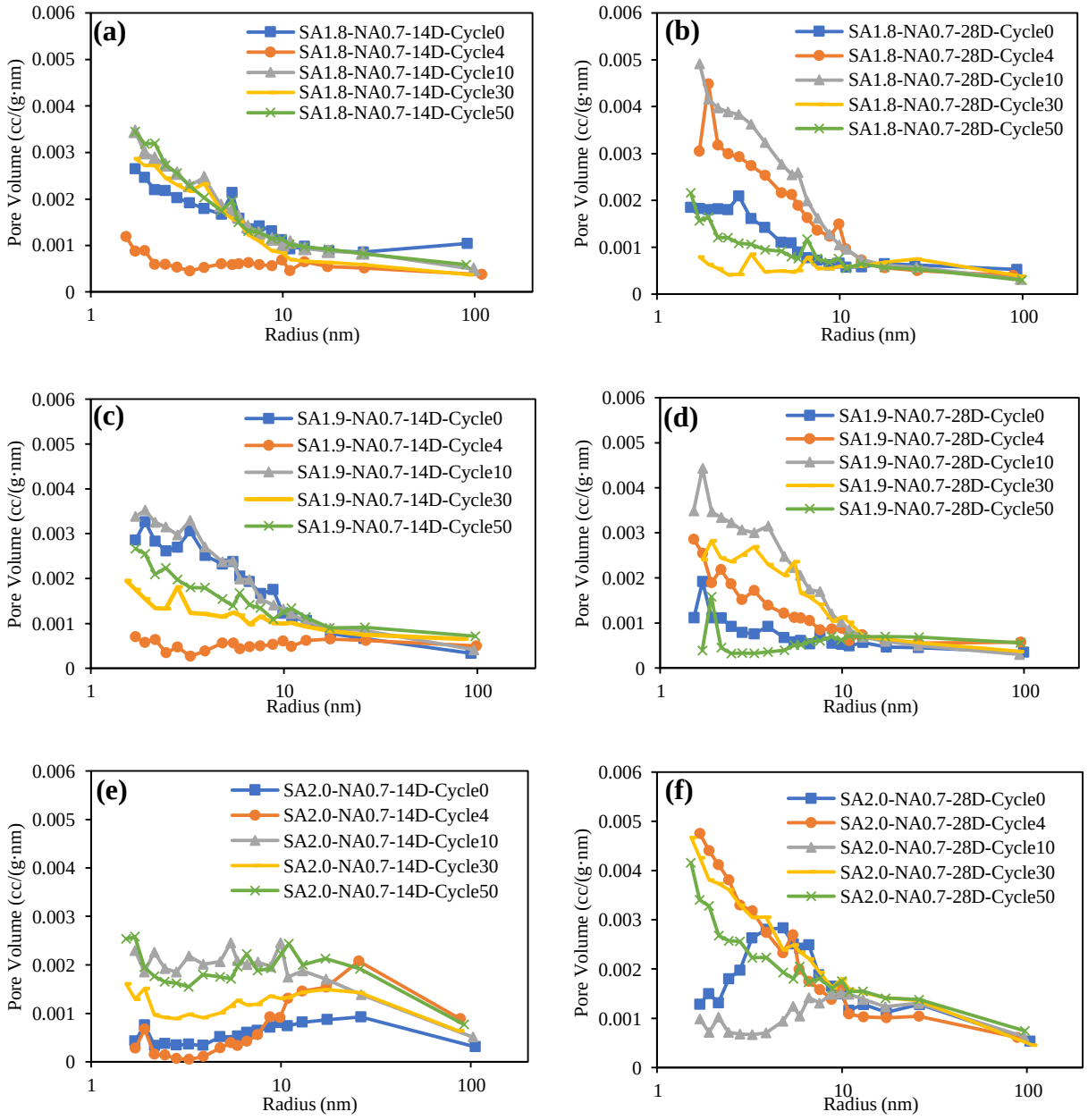

Figure 4-10 Pore size distribution of RMSFFA samples with different Si/Al molar ratios cured at 14 days (a)(c)(e) and 28 days (b)(d)(f) after subjected to various F-T conditioning cycles (up to 50).

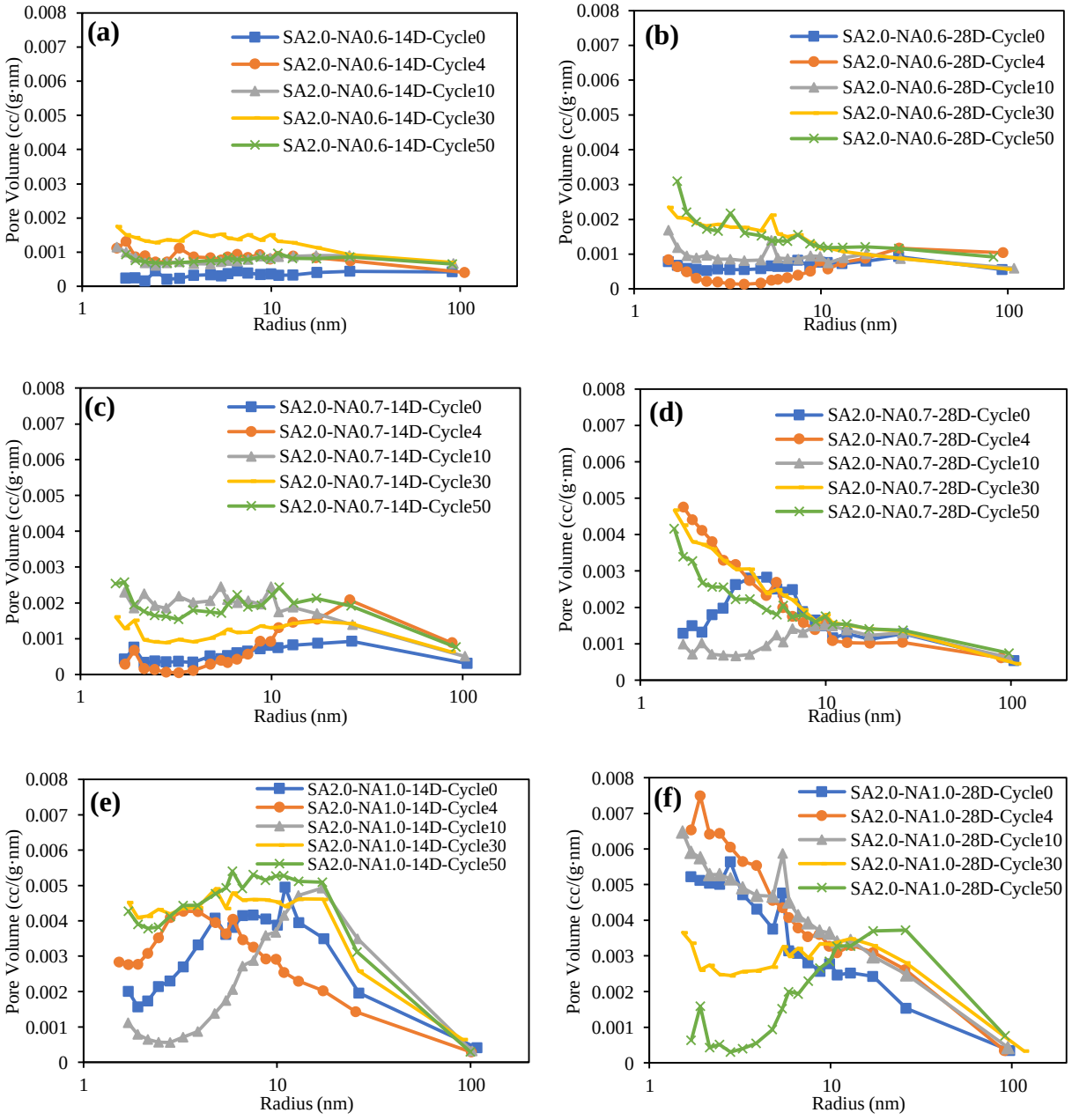

Figure 4-11 Pore size distribution of RMSFFA samples with different Na/Al molar ratios cured at 14 days (a)(c)(e) and 28 days (b)(d)(f) after subjected to various F-T conditioning cycles (up to 50).

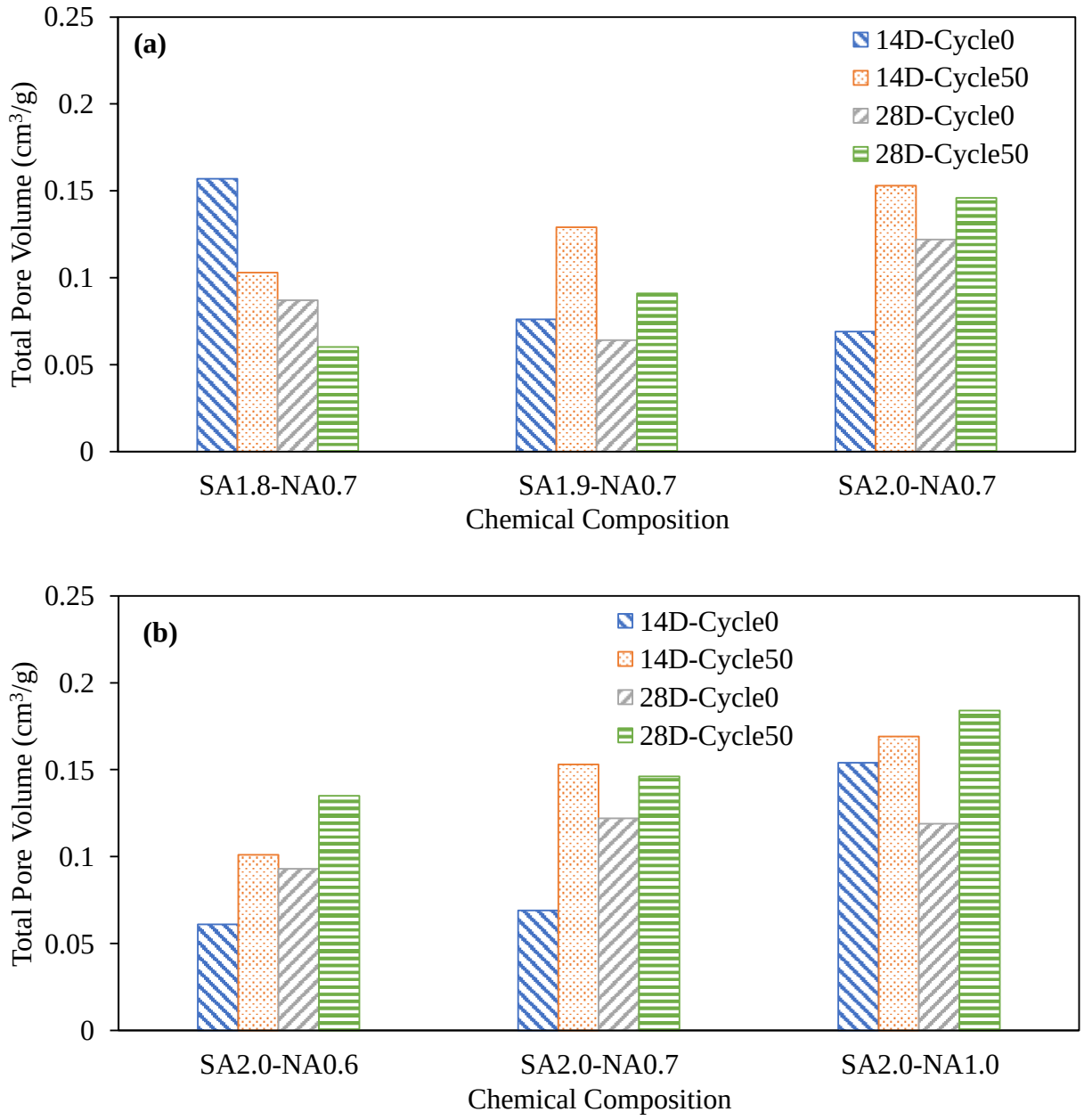

Figure 4-12 Changes in pore volumes of 14- and 28-day cured RMSFFA samples with different Na/Al molar ratios (a) and different Si/Al molar ratios (b) after subjected to various F-T conditioning cycles (up to 50).

4.4. CONCLUSIONS

An experimental study was performed to evaluate F-T resistance of RMSFFA, based on the sustained unconfined compressive strength after subjected to up to 50 F-T conditioning cycles. The processes underlying deterioration of RMSFFA samples during F-T conditioning were examined from the changes in chemical bonding, mineralogy, and porosity characteristics of the samples throughout F-T conditioning. In addition, the effect of curing temperature, curing time, and chemical compositions on the F-T durability of RMSFFA geopolymers were investigated in this study. The main findings are summarized below:

- Except those cured at room temperature, RMSFFA samples had fairly good F-T resistance. The remaining mechanical strength of 14-day cured RMSFFA samples after subjected to 50 F-T cycles was close to their respective initial values or did not deteriorate appreciably, while 28-day cured samples had sustained strength around 9 MPa, despite a more pronounced strength decrease after 50 F-T conditioning cycles. Regarding the effect of curing temperature, 50°C cured samples have a better F-T resistant, which has higher UCS compared to the other two groups regardless of the curing time.

- The difference in the variation of mechanical strength during F-T conditioning between 14-day and 28-day cured samples lies in the following facts: i. 14-day cured samples likely had geopolymer gels development during the early F-T conditioning which offset to some extent the deterioration effects caused by the F-T process; and ii. the 28-day cured samples might have already finished most of the strength development prior to F-T conditioning, with the strength decrease likely being caused by the geopolymer gel dissolution.

- Consistent with the variation of their mechanical strength during F-T conditioning, the changes in chemical bonding, mineralogy, and porosity characteristics of 14-day cured samples at elevated temperatures also indicate that appreciable further geopolymerization and the formation of geopolymer gels during the early stage of F-T conditioning while partial dissolution of geopolymer gel at the later stage of F-T conditioning. Similarly, the results of chemical bonding, mineralogy, and porosity characteristics of 28-day cured samples suggest the partial dissolution of geopolymer gel during F-T conditioning, which qualitatively agree with the variation of their mechanical strength.

- Si/Al molar ratio has more impact on the mechanical strength, while Na/Al molar ratio has more impact on the pore size distributions of the samples. Higher Si/Al molar ratio higher sustained compressive strength after 50 F-T cycles.

Based on this study, 14-day (curing time) and 50°C (curing temperature) are the more favorable curing conditions and Si/Al molar ratio of 2.0 and Na/Al molar ratio of 0.7 are the more favorable chemical compositions used in this study, which result in the samples with a good F-T resistance after subjected to 50 F-T cycles. The mechanical properties and F-T durability of RMSFFA geopolymer can be further improved by adjusting the synthesis parameters and curing conditions. Furthermore, the F-T durability of geopolymers synthesized with other raw materials should be investigated.

CHAPTER V - CONCLUSIONS AND FUTURE WORK

A holistic framework of synthesis and characterization of waste-based geopolymers for civil engineering applications is proposed in this Ph.D. study. The technological impact of this project is the development of the next generation, “green” cementitious binder for sustainable civil engineering. An integrated multiscale experimental approach was utilized to better understand the chemical composition - mechanical properties - durability behavior relationship of waste-based geopolymers. Two types of geopolymers were synthesized and characterized in this study: metakaolin-based geopolymer (MKG), and red mud slurry and Class F fly ash based geopolymers (RMSFFA). The effects of chemical molar ratios (Si/Al and Na/Al), curing temperature, and curing time on the mechanical properties of RMSFFA geopolymers were investigated. The UCS and Young’s modulus of RMSFFA geopolymers increased, with the increase of Si/Al molar ratio and the decrease of Na/Al molar ratio, based on the geopolymer recipes investigated in the current study. A higher curing temperature is more favorable for the strength development of RMSFFA geopolymers compared to room temperature. More specifically, 50°C is better than 80°C among the temperatures investigated in the study. FTIR results verified the formation of geopolymer gels while BET results showed the lower the total pore volume, the higher strength RMSFFA geopolymers had.

In the second part of this study, a comprehensive experimental study was performed to investigate the chemical volume change behavior of MKGs. There are four stages in chemical volume change of MKGs: Shrinkage, expansion, shrinkage, and stable stages, which reflected different chemical reaction processes during geopolymerization: the dissolution of metakaolin, the formation of Al-rich geopolymer gel and reaction products, the formation of the amorphous Si-

rich geopolymer gels with higher density, and the completion of the geopolymerization process. For the recipe used in this study, the AS group showed an overall expansion behavior except the first shrinkage stage, while the DIW group presented shrinkage behavior (i.e., its final chemical volume is reduced). Visual inspection indicates that the color of DIW group is similar to that of the control group besides the surface part, while the AS group is much darker. The ICC results show that AS filling solution caused further geopolymerization reactions and DIW filling solution dampened the geopolymerization process of the surface portion of the precursor. The FTIR and SEM-EDX results also indicate that the AS group samples exhibit relatively lower main band wavenumber, high Si/Al molar ratios and high Na/Al molar ratios, which implies higher geopolymerization/polycondensation degrees that promoted by the diffusion of Na ion from AS filling solution to being-cured geopolymer precursor. The center of the main band and the Si/Al and Na/Al molar ratios of AS group are closer to these of control group for the middle and bottom parts. Given that the much more porous DIW surface part with much larger size pores cannot be accurately characterized by the BET techniques, the total pore volume of DIW cannot be compared to the control group, although the total detected pore volume of the DIW sample is “seemingly” much closer to that of the control group. The AS group has a much smaller total pore volume compared to the other two groups and shows relatively smaller pore size distribution, largely attributed to further geopolymerization by the diffusion of Na ion from AS filling solution. The filling solutions affect the geopolymerization of MKGs and thus their micro-characteristics and chemical volume change, largely through complex, dynamic chemical exchanges between the filling solutions and the geopolymer precursor, particularly diffusion-based leaching or ingress of Na^+ and OH^-. Such chemical exchanges are governed by competing processes of

geopolymerization and diffusion, which is affected in turn by the type of raw materials, chemical composition of synthesis recipe, and chemical composition of filling solutions.

Although an appropriate filling solution for characterizing chemical volume change of geopolymer has not been identified, this study sheds light on the fundamental processes of a filling solution affecting geopolymerization and thus provides guidance for selecting filling solution. Ideally, an appropriate filling solution for geopolymers would be inert, non-volatile, with small molecular size, etc., for characterizing chemical volume change of geopolymer. Furthermore, an appropriate filling solution should suppress potential ion exchanges between filling solutions and geopolymer precursor. For RMSFFA geopolymers, there is no initial shrinkage stage as detected on the MKGs, which might be caused by the different geopolymerization process of different raw materials. All the RMSFFA geopolymers experienced overall expansion and similar chemical volume change behavior regardless of the geopolymer synthesize recipes. There is no clear trend of the effects of chemical compositions on the chemical volume change behavior of RMSFFA geopolymers. For MKGs and RMSFFA geopolymers investigated in this study, a total monitoring time of 20 days is adequate to capture their chemical volume change; however, different monitoring time might be required for other geopolymer systems that have different rate and kinetics of geopolymerization.

In the third part of this study, an experimental study was performed to evaluate F-T resistance of RMSFFA geopolymers, based on the sustained unconfined compressive strength after subjected to up to 50 F-T conditioning cycles. The processes underlying deterioration of RMSFFA samples during F-T conditioning were examined from the changes in chemical bonding, mineralogy, and porosity characteristics of the samples throughout F-T conditioning. In addition, the effect of curing temperature, curing time, and chemical compositions on the F-T durability of

RMSFFA geopolymers was investigated in this study. Except those cured at room temperature, RMSFFA samples had good F-T resistance. The remaining mechanical strength of 14-day cured RMSFFA samples after subjected to 50 F-T cycles was close to their respective initial values or did not deteriorate appreciably, while 28-day cured samples had sustained strength around 9 MPa, despite a more pronounced strength decrease after 50 F-T conditioning cycles. Regarding the effect of curing temperature, 50℃ cured samples have a better F-T resistance, which has higher UCS compared to the other two groups regardless of the curing time. The difference in the variation of mechanical strength during F-T conditioning between 14-day and 28-day cured samples lies in the following facts: i. 14-day cured samples likely had further geopolymer gels development during the early F-T conditioning which offset to some extent the deterioration effects caused by the F-T process; and ii. the 28-day cured samples might have already finished most of the strength development prior to F-T conditioning, with the strength decrease likely being caused by the geopolymer gel dissolution. Consistent with the variation of their mechanical strength during F-T conditioning, the changes in chemical bonding, mineralogy, and porosity characteristics of 14-day cured samples at elevated temperatures also indicate that appreciable further geopolymerization and the formation of geopolymer gels during the early stage of F-T conditioning while partial dissolution of geopolymer gel at the later stage of F-T conditioning. Similarly, the results of chemical bonding, mineralogy, and porosity characteristics of 28-day cured samples suggest the partial dissolution of geopolymer gel during F-T conditioning, which qualitatively agrees with the variation of their mechanical strength. Si/Al molar ratio has more impact on the mechanical strength, while Na/Al molar ratio has more impact on the pore size distributions of the samples. The higher Si/Al molar ratio, the higher sustained compressive strength after 50 F-T cycles. Based on this study, 14-day (curing time) and 50℃ (curing temperature) are the more favorable curing

conditions while Si/Al molar ratio of 2.0 and Na/Al molar ratio of 0.7 are the more favorable chemical compositions used in this study, which result in the geopolymer samples with a good F-T resistance after subjected to 50 F-T cycles. The mechanical properties and F-T durability of RMSFFA geopolymer can be further improved by adjusting the synthesis parameters and curing conditions. Furthermore, the F-T durability of geopolymers synthesized with other raw materials should be investigated.

Lastly, RMSFFA geopolymer results were plotted in Figure 5-1 to illustrate how such a holistic framework can be applied to synthesis of cementitious materials for civil engineering applications, in order to ensure their satisfactory performance. Three performance related indicators or properties, including UCS, durability (freeze and thaw durability), and chemical volume change are considered holistically. Ideally, a good recipe will give high strength, high free-thaw durability, and smaller chemical volume change. Among RMSFFA geopolymer recipes, Si/Al=2.0 works relatively better, with high UCS and higher freeze-thaw durability, but not the lowest chemical volume change. However, as long as the chemical volume change is small enough, this recipe is acceptable.

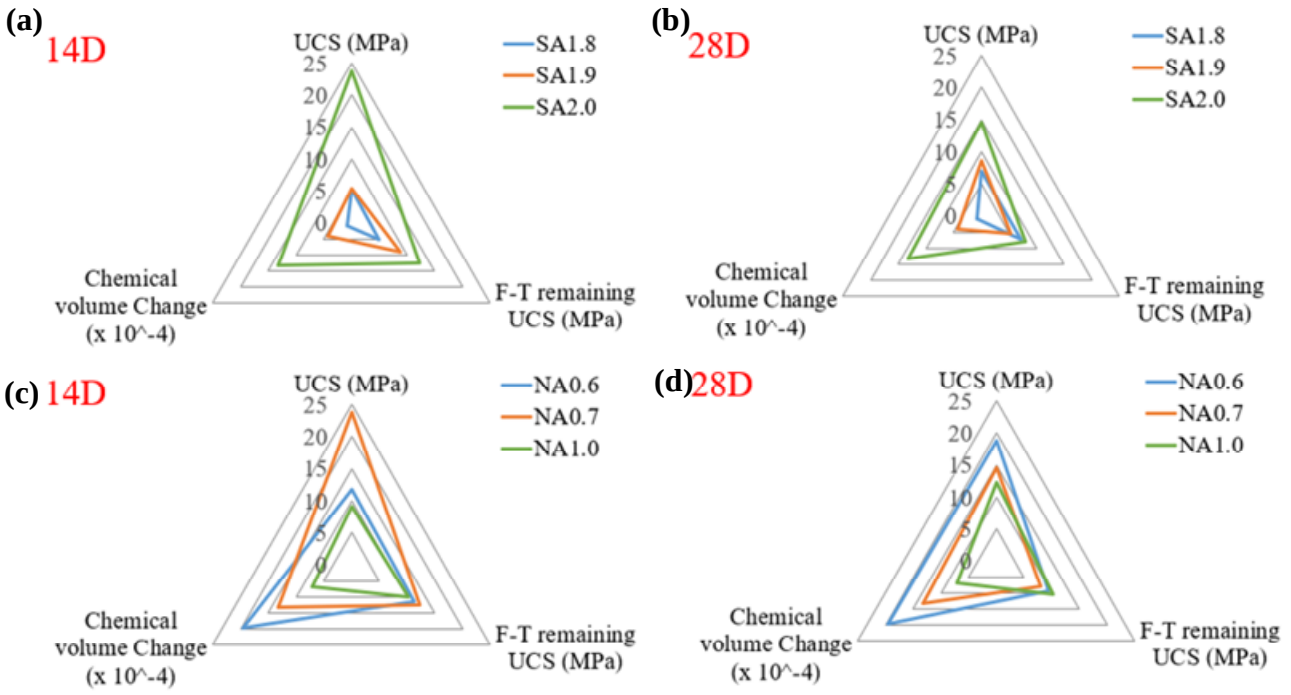

Figure 5-1 A holistic framework of geopolymer synthesis with the consideration of strength, F-T durability, and chemical volume change: RMSFFA geopolymers with different Si/Al molar ratios cured at 14 days (a) and 28 days (b); and RMSFFA geopolymers with different Na/Al molar ratios cured at 14 days (c) and 28 days (d).

In conclusion, geopolymers have very good mechanical properties comparable to OPC, and small chemical volume expansion, and good F-T resistance properties based on the recipes studied in this Ph.D. study. In the future, more geopolymer systems should be tested for various durability properties to better tailoring the recipes for different civil engineering applications.

REFERENCES

1. Monteiro, P.J., S.A. Miller, and A. Horvath, *Towards sustainable concrete.* Nature materials, 2017. **16**(7): p. 698-699.
2. Nuaklong, P., et al., *Influence of rice husk ash on mechanical properties and fire resistance of recycled aggregate high-calcium fly ash geopolymer concrete.* 2020. **252**: p. 119797.
3. Qu, F., et al., *High temperature resistance of fly ash/GGBFS-based geopolymer mortar with load-induced damage.* 2020. **53**(4): p. 1-21.
4. Zhang, M., et al., *Durability of red mud-fly ash based geopolymer and leaching behavior of heavy metals in sulfuric acid solutions and deionized water.* 2016. **124**: p. 373-382.
5. Aiken, T.A., et al., *Resistance of fly ash geopolymer binders to organic acids.* 2020. **53**(5): p. 1-18.
6. Davidovits, J. *Properties of geopolymer cements*. in *First international conference on alkaline cements and concretes*. 1994. Kiev State Technical University, Ukraine: Scientific Research Institute on ….
7. Turner, L.K., F.G.J.C. Collins, and B. Materials, *Carbon dioxide equivalent (CO2-e) emissions: A comparison between geopolymer and OPC cement concrete.* 2013. **43**: p. 125-130.
8. Loganayagan, S., et al., *Experimental investigation on characteristics of fly-ash based geo-polymer mixed concrete.* 2020.
9. Ji, Z., et al., *Porosity, mechanical strength and structure of waste-based geopolymer foams by different stabilizing agents.* 2020. **258**: p. 119555.
10. Wong, C.L., et al., *Mechanical strength and permeation properties of high calcium fly ash-based geopolymer containing recycled brick powder.* 2020: p. 101655.
11. Malone, P.G., C.A. Randall Jr, and T. Kirkpatrick, *Potential applications of alkali-activated alumino-silicate binders in military operations*. 1985, ARMY ENGINEER WATERWAYS EXPERIMENT STATION VICKSBURG MS GEOTECHNICAL LAB.
12. Giancaspro, J., P. Balaguru, and R.E. Lyon, *Use of inorganic polymer to improve the fire response of balsa sandwich structures.* Journal of materials in civil engineering, 2006. **18**(3): p. 390-397.
13. Lyon, R.E., et al., *Fire‐resistant aluminosilicate composites.* Fire and materials, 1997. **21**(2): p. 67-73.
14. Goretta, K., J. Fuller, and E. Crawley, *Geopolymers.* Air Force Office of Scientific Research Report, 2006.
15. Buchwald, A., et al. *Stabilised foam clay material with high performance thermal insulation properties*. in *CFI (Ceramic Forum International/Berichte der DKG)*. 2004.
16. Balaguru, P.N., *Geopolymer for protective coating of transportation infrastructures*. 1998, New Jersey. Dept. of Transportation.
17. Bell, J.L., P.E. Driemeyer, and W.M. Kriven, *Formation of ceramics from metakaolin‐based geopolymers. Part II: K‐based geopolymer.* Journal of the American Ceramic Society, 2009. **92**(3): p. 607-615.
18. Li, Z. and S. Liu, *Influence of slag as additive on compressive strength of fly ash-based geopolymer.* Journal of Materials in civil engineering, 2007. **19**(6): p. 470-474.

19. Zhang, S., K. Gong, and J. Lu, *Novel modification method for inorganic geopolymer by using water soluble organic polymers.* Materials letters, 2004. **58**(7-8): p. 1292-1296.
20. Fletcher, R.A., et al., *The composition range of aluminosilicate geopolymers.* Journal of the European Ceramic Society, 2005. **25**(9): p. 1471-1477.
21. Davidovits, J., *Geopolymers: inorganic polymeric new materials.* Journal of Thermal Analysis and calorimetry, 1991. **37**(8): p. 1633-1656.
22. Duxson, P., et al., *Geopolymer technology: the current state of the art.* Journal of materials science, 2007. **42**(9): p. 2917-2933.
23. Duxson, P., et al., *Understanding the relationship between geopolymer composition, microstructure and mechanical properties.* Colloids and Surfaces A: Physicochemical and Engineering Aspects, 2005. **269**(1-3): p. 47-58.
24. Xu, H. and J. Van Deventer, *The geopolymerisation of alumino-silicate minerals.* International journal of mineral processing, 2000. **59**(3): p. 247-266.
25. Medri, V., et al., *Metakaolin-based geopolymer beads: Production methods and characterization.* 2020. **244**: p. 118844.
26. Gomes, S., et al., *Temperature stability of a pure metakaolin based K-geopolymer: Part 1. Variations in the amorphous mineral network.* 2020.
27. He, J., et al., *Synthesis and characterization of red mud and rice husk ash-based geopolymer composites.* 2013. **37**: p. 108-118.
28. Liu, J., et al., *Effects of Na/Al ratio on mechanical properties and microstructure of red mud-coal metakaolin geopolymer.* 2020. **263**: p. 120653.
29. Wang, Y., et al., *Effects of Si/Al ratio on the efflorescence and properties of fly ash based geopolymer.* 2020. **244**: p. 118852.
30. Jin, Y., et al., *Structure refinement of fly ash in connection with its reactivity in geopolymerization.* 2020. **118**: p. 350-359.
31. He, J., et al., *The strength and microstructure of two geopolymers derived from metakaolin and red mud-fly ash admixture: a comparative study.* 2012. **30**: p. 80-91.
32. He, J., et al., *Synthesis and characterization of red mud and rice husk ash-based geopolymer composites.* Cement and Concrete Composites, 2013. **37**: p. 108-118.
33. Ayres, R.U., J. Holmberg, and B. Andersson, *Materials and the global environment: Waste mining in the 21st century.* MRS Bulletin, 2001. **26**(6): p. 477-480.
34. Badanoiu, A.I., et al., *Preparation and characterization of foamed geopolymers from waste glass and red mud.* Construction and Building Materials, 2015. **84**: p. 284-293.
35. Sutar, H., et al., *Progress of red mud utilization: an overview.* 2014.
36. Ye, N., et al., *Synthesis and characterization of geopolymer from Bayer red mud with thermal pretreatment.* Journal of the American Ceramic Society, 2014. **97**(5): p. 1652-1660.
37. Cooling, D. and D. Clenister, *Practical aspects of dry residue disposal.* Light Metals 1992, 1992: p. 25-31.
38. Klauber, C., M. Gräfe, and G. Power, *Bauxite residue issues: II. Options for residue utilization.* Hydrometallurgy, 2011. **108**(1-2): p. 11-32.
39. Rai, S., et al., *Neutralization and utilization of red mud for its better waste management.* World, 2012. **6**: p. 5410.
40. Antunes, M.L.P., et al., *Red mud from Brazil: thermal behavior and physical properties.* Industrial & Engineering Chemistry Research, 2011. **51**(2): p. 775-779.

41. Zhang, G., J. He, and R. Gambrell, *Synthesis, characterization, and mechanical properties of red mud-based geopolymers.* Transportation Research Record: Journal of the Transportation Research Board, 2010(2167): p. 1-9.
42. Dimas, D.D., I.P. Giannopoulou, and D. Panias, *Utilization of alumina red mud for synthesis of inorganic polymeric materials.* Mineral processing & Extractive metallurgy review, 2009. **30**(3): p. 211-239.
43. Testing, A.S.f., M.C.C.-o. Concrete, and C. Aggregates, *Standard specification for coal fly ash and raw or calcined natural pozzolan for use in concrete*. 2005: ASTM International.
44. Ferguson, G., *Use of self-cementing fly ashes as a soil stabilization agent.* FLY ASH FOR SOIL IMPROVEMENT. ASCE GEOTECHNICAL SPECIAL PUBLICATION NO. 36, 1993.
45. Haiying, Z., Z. Youcai, and Q. Jingyu, *Characterization of heavy metals in fly ash from municipal solid waste incinerators in Shanghai.* Process Safety and Environmental Protection, 2010. **88**(2): p. 114-124.
46. Kumar, A. and S. Kumar, *Development of paving blocks from synergistic use of red mud and fly ash using geopolymerization.* Construction and building Materials, 2013. **38**: p. 865-871.
47. Zhang, M., et al., *Synthesis factors affecting mechanical properties, microstructure, and chemical composition of red mud–fly ash based geopolymers.* Fuel, 2014. **134**: p. 315-325.
48. Rashad, A.M., *Metakaolin as cementitious material: History, scours, production and composition–A comprehensive overview.* Construction and building materials, 2013. **41**: p. 303-318.
49. Sakulich, A.R., *Reinforced geopolymer composites for enhanced material greenness and durability.* Sustainable Cities and Society, 2011. **1**(4): p. 195-210.
50. Kuenzel, C., et al., *Ambient temperature drying shrinkage and cracking in metakaolin-based geopolymers.* Journal of the American Ceramic Society, 2012. **95**(10): p. 3270-3277.
51. Criado, M., A. Palomo, and A. Fernández-Jiménez, *Alkali activation of fly ashes. Part 1: Effect of curing conditions on the carbonation of the reaction products.* Fuel, 2005. **84**(16): p. 2048-2054.
52. García-Lodeiro, I., et al., *FTIR study of the sol–gel synthesis of cementitious gels: C–S–H and N–A–S–H.* Journal of Sol-Gel Science and Technology, 2008. **45**(1): p. 63-72.
53. Furlani, E., et al., *Synthesis and characterization of geopolymers containing blends of unprocessed steel slag and metakaolin: The role of slag particle size.* Ceramics International, 2018. **44**(5): p. 5226-5232.
54. Lodeiro, I.G., et al., *Effect on fresh CSH gels of the simultaneous addition of alkali and aluminium.* Cement and Concrete Research, 2010. **40**(1): p. 27-32.
55. Faucon, P., et al., *Silicon substitution for aluminum in calcium silicate hydrates.* Journal of the American Ceramic Society, 1999. **82**(5): p. 1307-1312.
56. Taylor, H.W., *726. Hydrated calcium silicates. Part I. Compound formation at ordinary temperatures.* Journal of the Chemical Society (Resumed), 1950: p. 3682-3690.
57. Van Chanh, N., B.D. Trung, and D. Van Tuan. *Recent research geopolymer concrete*. in *The 3rd ACF international conference-ACF/VCA, Vietnam*. 2008.

58. Moradikhou, A.B., M. Safehian, and E.M. Golafshani, *High-strength geopolymer concrete based on coal washing waste.* Construction and Building Materials, 2023. **362**: p. 129675.
59. Mermerdaş, K., Z. Algın, and Ş. Ekmen, *Experimental assessment and optimization of mix parameters of fly ash-based lightweight geopolymer mortar with respect to shrinkage and strength.* Journal of Building Engineering, 2020. **31**: p. 101351.
60. Li, F., et al., *Influence of mixed fibers on fly ash based geopolymer resistance against freeze-thaw cycles.* Journal of Non-Crystalline Solids, 2022. **584**: p. 121517.
61. Tan, J., H. Dan, and Z. Ma, *Metakaolin based geopolymer mortar as concrete repairs: Bond strength and degradation when subjected to aggressive environments.* Ceramics International, 2022.
62. Villca, A.R., et al., *Hybrid Lime–Pozzolan Geopolymer Systems: Microstructural, Mechanical and Durability Studies.* Materials, 2022. **15**(8): p. 2736.
63. Tang, J., et al., *Elastic geopolymer based on nanotechnology: Synthesis, characterization, properties, and applications.* Ceramics International, 2022. **48**(5): p. 5965-5971.
64. Cartwright, C., F. Rajabipour, and A. Radlińska, *Shrinkage characteristics of alkali-activated slag cements.* Journal of materials in civil engineering, 2014. **27**(7): p. B4014007.
65. Ye, H., et al., *Effect of drying rate on shrinkage of alkali-activated slag cements.* 2014.
66. Neto, A.A.M., M.A. Cincotto, and W. Repette, *Drying and autogenous shrinkage of pastes and mortars with activated slag cement.* Cement and Concrete Research, 2008. **38**(4): p. 565-574.
67. Hardjito, D., et al., *On the development of fly ash-based geopolymer concrete.* Materials Journal, 2004. **101**(6): p. 467-472.
68. Fernandez-Jimenez, A.M., A. Palomo, and C. Lopez-Hombrados, *Engineering properties of alkali-activated fly ash concrete.* ACI Materials Journal, 2006. **103**(2): p. 106.
69. Rajayogan, V., *Autogenous shrinkage in cementitious systems*. 2009: University of New South Wales, Australian Defence Force Academy, School of ….
70. Holt, E.E., *Early age autogenous shrinkage of concrete*. Vol. 446. 2001: Technical Research Centre of Finland Espoo, Finland.
71. Holt, E.E., *Where did these cracks come from?* Concrete International, 2000. **22**(9): p. 57-60.
72. Hojati, M. and A. Radlińska, *Shrinkage and strength development of alkali-activated fly ash-slag binary cements.* Construction and Building Materials, 2017. **150**: p. 808-816.
73. Tazawa, E.-i., S. Miyazawa, and T. Kasai, *Chemical shrinkage and autogenous shrinkage of hydrating cement paste.* Cement and concrete research, 1995. **25**(2): p. 288-292.
74. Bentz, D.P. and K.A. Snyder, *Protected paste volume in concrete: Extension to internal curing using saturated lightweight fine aggregate.* Cement and concrete research, 1999. **29**(11): p. 1863-1867.
75. Lura, P., O.M. Jensen, and K. van Breugel, *Autogenous shrinkage in high-performance cement paste: An evaluation of basic mechanisms.* Cement and Concrete Research, 2003. **33**(2): p. 223-232.
76. Bouasker, M., et al., *Chemical shrinkage of cement pastes and mortars at very early age: effect of limestone filler and granular inclusions.* Cement and Concrete Composites, 2008. **30**(1): p. 13-22.

77. Scherer, G.W., et al., *Hydration and percolation at the setting point.* Cement and Concrete Research, 2012. **42**(5): p. 665-672.
78. Zhang, J., et al., *Early hydration and setting of oil well cement.* Cement and Concrete research, 2010. **40**(7): p. 1023-1033.
79. Mounanga, P., et al., *Autogenous deformations of cement pastes: Part I. Temperature effects at early age and micro–macro correlations.* Cement and Concrete Research, 2006. **36**(1): p. 110-122.
80. Baroghel-Bouny, V., et al., *Autogenous deformations of cement pastes: part II. W/C effects, micro–macro correlations, and threshold values.* Cement and Concrete Research, 2006. **36**(1): p. 123-136.
81. Sakulich, A.R. and D.P. Bentz, *Mitigation of autogenous shrinkage in alkali activated slag mortars by internal curing.* Materials and structures, 2013. **46**(8): p. 1355-1367.
82. Lee, N., J. Jang, and H. Lee, *Shrinkage characteristics of alkali-activated fly ash/slag paste and mortar at early ages.* Cement and Concrete Composites, 2014. **53**: p. 239-248.
83. Bentz, D.P. and W.J. Weiss, *Internal curing: a 2010 state-of-the-art review*. 2011: US Department of Commerce, National Institute of Standards and Technology Gaithersburg, Maryland.
84. Justnes, H., et al., *Chemical shrinkage of cement pastes with plasticizing admixtures.* NORDIC CONCRETE RESEARCH-PUBLICATIONS-, 2000. **24**: p. 39-54.
85. *A. International, Standard test method for chemical shrinkage of hydraulic cement paste.* West Conshohocken, 2007. **PA**(ASTM C1608-07).
86. Bentz, D.P., *A review of early-age properties of cement-based materials.* Cement and Concrete Research, 2008. **38**(2): p. 196-204.
87. Lemly, A.D., *Damage cost of the Dan River coal ash spill.* Environmental Pollution, 2015. **197**: p. 55-61.
88. Hojati, M., A.J.C. Radlińska, and B. Materials, *Shrinkage and strength development of alkali-activated fly ash-slag binary cements.* 2017. **150**: p. 808-816.
89. Lee, N., et al., *Shrinkage characteristics of alkali-activated fly ash/slag paste and mortar at early ages.* 2014. **53**: p. 239-248.
90. Sakulich, A.R., D.P.J.M. Bentz, and structures, *Mitigation of autogenous shrinkage in alkali activated slag mortars by internal curing.* 2013. **46**(8): p. 1355-1367.
91. Cartwright, C.P., F. Rajabipour, and A. Radlińska, *Measuring the chemical shrinkage of alkali-activated slag cements using the buoyancy method*, in *Mechanics and Physics of Creep, Shrinkage, and Durability of Concrete: A Tribute to Zdeňk P. Bažant*. 2013. p. 308-315.
92. Li, Z., et al., *Chemical deformation of metakaolin based geopolymer.* 2019. **120**: p. 108-118.
93. Lolli, F., et al., *Early age volume changes in metakaolin geopolymers: Insights from molecular simulations and experiments.* Cement and Concrete Research, 2021. **144**: p. 106428.
94. Yang, T., H. Zhu, and Z. Zhang, *Influence of fly ash on the pore structure and shrinkage characteristics of metakaolin-based geopolymer pastes and mortars.* Construction and Building Materials, 2017. **153**: p. 284-293.
95. Ma, J. and F. Dehn, *Investigations on the coefficient of thermal expansion of a low-calcium fly ash-based geopolymer concrete.* Structural Concrete, 2017.

96. Thomas, R., D. Lezama, and S. Peethamparan, *On drying shrinkage in alkali-activated concrete: Improving dimensional stability by aging or heat-curing.* Cement and Concrete Research, 2017. **91**: p. 13-23.
97. Mu, S., et al., *Property and microstructure of aluminosilicate inorganic coating for concrete: Role of water to solid ratio.* Construction and Building Materials, 2017. **148**: p. 846-856.
98. Bakharev, T., J. Sanjayan, and Y.-B. Cheng, *Effect of admixtures on properties of alkali-activated slag concrete.* Cement and Concrete Research, 2000. **30**(9): p. 1367-1374.
99. Brooks, J. and M.M. Johari, *Effect of metakaolin on creep and shrinkage of concrete.* Cement and Concrete Composites, 2001. **23**(6): p. 495-502.
100. Zhang, M., C. Tam, and M. Leow, *Effect of water-to-cementitious materials ratio and silica fume on the autogenous shrinkage of concrete.* Cement and Concrete Research, 2003. **33**(10): p. 1687-1694.
101. Bentz, D.P. and O.M. Jensen, *Mitigation strategies for autogenous shrinkage cracking.* Cement and Concrete Composites, 2004. **26**(6): p. 677-685.
102. Henkensiefken, R., et al., *Internal curing improves concrete performance throughout its life.* Concrete InFocus, 2009. **8**(5): p. 22-30.
103. Ma, Y. and G. Ye, *The shrinkage of alkali activated fly ash.* Cement and Concrete Research, 2015. **68**: p. 75-82.
104. Song, C., Y.C. Choi, and S. Choi, *Effect of internal curing by superabsorbent polymers–Internal relative humidity and autogenous shrinkage of alkali-activated slag mortars.* Construction and Building Materials, 2016. **123**: p. 198-206.
105. *A. International,Standard test method for autogenous strain of cement paste and mortar.* West Conshohocken, 2009. **ASTM C1698-09**(PA).
106. Bentz, D.P., *A three-dimensional cement hydration and microstructure program: I. hydration rate, heat of hydration, and chemical shrinkage*. 1995: Building and Fire Research Laboratory, National Institute of Technology.
107. Tanpure, S.M., M.N. Shirsath, and S.L. Hake, *State of Art-Lime Added Geopolymer Concrete.* 2017.
108. Carabba, L., et al., *Steel fiber reinforced geopolymer matrix (S-FRGM) composites applied to reinforced concrete structures for strengthening applications: A preliminary study.* Composites Part B: Engineering, 2017.
109. Huseien, G.F., et al., *Geopolymer mortars as sustainable repair material: A comprehensive review.* Renewable and Sustainable Energy Reviews, 2017. **80**: p. 54-74.
110. Hawa, A., D. Tonnayopas, and W. Prachasaree, *Performance evaluation and microstructure characterization of metakaolin-based geopolymer containing oil palm ash.* The Scientific World Journal, 2013. **2013**.
111. Nmai, C., et al., *Shrinkage-reducing admixtures.* Concrete International, 1998. **20**(4): p. 31-37.
112. Collins, F. and J.G. Sanjayan, *Strength and shrinkage properties of alkali-activated slag concrete containing porous coarse aggregate.* Cement and Concrete Research, 1999. **29**(4): p. 607-610.
113. Li, J. and Y. Yao, *A study on creep and drying shrinkage of high performance concrete.* Cement and Concrete Research, 2001. **31**(8): p. 1203-1206.
114. Abdollahnejad, Z., et al., *Comparative Study on the Effects of Recycled Glass–Fiber on Drying Shrinkage Rate and Mechanical Properties of the Self-Compacting Mortar and*

Fly Ash–Slag Geopolymer Mortar. Journal of Materials in Civil Engineering, 2017. **29**(8): p. 04017076.

115. Zanotti, C., et al., *Bond strength between concrete substrate and metakaolin geopolymer repair mortar: Effect of curing regime and PVA fiber reinforcement.* Cement and Concrete Composites, 2017. **80**: p. 307-316.
116. Naganur, I.K., et al., *A STUDY ON SELF-COMPACTING GEOPOLYMER CONCRETE WITH AN ALKALINE ACTIVATOR RATIO AND DIFFERENT ALKALINE ACTIVATOR TO CEMENTITIOUS BINDER RATIOS.* 2017.
117. Nikolov, A., I. Rostovsky, and H. Nugteren, *Geopolymer materials based on natural zeolite.* Case Studies in Construction Materials, 2017. **6**: p. 198-205.
118. Gao, X., et al., *Evaluation of hybrid steel fiber reinforcement in high performance geopolymer composites.* Materials and Structures, 2017. **50**(2): p. 165.
119. Khater, H. and H.A. el Gawaad, *Characterization of alkali activated geopolymer mortar doped with MWCNT.* Construction and Building Materials, 2016. **102**: p. 329-337.
120. Ridtirud, C., P. Chindaprasirt, and K. Pimraksa, *Factors affecting the shrinkage of fly ash geopolymers.* International Journal of Minerals, Metallurgy, and Materials, 2011. **18**(1): p. 100-104.
121. Chindaprasirt, P., et al., *High-strength geopolymer using fine high-calcium fly ash.* Journal of Materials in Civil Engineering, 2010. **23**(3): p. 264-270.
122. Temuujin, J. and A. Van Riessen, *Effect of fly ash preliminary calcination on the properties of geopolymer.* Journal of Hazardous Materials, 2009. **164**(2): p. 634-639.
123. Atiş, C.D., et al., *Influence of activator on the strength and drying shrinkage of alkali-activated slag mortar.* Construction and building materials, 2009. **23**(1): p. 548-555.
124. Zuhua, Z., et al., *Role of water in the synthesis of calcined kaolin-based geopolymer.* Applied Clay Science, 2009. **43**(2): p. 218-223.
125. Palacios, M. and F. Puertas, *Effect of shrinkage-reducing admixtures on the properties of alkali-activated slag mortars and pastes.* Cement and concrete research, 2007. **37**(5): p. 691-702.
126. He, J., et al., *The strength and microstructure of two geopolymers derived from metakaolin and red mud-fly ash admixture: A comparative study.* Construction and Building Materials, 2012. **30**: p. 80-91.
127. Nie, Q., et al., *Strength properties of geopolymers derived from original and desulfurized red mud cured at ambient temperature.* 2016. **125**: p. 905-911.
128. Hu, W., et al., *Mechanical and microstructural characterization of geopolymers derived from red mud and fly ashes.* 2018. **186**: p. 799-806.
129. Hu, W., et al., *Mechanical property and microstructure characteristics of geopolymer stabilized aggregate base.* 2018. **191**: p. 1120-1127.
130. Hu, W., et al., *Investigation of the strength development of cast-in-place geopolymer piles with heating systems.* 2019.
131. Zhang, M., et al., *Durability of red mud-fly ash based geopolymer and leaching behavior of heavy metals in sulfuric acid solutions and deionized water.* Construction and Building Materials, 2016. **124**: p. 373-382.
132. Fu, Y., L. Cai, and W. Yonggen, *Freeze–thaw cycle test and damage mechanics models of alkali-activated slag concrete.* Construction and Building Materials, 2011. **25**(7): p. 3144-3148.
133. http://www.concrete-experts.com/pages/ft.htm, *Freeze-thaw deterioration of concrete.*

134. Sun, P. and H.-C. Wu, *Chemical and freeze–thaw resistance of fly ash-based inorganic mortars.* Fuel, 2013. **111**: p. 740-745.
135. Slavik, R., et al., *Preparation of geopolymer from fluidized bed combustion bottom ash.* Journal of Materials Processing Technology, 2008. **200**(1): p. 265-270.
136. Topcu, I.B. and M.U. Toprak, *Properties of geopolymer from circulating fluidized bed combustion coal bottom ash.* Materials Science and Engineering: A, 2011. **528**(3): p. 1472-1477.
137. Topcu, I.B., M.U. Toprak, and T. Uygunoğlu, *Durability and microstructure characteristics of alkali activated coal bottom ash geopolymer cement.* Journal of Cleaner Production, 2014. **81**: p. 211-217.
138. Li, Q., et al., *Immobilization of simulated radionuclide 133Cs+ by fly ash-based geopolymer.* Journal of hazardous materials, 2013. **262**: p. 325-331.
139. Wang, S., et al., *Durability of biomass fly ash concrete: freezing and thawing and rapid chloride permeability tests.* Fuel, 2008. **87**(3): p. 359-364.
140. Yunsheng, Z., et al., *Impact properties of geopolymer based extrudates incorporated with fly ash and PVA short fiber.* Construction and Building Materials, 2008. **22**(3): p. 370-383.
141. Zhang, G., J. He, and R.P. Gambrell, *Synthesis, Characterization, and Mechanical Properties of Red Mud-Based Geopolymers.* Transportation research record, 2010. **2167**(01).
142. Mohammad, L.N. and S.B. Cooper III, *AAPT Symposium: Implementation of a Balanced Asphalt Mixture Design Procedure: Louisiana's Approach.* Journal of the Association of Asphalt Paving Technologists, 2016(85).
143. Khale, D. and R. Chaudhary, *Mechanism of geopolymerization and factors influencing its development: a review.* Journal of materials science, 2007. **42**(3): p. 729-746.
144. Duxson, P., et al., *Geopolymer technology: the current state of the art.* Journal of Materials Science, 2007. **42**(9): p. 2917-2933.
145. Fernandez-Jimenez, A., I. García-Lodeiro, and A. Palomo, *Durability of alkali-activated fly ash cementitious materials.* Journal of Materials Science, 2006. **42**(9): p. 3055-3065.
146. de Vargas, A.S., et al., *The effects of Na2O/SiO2molar ratio, curing temperature and age on compressive strength, morphology and microstructure of alkali-activated fly ash-based geopolymers.* Cement and Concrete Composites, 2011. **33**(6): p. 653-660.
147. Chindaprasirt, P., et al., *High-strength geopolymer using fine high-calcium fly ash.* Journal of Materials in Civil Engineering, 2011. **23**(3): p. 264-270.
148. Cheng, T. and J. Chiu, *Fire-resistant geopolymer produced by granulated blast furnace slag.* Minerals Engineering, 2003. **16**(3): p. 205-210.
149. Yunsheng, Z., et al., *Synthesis and heavy metal immobilization behaviors of slag based geopolymer.* Journal of Hazardous Materials, 2007. **143**(1): p. 206-213.
150. Detphan, S. and P. Chindaprasirt, *Preparation of fly ash and rice husk ash geopolymer.* International Journal of Minerals, Metallurgy and Materials, 2009. **16**(6): p. 720-726.
151. Rowles, M. and B. O'connor, *Chemical optimisation of the compressive strength of aluminosilicate geopolymers synthesised by sodium silicate activation of metakaolinite.* journal of Materials Chemistry, 2003. **13**(5): p. 1161-1165.
152. Barbosa, V.F., K.J. MacKenzie, and C. Thaumaturgo, *Synthesis and characterisation of materials based on inorganic polymers of alumina and silica: sodium polysialate polymers.* International Journal of Inorganic Materials, 2000. **2**(4): p. 309-317.

153. Pacheco-Torgal, F., et al., *Composition, strength and workability of alkali-activated metakaolin based mortars.* Construction and Building Materials, 2011. **25**(9): p. 3732-3745.
154. Puertas, F., et al., *Alkali-activated fly ash slag cements Strength behaviour and hydration products.* Cement and Concrete Research, 2000. **30**: p. 1625-1632.
155. Zhang, G., J. He, and R.P. Gambrell, *Synthesis, characterization, and mechanical properties of red mud-based geopolymers*, in *Transportation Research Record*. 2010. p. 1-9.
156. Kavas, T., *Use of boron waste as a fluxing agent in production of red mud brick.* Building and Environment, 2006. **41**(12): p. 1779-1783.
157. Yang, J. and B. Xiao, *Development of unsintered construction materials from red mud wastes produced in the sintering alumina process.* Construction and Building Materials, 2008. **22**(12): p. 2299-2307.
158. Marabini, A.M., et al., *New materials from industrial and mining wastes: glass-ceramics and glass-and rock-wool fibre.* International journal of mineral processing, 1998. **53**(1-2): p. 121-134.
159. Yang, J., et al., *Preparation of glass-ceramics from red mud in the aluminium industries.* Ceramics International, 2008. **34**(1): p. 125-130.
160. Zuhua, Z., et al., *Role of water in the synthesis of calcined kaolin-based geopolymer.* 2009. **43**(2): p. 218-223.
161. Winnefeld, F., et al., *Assessment of phase formation in alkali activated low and high calcium fly ashes in building materials.* Construction and building materials, 2010. **24**(6): p. 1086-1093.
162. Rees, C.A., et al., *In situ ATR-FTIR study of the early stages of fly ash geopolymer gel formation.* 2007. **23**(17): p. 9076-9082.
163. Rees, C.A., et al., *Attenuated total reflectance fourier transform infrared analysis of fly ash geopolymer gel aging.* 2007. **23**(15): p. 8170-8179.
164. Rovnaník, P., *Effect of curing temperature on the development of hard structure of metakaolin-based geopolymer.* Construction and building materials, 2010. **24**(7): p. 1176-1183.
165. Hajimohammadi, A., J.L. Provis, and J.S. Van Deventer, *One-part geopolymer mixes from geothermal silica and sodium aluminate.* Industrial & Engineering Chemistry Research, 2008. **47**(23): p. 9396-9405.
166. Criado, M., A. Fernández-Jiménez, and A. Palomo, *Alkali activation of fly ash: Effect of the SiO2/Na2O ratio: Part I: FTIR study.* Microporous and mesoporous materials, 2007. **106**(1-3): p. 180-191.
167. Zhang, Z., et al., *Quantitative kinetic and structural analysis of geopolymers. Part 1. The activation of metakaolin with sodium hydroxide.* Thermochimica acta, 2012. **539**: p. 23-33.
168. Çelik, Ö., E. Damcı, and S. Pişkin, *Characterization of fly ash and it effects on the compressive strength properties of Portland cement.* 2008.
169. Lee, W. and J. Van Deventer, *The effects of inorganic salt contamination on the strength and durability of geopolymers.* Colloids and Surfaces A: Physicochemical and Engineering Aspects, 2002. **211**(2-3): p. 115-126.

170. Zhang, Z., et al., *Quantitative kinetic and structural analysis of geopolymers. Part 2. Thermodynamics of sodium silicate activation of metakaolin.* Thermochimica acta, 2013. **565**: p. 163-171.
171. Lyu, S.-J., et al., *Microstructure of geopolymer accounting for associated mechanical characteristics under various stress states.* Cement and concrete research, 2013. **54**: p. 199-207.
172. Rahier, H., et al., *Reaction mechanism, kinetics and high temperature transformations of geopolymers.* Journal of materials science, 2007. **42**(9): p. 2982-2996.
173. Yunsheng, Z., S. Wei, and L. Zongjin, *Composition design and microstructural characterization of calcined kaolin-based geopolymer cement.* Applied Clay Science, 2010. **47**(3-4): p. 271-275.
174. Powers, T.J.I. and E. Chemistry, *Absorption of water by Portland cement paste during the hardening process.* 1935. **27**(7): p. 790-794.
175. Standard, A.J.S.T.M.f.C.S.o.H.C.P., " ASTM International, West Conshohocken, PA, *C1608, 2012,"*. 2012.
176. Tazawa, E.-i., et al., *Chemical shrinkage and autogenous shrinkage of hydrating cement paste.* 1995. **25**(2): p. 288-292.
177. Zhang, Z., G.W.J.C. Scherer, and C. Composites, *Measuring chemical shrinkage of ordinary Portland cement pastes with high water-to-cement ratios by adding cellulose nanofibrils.* 2020: p. 103625.
178. Zhang, M., et al., *A multiscale investigation of reaction kinetics, phase formation, and mechanical properties of metakaolin geopolymers.* Cement and Concrete Composites, 2017. **78**: p. 21-32.
179. Zhang, M., et al., *A multiscale investigation of reaction kinetics, phase formation, and mechanical properties of metakaolin geopolymers.* 2017. **78**: p. 21-32.
180. Rees, C.A., et al., *The mechanism of geopolymer gel formation investigated through seeded nucleation.* Colloids and Surfaces A: Physicochemical and Engineering Aspects, 2008. **318**(1-3): p. 97-105.
181. Tennakoon, C., et al., *Influence and role of feedstock Si and Al content in Geopolymer synthesis.* Journal of Sustainable Cement-Based Materials, 2015. **4**(2): p. 129-139.
182. Hajimohammadi, A., J.L. Provis, and J.S. Van Deventer, *Time-resolved and spatially-resolved infrared spectroscopic observation of seeded nucleation controlling geopolymer gel formation.* Journal of colloid and interface science, 2011. **357**(2): p. 384-392.
183. Duxson, P., et al., *Geopolymer technology: the current state of the art.* 2007. **42**(9): p. 2917-2933.
184. Ge, X., et al., *Characteristics of underwater cast and cured geopolymers.* Cement and Concrete Composites, 2020. **114**: p. 103783.
185. Fernández-Jiménez, A. and A. Palomo, *Composition and microstructure of alkali activated fly ash binder: Effect of the activator.* Cement and concrete research, 2005. **35**(10): p. 1984-1992.
186. van Jaarsveld, J. and J. Van Deventer, *Effect of the alkali metal activator on the properties of fly ash-based geopolymers.* Industrial & engineering chemistry research, 1999. **38**(10): p. 3932-3941.
187. Zhang, F., et al., *Role of alkali cation in compressive strength of metakaolin based geopolymers.* Ceramics International, 2017. **43**(4): p. 3811-3817.

188. Zhang, M., et al., *Reaction kinetics of red mud-fly ash based geopolymers: Effects of curing temperature on chemical bonding, porosity, and mechanical strength.* 2018. **93**: p. 175-185.
189. Nath, S.J.C. and B. Materials, *Geopolymerization behavior of ferrochrome slag and fly ash blends.* 2018. **181**: p. 487-494.
190. Rovnaník, P.J.C. and b. materials, *Effect of curing temperature on the development of hard structure of metakaolin-based geopolymer.* 2010. **24**(7): p. 1176-1183.
191. Zhang, M., et al., *Synthesis factors affecting mechanical properties, microstructure, and chemical composition of red mud–fly ash based geopolymers.* 2014. **134**: p. 315-325.
192. Yunsheng, Z., S. Wei, and L.J.A.C.S. Zongjin, *Composition design and microstructural characterization of calcined kaolin-based geopolymer cement.* 2010. **47**(3-4): p. 271-275.
193. Kaya, K. and S.J.C.I. Soyer-Uzun, *Evolution of structural characteristics and compressive strength in red mud–metakaolin based geopolymer systems.* 2016. **42**(6): p. 7406-7413.
194. Kumar, A., S.J.C. Kumar, and B. Materials, *Development of paving blocks from synergistic use of red mud and fly ash using geopolymerization.* 2013. **38**: p. 865-871.
195. Zhao, M., et al., *Freeze-thaw durability of red mud slurry-class F fly ash-based geopolymer: Effect of curing conditions.* 2019. **215**: p. 381-390.
196. Komljenović, M., Z. Baščarević, and V. Bradić, *Mechanical and microstructural properties of alkali-activated fly ash geopolymers.* Journal of Hazardous Materials, 2010. **181**(1-3): p. 35-42.
197. Rowles, M.R. and B.H. O'Connor, *Chemical and structural microanalysis of aluminosilicate geopolymers synthesized by sodium silicate activation of metakaolinite.* Journal of the American Ceramic Society, 2009. **92**(10): p. 2354-2361.
198. Turner, L.K. and F.G. Collins, *Carbon dioxide equivalent (CO2-e) emissions: A comparison between geopolymer and OPC cement concrete.* Construction and Building Materials, 2013. **43**: p. 125-130.
199. Davidovits, J. *Environmentally driven geopolymer cement applications*. in *Proceedings of 2002 Geopolymer Conference. Melbourne. Australia*. 2002.
200. Van Jaarsveld, J., J. Van Deventer, and L. Lorenzen, *The potential use of geopolymeric materials to immobilise toxic metals: Part I. Theory and applications.* Minerals engineering, 1997. **10**(7): p. 659-669.
201. Duxson, P., et al., *Geopolymer technology: the current state of the art.* Journal of Materials Science, 2007. **42**(9): p. 2917-2933.
202. Bakharev, T., *Resistance of geopolymer materials to acid attack.* Cement and Concrete Research, 2005. **35**(4): p. 658-670.
203. Zhang, H.Y., et al., *Development of metakaolin–fly ash based geopolymers for fire resistance applications.* Construction and Building Materials, 2014. **55**: p. 38-45.
204. *Standard Test Method for Compressive Strength of Hydraulic Cement Mortars (Using 2-in. or [50-mm] Cube Specimens)*.
205. Criado, M., A. Fernández-Jiménez, and A. Palomo, *Alkali activation of fly ash: effect of the SiO 2/Na 2 O ratio: Part I: FTIR study.* Microporous and mesoporous materials, 2007. **106**(1): p. 180-191.
206. Jr, S. and W. Wb, *Study of Sodium Silicate Glasses and Liquids by Infrared Reflectance Spectroscopy*. Vol. 10. 1969. 246-251.

207. Roy, B.N., *Infrared Spectroscopy of Lead and Alkaline-Earth Aluminosilicate Glasses.* Journal of the American Ceramic Society, 1990. **73**(4): p. 846-855.
208. JEWER, S., *Structural Analysis by Infrared Spectroscopy.* Zeolite Chemistry, 1985. **2**: p. 80-117.
209. Catauro, M., et al., *Investigation of the sample preparation and curing treatment effects on mechanical properties and bioactivity of silica rich metakaolin geopolymer.* Materials Science and Engineering: C, 2014. **36**: p. 20-24.
210. Rees, C.A., et al., *In situ ATR-FTIR study of the early stages of fly ash geopolymer gel formation.* Langmuir, 2007. **23**(17): p. 9076-9082.
211. Parler, C.M., J.A. Ritter, and M.D. Amiridis, *Infrared spectroscopic study of sol–gel derived mixed-metal oxides.* Journal of non-crystalline solids, 2001. **279**(2): p. 119-125.
212. Ismail, I., et al., *Modification of phase evolution in alkali-activated blast furnace slag by the incorporation of fly ash.* Cement and Concrete Composites, 2014. **45**: p. 125-135.
213. Ismail, I., et al., *Influence of fly ash on the water and chloride permeability of alkali-activated slag mortars and concretes.* Construction and Building Materials, 2013. **48**: p. 1187-1201.
214. Ismail, I., et al., *Microstructural changes in alkali activated fly ash/slag geopolymers with sulfate exposure.* Materials and structures, 2013. **46**(3): p. 361-373.
215. Ranjbar, N., et al., *Compressive strength and microstructural analysis of fly ash/palm oil fuel ash based geopolymer mortar.* 2014. **59**: p. 532-539.